A new paradigm towards advanced Li-based batteries: a true polymeric approach

POLITECNICO DI TORINO
Ph.D. in Materials Science and Technology (Cycle XXVIII)


# A new paradigm towards advanced Li-based batteries: a true polymeric approach

Ph.D. candidate: Luca Porcarelli

Supervisor: Prof. Claudio Gerbaldi

**2013 - 2016**

*To my family*

# TABLE OF CONTENTS

# *PREFACE*

Today, the global energy demand is mainly fulfilled by combustion of non-renewable fossil fuels. Greenhouse gases, i.e. carbon dioxide, are produced in large quantities and the always-increasing emissions of $CO_2$ in the atmosphere have been identified as one of the principal causes of global warming. As the world energy consumption is expected to rise tremendously in the next twenty years, global efforts are required to change the current energy economy, in order to avoid catastrophic consequences for both human health and the environment. The exploitation of renewable energy sources and the replacement of internal combustion engines with electric motors for propulsion needs are the most viable strategies to accomplish the goal. Of course, both of these approaches will require efficient technologies to store electrical energy.

To date, lithium-ion batteries (LIBs) are the best candidates to face these challenges and their fields of application are rapidly expanding towards new performance-demanding applications such as electric/hybrid electric vehicles (EVs / HEVs) and large-scale stationary energy storage to power the grid. The success of LIBs owes mainly to their high energy density, lightweight, rapid charge/discharge and relatively long lifetime. Despite the mentioned advantages, safety issues deriving from the use of conventional liquid electrolytes are, at present, one of the major drawbacks of this technology.

In the past years, a great deal of research work has been focused on the development of safer electrolytes. Soon after the discovery of ion conductivity of alkali metal ions in poly(ethylene oxide) (PEO), the use of solid-state polymer electrolytes (SPEs) was proposed to replace conventional liquid electrolytes. The most striking advantages of SPEs are non-volatility, non-flammability, and good mechanical robustness that allow their use as electrode separator, which accounts for safer and overall higher energy density LIBs. On the other hand, the practical application of polymer electrolytes in real devices has been precluded so far due to their intrinsic low ionic conductivity values. Still, a lot of research work has to be done to improve the performance of polymer electrolytes, thus favoring their widespread use in commercial devices.

It is universally accepted that ion conduction can occur exclusively in the amorphous phase of PEO-based electrolytes, and the crystalline domains are usually considered as ionic insulator. Due to the semi-crystalline nature of PEO, strategies to increase ionic conductivity have been mainly focused on increasing the degree of disorder in the polymer. Modification of the macromolecular design, such as branching, brushing, random and block copolymerization demonstrated to suppress effectively crystallinity. Another popular approach has been the incorporation of plasticizing agents or small-molecule organic solvents, thus forming gel polymer electrolytes (GPEs).

Considering such a scenario, during the three years of this Ph.D. course the research work has been focused on the development of different families of polymer electrolytes based on PEO. The goal has been achieved by exploiting a series of smart engineering strategies and synthetic

pathways. Then, all of the newly designed materials were characterized in terms of their physicochemical and electrochemical properties. The experimental work has been carried out in the GAME Lab at the Department of Applied Science and Technology – DISAT of Politecnico di Torino and also in the laboratories of the Institute for Polymer Materials - POLYMAT (University of the Basque Country), during an 11 months visiting stage.

During the first half of the Ph.D., a progressive pathway has been followed, which started from the idea of using UV-induced cross-linking as a versatile tool to incorporate substantial amounts of high boiling liquid plasticizers in the polymeric matrix, with the aim to increase the ionic conductivity at room temperature, without sacrificing the mechanical properties of the polymer. The second half of this Ph.D. was instead devoted to the development of synthetic strategies to increase another important transport parameter of polymer electrolytes, which is the lithium-ion transference number. The goal was achieved by covalently immobilizing anions to the polymer backbone and obtaining single (lithium) ion conduction in polymer electrolytes.

In Chapter 1, the current global energy scenario is briefly overviewed, along with the challenges that actual energy storage technologies must address. Furthermore, the basic concepts of lithium-based cells are discussed and a short review is given on the state-of-the-art of materials and components for LIBs.

In Chapter 2, a simple and easily up-scalable preparation of UV crosslinked polymer electrolytes encompassing room temperature ionic liquids (RTILs) is presented. The polymer electrolyte membranes were prepared by mixing PEO as the polymer matrix, 1-ethyl-3-methylimidazolium

bis(trifluoromethylsulfonyl)imide (EMI TFSI) as the high boiling point plasticizer, lithium bis(trifluoromethylsulfonyl)imide (LiTFSI) as the source of $Li^+$ ions and 4-methyl benzophenone (MBP) as the UV-induced hydrogen abstraction mediator. Under UV excitation, MBP may abstract acidic protons from methylene groups and generate free radicals on the polymer backbone. Then, the recombination of free radicals may create multiple crosslinking points. The prepared materials displayed remarkable thermal stability, reduced crystallinity and showed outstanding mechanical properties due to the induced crosslinking, regardless of the relatively high weight content of RTIL in the membranes. Improved ionic conductivity at room temperature was achieved (up to $2.5 \times 10^{-4}$ S $cm^{-1}$ at 25 °C) along with a 4.6 V electrochemical window for safe operation. The promising prospect of this polymer electrolyte were demonstrated by the results of tests in lab-scale lithium cells operating at ambient temperature as well as 55 °C. Finally, it is worth to be noted that the newly developed preparation method has led to an international patent recently published.

Chapter 3 describes the preparation of a polymer electrolyte system based on PEO and glycol dimethyl ether. The UV crosslinking procedure described in the previous chapter was adapted and applied to this novel concept of soft polymer electrolyte, which was designed by regulating the mobility of classic ethylene oxide backbones. In particular, polymer electrolytes were obtained by UV-induced crosslinking between the ethylene oxide chains, plasticized by glycol dimethyl ether at various lithium salt concentrations. The macromolecular networks exhibited sterling mechanical robustness, low glass-transition temperature, high ionic conductivity (up to $4.0 \times 10^{-4}$ S $cm^{-1}$ at 25 °C) and a wide 5.2 V

electrochemical window. All solid lithium-based polymer cells were assembled, which showed outstanding cycling behavior in terms of rate capability and stability over a wide range of operating temperatures.

In Chapter 4, a novel family of block copolymer SPEs was obtained via RAFT controlled radical polymerization of a specifically designed anionic liquid monomer, namely lithium 1-[3-(methacryloxy)propylsulfonyl]-1-(trifluoromethanesulfonyl)imide, with poly(ethylene glycol) methyl ether methacrylate. The proposed synthetic approach enabled to obtain anionic polyelectrolytes displaying single lithium-ion conduction, as for the lithium-ion transference number approaching the unity (0.84). This characteristic is expected to prevent polarization phenomena within the polymer electrolyte. Low glass-transition temperatures, absence of crystallinity, comparatively high ionic conductivity for a solvent-free solid polymer electrolyte (up to $1.0 \times 10^{-5}$ S $cm^{-1}$ at 55 °C) and a 4.5 V electrochemical window were achieved. Owing to the combination of all mentioned properties, the prepared polymer materials were used as solid polyelectrolytes as well as binders in the elaboration of lithium-metal battery prototypes with high charge/discharge efficiency and good rate capability.

In Chapter 5, the anionic monomer proposed in the previous chapter was employed with poly(ethylene glycol)dimethacrylate to prepare networked single-ion conducting GPEs. Enhanced ionic conductivities for a single-ion conductor type electrolyte were obtained upon incorporation of propylene carbonate in the polymer network (up to $8.6 \times 10^{-5}$ S $cm^{-1}$ at 20 °C), along with a 5.5 V electrochemical window for safe battery operation. Despite the significant solvent content, the synthesized thermoset polymer showed

good mechanical stability, thus it was possible to prepare them in the form of thin, self-standing films. Excellent rate capabilities were achieved in a wide temperature operating range (up to 5C and 1C current rates respectively at 70 °C and ambient temperature) and lab-scale lithium cells demonstrated stable cycling and high capacity retention upon prolonged cycling. Based on the experiments carried out and the literature data, the obtained findings outperform the current reports on single-ion conducting gel electrolytes. This represents a concrete step forward for the next generation of high performing, safe and durable lithium-based energy storage devices to be successful in the contest of a sustainable global energy supply system.

# CHAPTER ONE

## *Towards the development of advanced lithium-ion batteries*

### 1.1 INTRODUCTION

Modern society is strongly dependent on electrochemical energy storage and conversion devices, and the importance of such technologies is expected to increase in the near future. The use of sophisticated portable electronic devices, including cell phones and laptop computers, has revolutionized our every-day life, and it would not be possible without high-energy density power sources. Lithium-ion batteries (LIBs) were introduced in the market almost three decades ago and since then have been dominantly used in portable electronics [1–5]. Nowadays, the market of lithium-ion batteries is rapidly moving towards more challenging applications, such as electric vehicles (xEV) and stationary large scale energy storage [2,3,5,6]. **Figure 1.1** shows the quick expansion of the LIBs market during the past years and the predicted trends for the near future. To explain

the increasing demand for energy storage, a discussion on the current global energy scenario is required.

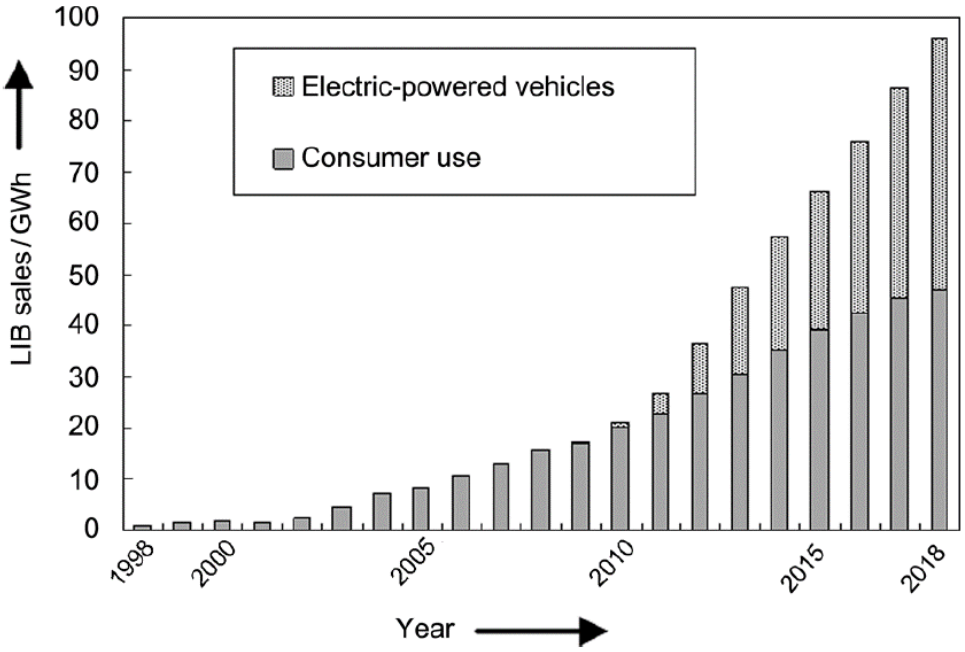


**Figure 1.1** Forecasted expansion in demand for lithium-ion batteries. GWh=gigawatt hours. Reproduced with permission from [3]

## 1.2. THE GLOBAL ENERGY SCENARIO

Nowadays, the annual world energy consumption is calculated to be around 18 TW. As a consequence of the increasing world population and raise in the average energy use per person, the world energy consumption

is expected to exceed 25 TW in the next twenty years [7]. The production of energy and economic welfare is mainly based on the combustion of cheap and abundant non-renewable fossil fuels such as oil, natural gas, and coal (**Figure 1.2**). Coal and natural gases are intensively used for electric energy production, whereas refined products of oil are used for transportation needs [7].

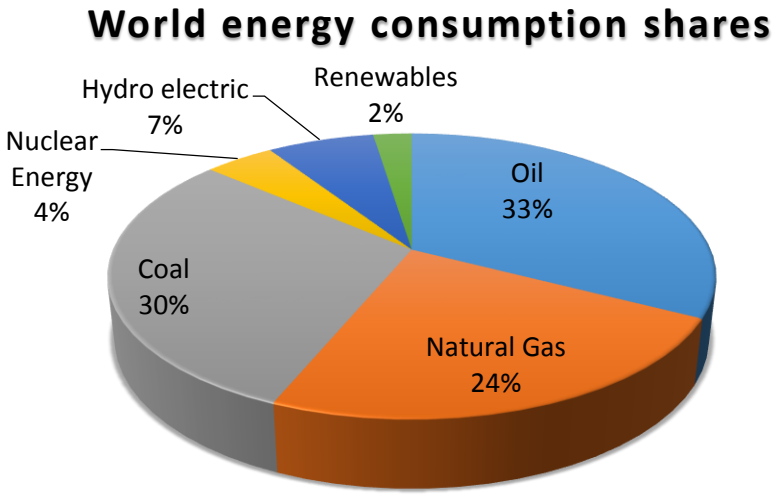


**Figure 1.2** World primary energy consumption shares during 2014. Adapted from [7].

Although the depletion of these resources is not an issue in the short term, environmental damages resulting from their use are tremendously evident. Greenhouse gases, particularly carbon dioxide - $CO_2$, are produced in large quantities upon combustion of fossil fuels, and the raising level of

$CO_2$ in the atmosphere has been identified as one of the major causes of global warming and associated global climate changes [8]. Greenhouse gases are not the only emissions deriving from energy production and consumption. Indeed, large amounts of pollutants such as sulphur oxides ($SO_x$), mono-nitrogen oxides ($NO_x$), and particulate matter are produced from the combustion of fossil fuels. Renewable energy harvesting technologies have evolved much in the recent years; however, due to the intermittency of the main sources of alternative energy, such as sun and wind [9,10], intensive exploitation of these resources requires efficient systems for energy storage [6]. The development of electric propulsion technologies for ground transportation is facing very similar challenges. Both of these applications will require newly developed battery technologies, with enhanced energy density, prolonged cycle life, and excellent safety. To date, LIBs are the best candidates to face these challenges. The most striking advantage of LIBs is their superior energy density compared to other energy storage technologies [11], such as lead-acid (Pb-acid), nickel-cadmium (Ni-Cd) and nickel-metal hydride (NiMH) batteries [12]. The Ragone plot of specific gravimetric and volumetric energy density for various energy storage technologies is shown in **Figure 1.3.** The other successful characteristics of LIBs are rapid charge and discharge rates, absence of memory effect, low self-discharge, and both long shelf and cycle life [5]. The challenges imposed by these new applications will be discussed in the next two paragraphs.

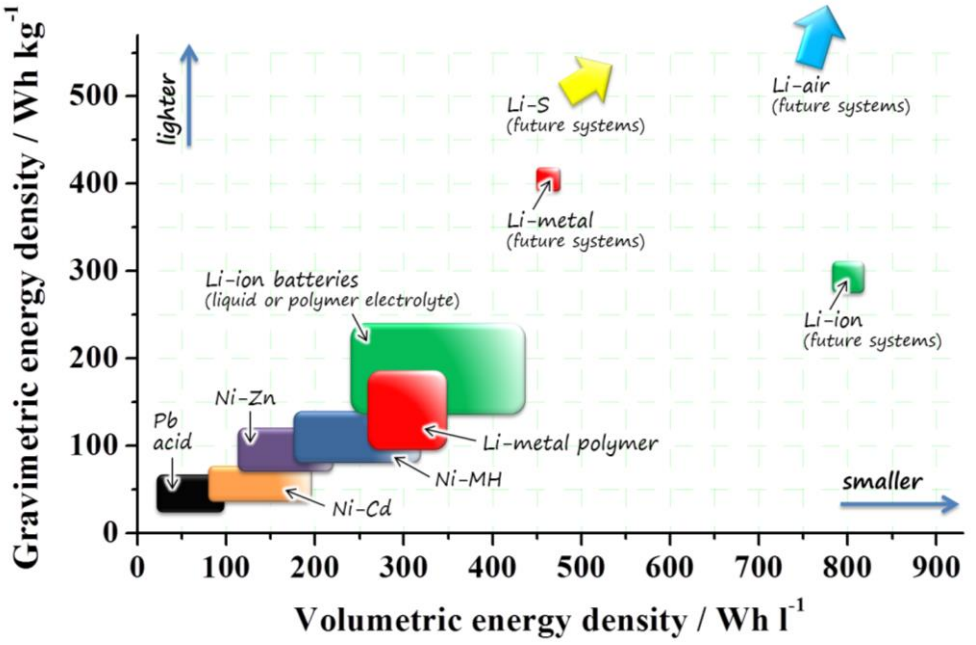


**Figure 1.3.** Plot of gravimetric and volumetric energy densities for different energy storage technologies. Reproduced with permission from [13].

### 1.2.1 ON THE CHALLENGE TOWARDS ELECTRIC PROPULSION

The development of electric propulsion for transportation needs is mainly driven by ambitious emission reduction plans. Indeed, considering the average increasing price of this raw material during the past years and the detrimental effects on the environment and human health, we will become more and more reluctant to burn petroleum in ICE for ground transportation in the future.

Electric vehicles (xEV) can be classified into three main categories: hybrid electric vehicles (HEVs), full electric vehicles (EVs) and plug-in hybrid electric vehicles (PHEVs) [2]. HEVs are powered mainly by a conventional ICE that takes advantage of an electric propulsion system to achieve better fuel economy and/or better performance. Batteries of an HEV are charged by the ICE as well as during regenerative braking mode. EVs depend only on the electric propulsion system and their only source of power is the internal battery pack; the battery pack is then recharged connecting the vehicle to the external electrical grid. PHEVs are similar to HEV but their battery pack is recharged externally. Performance requirements for batteries are dependent on the propulsion system of the xEV; power density is especially required for HEV, whereas energy density is more important for EV as shown in **figure 1.4**. Power density is a critical factor in HEV since the battery pack is required to provide current delivery at high rates during acceleration and regenerative braking. In contrast, energy density is more relevant in EVs since the vehicle autonomy is depending only on the overall capacity of the battery [2]. Cycle life of batteries for xEVs is another important parameter. Since the average lifetime expectancy of a new car is more than 10 years, batteries for xEV applications are expected to have similar cycle life. From a merely economic point of view, consumers are not willing to replace a whole battery before purchasing a new car.

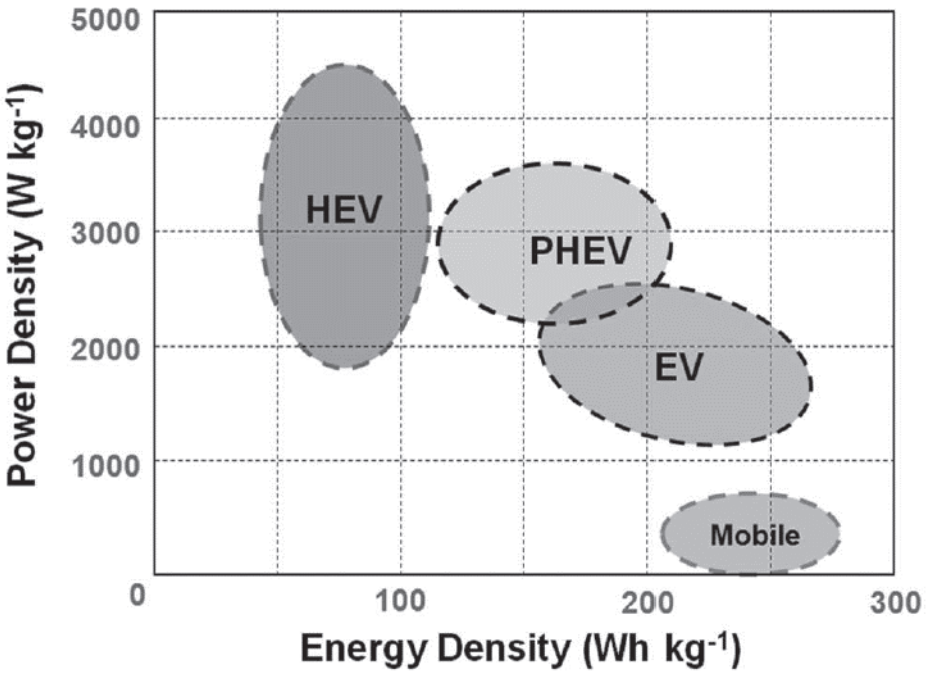


**Figure 1.4** Power and energy density requirement of LIBs for xEVs and small mobile applications. Reproduced with permission from [2].

Safely is another key issue for xEV applications. Since the early years of LIBs, consumers have sporadically experienced incidents of firing and/or explosions of electronic devices caused by battery failures. As the size of LIBs for xEV applications is significantly bigger than that of portable electronics, increased safety levels must be guaranteed. Although LIBs for xEVs are already commercialized, their performance still need to be improved to meet the customer expectations, especially for the full EV sector. To date, state-of-the-art LIBs allow for maximum driving autonomies of 150 km. Since

xEVs have to be similar to conventional vehicles in terms of size and weight, it is not possible to increase driving autonomies and power performances just by increasing the size of batteries. Therefore, improvements to the current lithium-ion chemistry are required to double, at least, the autonomy of xEVs. Moreover, quick recharge times (less than half an hour) are other important requirements to be meet, as to date, the time for full recharge of EVs and PHEVs is around 3-4 hours.

### 1.2.2 ON THE CHALLENGE OF LOAD LEVELLING

The electric energy demand is not constant during the day, and electric power grids have time dependent power loads. The typical daily power load profile in different seasons is depicted in **Figure 1.5**. To satisfy the intermediate demands, energy power plants are switched on and off to match the electric grid request at all times. However, some plants sit idle for 95 percent of the time, and are only used to satisfy the peak demand [2]. For higher efficiency, electric energy should be stored during low load time and utilized at high load time. To do so, large scale-energy storage plants must be integrated in the current grids. In the short terms, LIBs are the most promising technology for this task [6]. The challenges associated to the development of LIBs for this application are similar to those for xEVs, except maybe for energy density. In fact, high energy density is not mandatory in large-scale energy plants, where battery sizes are not limited. Moreover, for a better exploitation of electric energy coming from renewable sources, load levelling is also required. In fact, one of the weakest point of renewable

energies is that their production rate cannot be controlled. In fact, sun and wind are intermittent energy sources. Efficient load levelling systems of the energy coming from renewable resources must be developed to integrate renewable energy plants into conventional grids.

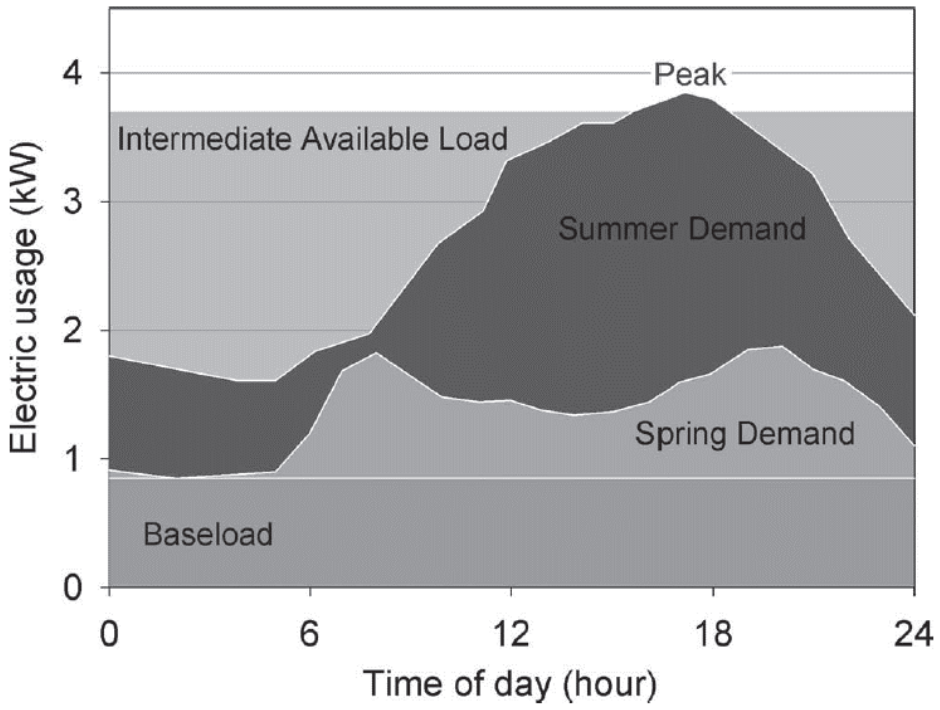


**Figure 1.5** The typical daily power load profile of electrid grids in different seasons. Reproduced with permission from [2]

## 1.3 LITHIUM-ION BATTERIES: WORKING PRINCIPLES AND STATE-OF-THE-ART

The working principle of a standard lithium-ion cell is schematically illustrated in **Figure 1.6**, typical state-of-the-art materials are used in this example. The typical cell assembly is obtained by sandwiching the positive electrode, based on a layered transition metal oxide ($LiCoO_2$), and the negative one, based on graphitic carbon, with a polymeric microporous polyolefin separator in between. The separator is filled with an aprotic liquid electrolyte, i.e. a solution of lithium fluorinated salt ($LiPF_6$) in a mixture of solvents comprising ethylene carbonate and at least one linear organic carbonate. The two electrodes are connected externally through an electric circuit [1]. Lithium-ion cells are fabricated in the discharged state; discharged electrode materials are more stable and can be easily handled during assembly [11]. During charge, electrons are forced to leave the positive electrode and move through the external circuit to the negative one. Since this process is not thermodynamically favored, the use of an external power source is required. At the same time, lithium-ions leave the hosting structure of lithium cobalt oxide and, migrating through the electrolyte, intercalate in between the graphitic layers. In this way, the external electric energy is stored in the battery in the form of chemical energy.

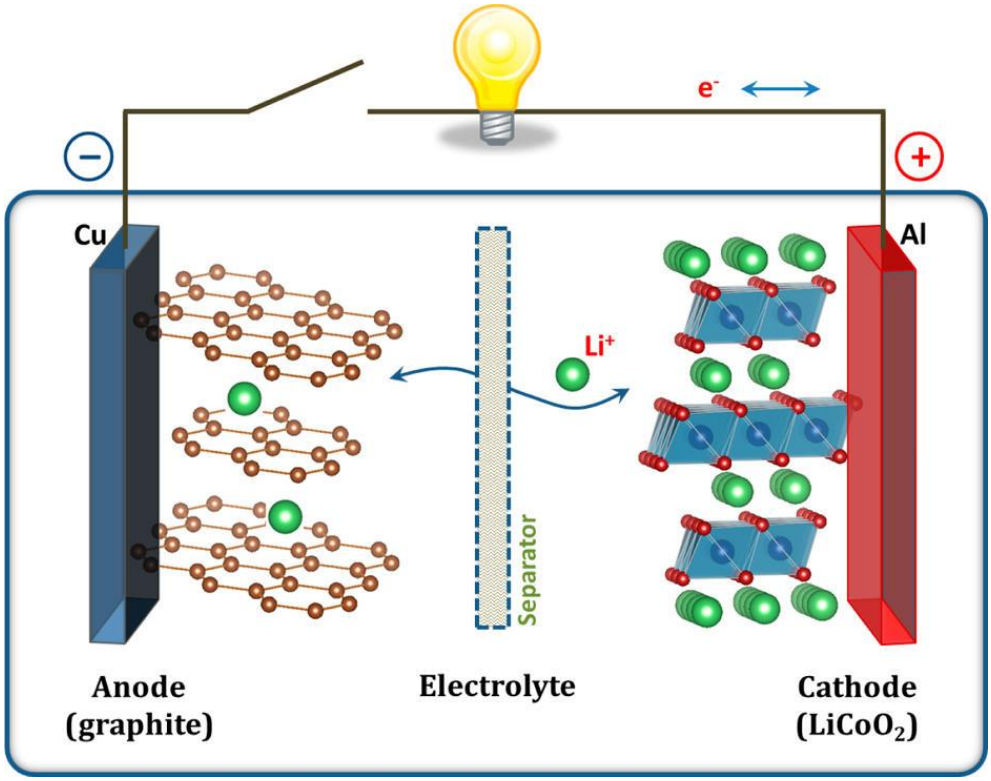


**Figure 1.6** Schematic representation of a lithium-ion cell. Reproduced with permission from [4].

During discharge, lithium-ions shuttle back spontaneously, and the electric current flow in the external circuit is used to produce work. The role of lithium-ions in this system is merely to balance the electric charge inside the electrodes. Lithium-ions never change their oxidation state during the whole cycle, and lithium metal deposition should not occur under normal operating conditions. In fact, LIBs owe their name to this. The reactions

occurring at the electrodes during charge and discharge are described by the following equation:

$$LiCoO_2 + C_6 \leftrightarrow Li_{1-x}CoO_2 + Li_xC_6$$

In the field of lithium ion batteries, positive and negative electrodes are also called cathode and anode, respectively, although by a more strict definition, this convention is only correct during discharge. Nevertheless, this thesis will conform to the convention and the terms “cathode” and “anode” will be used in place of “positive electrode” and “negative electrode”. Electrodes for LIBs are usually in the form of composites [3,12]. The redox-active material is the main component in weight of a standard electrode; a polymeric binder is also used in small quantity to guarantee adhesion between the active material particles and the current collector, along with a carbonaceous additive to ensure optimal electrical conduction. Composite electrodes are usually coated onto metallic current collectors: aluminum and copper for the positive and the negative electrodes, respectively.

During the first charge, irreversible reactions of the electrolyte with the graphite electrode lower the Coulombic efficiency; however, the subsequent cycles proceed with Coulombic efficiencies approaching 100 percent. This process, also called solid electrolyte interface (SEI) formation, is essential for batteries based on graphitic carbons [14]. During SEI formation, some of the electrolyte components decompose reductively at the surface of the negative electrodes, forming a protective film. When the graphite surface is covered, further electrolyte decomposition is kinetically

suppressed by the film. Additionally, the SEI layer effectively prevent graphite exfoliation caused by co-intercalation of lithium ions and solvent molecules (**Figure 1.7**). Ethylene carbonate was found to be the most efficient organic solvent for a stable SEI layer formation and, as a result, has become the essential component in all commercial electrolyte formulations.

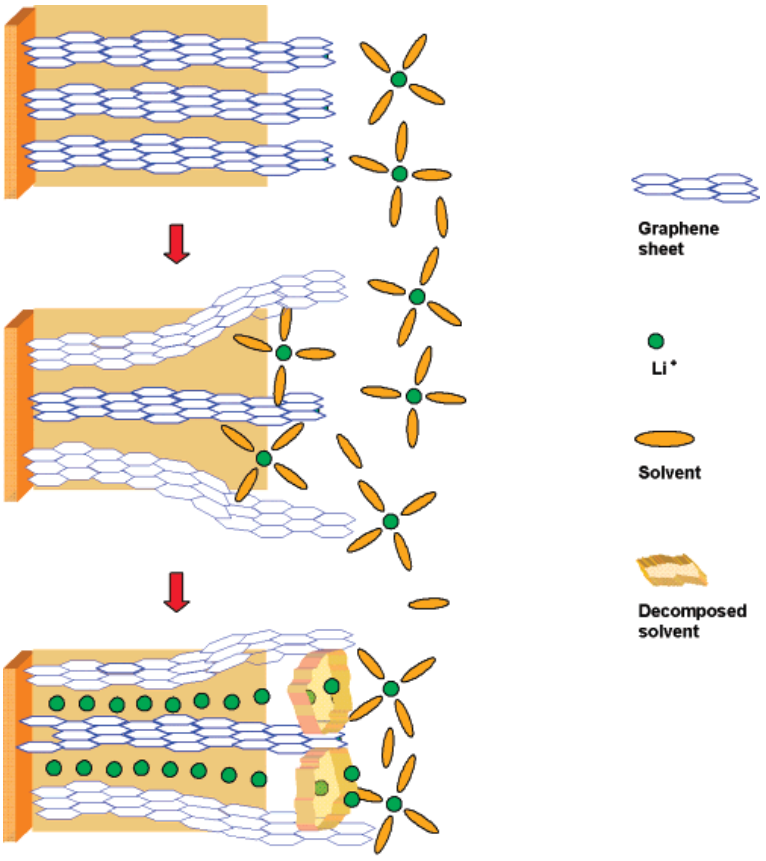


**Figure 1.7** Schematic illustration of the SEI formation mechanism. Reproduced with permission from [15].

Lithium-ion cells can be easily fabricated in different shapes, however the most common ones on the market are prismatic and cylindrical (**Figure 1.8**).

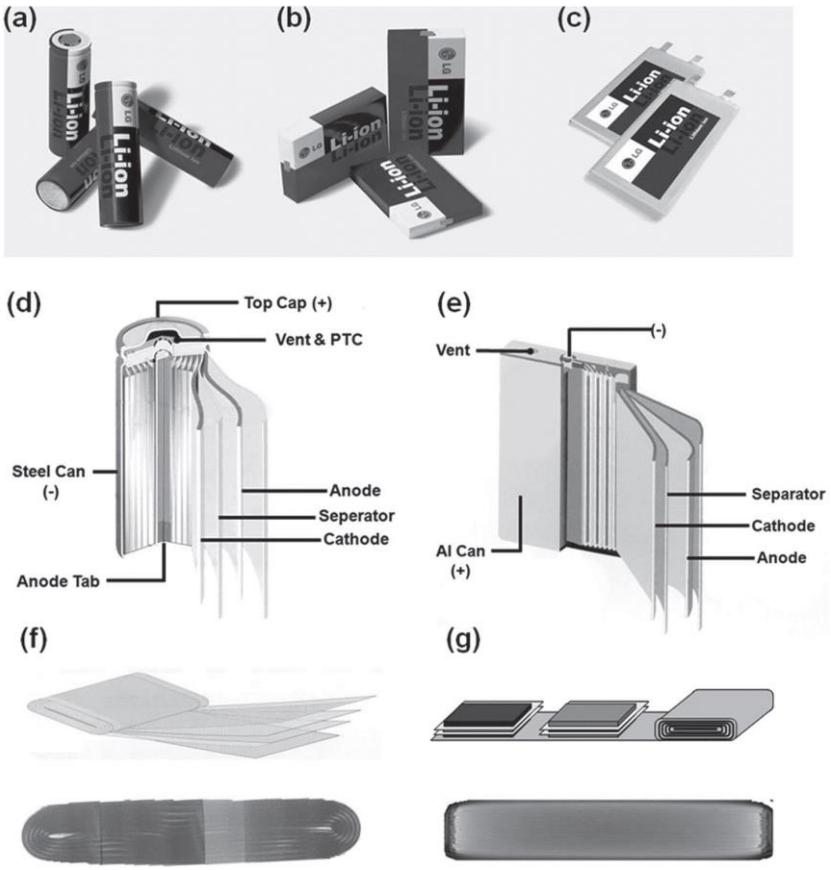


**Figure 1.8** Three different types of commercially available cells of lithium ion batteries: cylindrical (a, d), prismatic (b, e) and polymer (c, f, g) cells. The assembly of cathode, separator and anode is winded (f) or stacked (g) in a pouch of polymer type cells. Reproduced with permission from [2].

The assembly of electrodes inside a cell can be winded or stacked, thus allowing more than two layers to be packed inside a single cell. Prismatic and cylindrical cells are usually covered by a rigid case. When the packaging material is a thin polymeric film, cells are commercially known as polymeric although their shape is prismatic and all the other cell components are conventional. Prismatic and polymeric cells are preferred for application in portable electronics since the size of modern devices, such as cellphones and tablets, have evolved to be always thinner and lighter [2].

A number of cells, connected together in series or in parallel depending on the required battery output, form a battery pack. The nominal potential of a battery pack is determined by how the cell connections are made. The combination of multiple battery packs, together with electrical and mechanical components form a battery system. These systems are used for xEV and electrical energy storage applications. The function of the electrical components is to monitor the temperature inside the battery pack, the potential and current for each cell, to disconnect short circuited or malfunctioning cells in order to preserve the battery pack health-state and efficiency. All the information is collected and operated by the battery management system (BMS) that can also work as user interface (**Figure 1.9**).

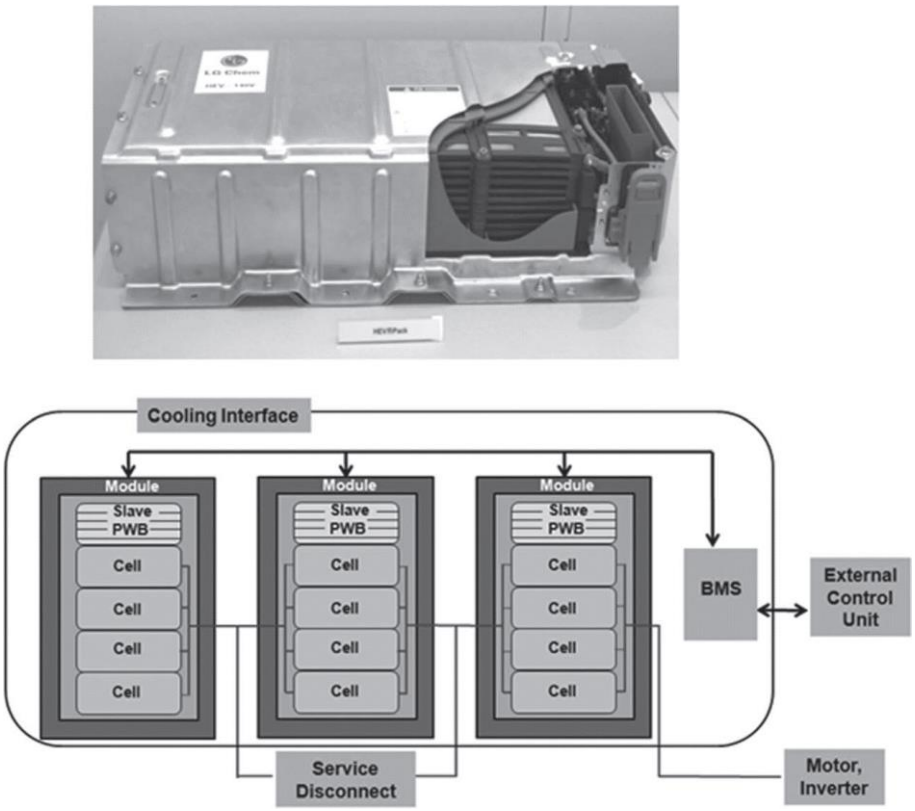


**Figure 1.9.** A battery pack for HEVs. Reproduced with permission from [2].

Early strategies to increment efficiency and performance of LIBs were mainly focused on the optimization of the battery design [2]. Despite such engineering efforts, electrode and electrolyte materials have not changed much in the years. At the present stage, design optimization is no longer sufficient to satisfy the requirement of the new performance demanding applications. Research of novel materials with enhanced performance is currently the most promising approach to enable advanced LIBs.

## 1.4 MATERIALS FOR LITHIUM-ION BATTERIES

A small review of the most promising materials developed for advanced LIBs will be given in the next section, with reference to state-of-the-art materials, for comparison purposes.

### 1.4.1 CATHODE MATERIALS

Cathode materials for LIBs are classified based on their crystalline structure [16]. Discharge potential profiles plots against specific capacity of different cathode materials are shown in **Figure 1.10** for a quick comparison. Key requirements to face and solve the challenges of the new high-performing applications can be summarized as follow:

(1) High energy density: both by increasing the specific capacity of both the electrode materials or/and the operating potential of the positive electrode material it is possible to increase the energy density of LIBs. Increasing the operating potential is sometime problematic as common electrolytes might decompose above 4.5 V vs. $Li^+/Li$.
(2) Structural stability: this is an essential parameter as it strongly affects the lifetime of the battery; a good electrode material should be able to perform more than 1000 cycles of reversible charge and discharge before disposal.
(3) Cost: primarily related to the abundancy of raw materials and secondly to the production process employed. To date, the high cost of LIBs is still making them less attractive for some kind of applications. For example,

the price per kg of a lead-acid battery can be ten times lower than that of a LIB.

(4) Lastly, the use of cheap, abundant, and environmental friendly materials is another key requirement for the next-gen LIBs. The choice of materials that can be recycled, at least partially, should be emphasized since an increased use of LIBs will also require increased efforts for an effective disposal at the end of life.

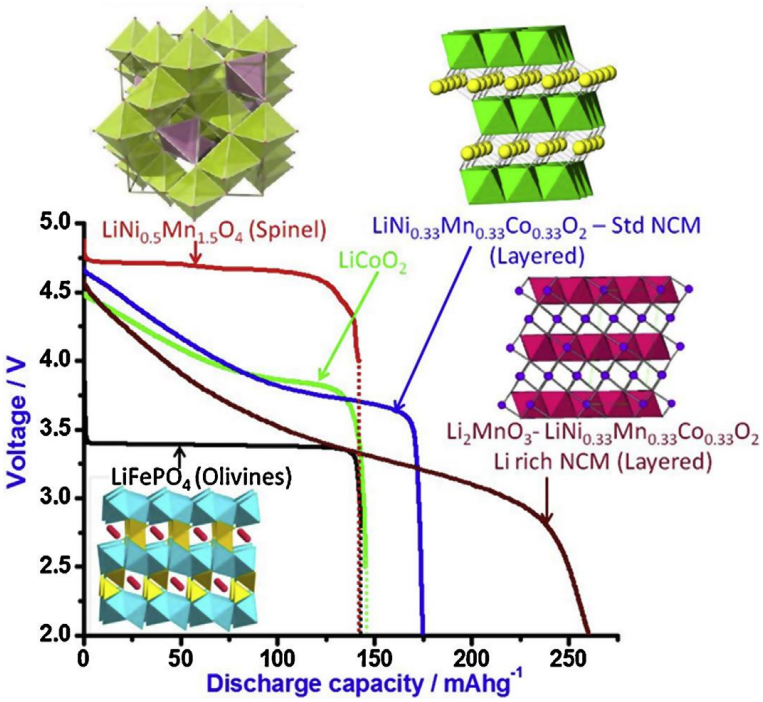


**Figure 1.10** Li-ion battery cathodes: important formulae, structures and voltage profiles during discharge. The potentials are versus Li reference electrodes. Reprinted with permission from [5].

#### 1.4.1.1 LAYERED OXIDE MATERIALS

Layered metal oxide materials are characterized by a rhombohedral structure with alternate layers of lithium ions and transition metal atoms. The relatively open structure of layered metal oxide materials allows for migration of lithium-ions through a two-dimensional pathway during the charge/discharge process. Lithium Cobalt Oxide ($LiCoO_2$) has been commonly used as cathode material since the introduction of LIBs on the market and, to date, continues to be the most employed material for portable electronic applications [17]. $LiCoO_2$ has a practical capacity of 130-150 mAh $g^{-1}$ and an average operating potential of 3.9 V *vs*. $Li/Li^+$. The major drawbacks of this material are related to cost and toxicity of Cobalt. Layered oxides based on Nickel ($LiNiO_2$) have been proposed as a possible replacement due to their relatively lower cost and increased capacity delivery. However, their tendency to form non-stoichiometric compounds with poor performance has strongly limited their use so far [18]. The usage of solid solutions of $LiCoO_2$ and $LiNiO_2$ were also discarded due to safety issues despite higher capacity delivery. Mixes oxides of Nickel, Manganese and Cobalt, $LiNi_{1/3}Mn_{1/3}Co_{1/3}O_2$, represent the only commercially available alternative to $LiCoO_2$ in the family of layered oxides. Their superior specific capacity (170 mAh $g^{-1}$) and operating potential (4.4 V *vs*. $Li^+/Li$) make these materials well suited for applications also in the transportation sector [19].

### 1.4.1.2 SPINEL OXIDE MATERIALS

Manganese spinel oxides ($LiMn_2O_4$) have the three main advantages of low cost due to natural abundancy, increased safety and superior environmental compatibility with respect to Nickel and Cobalt based materials; these characteristics make $LiMn_2O_4$ an ideal candidate for stationary energy storage despite the rather limited delivered capacity (120 mAh $g^{-1}$) with respect to layered materials [20]. Indeed, energy density is less crucial for large-scale applications, like energy storage plants, where the size of batteries is not limited by the size of the device, like in mobile applications. However, the spinel structure shown to be damaged by Jahn-Teller distortions of Mn atoms during prolonged cycling and therefore make this material unsuited for practical applications [4]. Mixed Manganese and Nickel spinel oxides ($LiNi_xMn_{2-x}O_4$) with improved structural stability have been also developed [21] and although the capacity of these spinels remains low, the operating potential approaches 5 V *vs*. $Li^+/Li$. Higher operating potentials are obviously advantageous in terms of specific energy, but may also bring safety problems caused by oxidative degradation of the electrolyte.

### 1.4.1.3 PHOSPHO-OLIVINE MATERIALS

Among this family, lithium iron phosphate ($LiFePO_4$) is the most promising candidate for application in the transportation sector [22]. This material has a theoretical capacity of 170 mAh $g^{-1}$ and an average operating

potential of 3.4 V *vs*. Li/$Li^+$. Despite the relatively low energy density of this material, the main advantages of $LiFePO_4$ lie in its low cost, eco-friendliness and high structural stability thanks to the strong phosphate bonds that strongly reduce the structural degradation process [23]. The issues raising from the intrinsic low electronic conductivity of $LiFePO_4$ have been overcome by nano-sizing the particles of active material, by specifically coating the nanoparticles with conductive layers and by bulk doping with metal particles. $LiFePO_4$ is already being commercialized and used in industrial products by several companies. Cobalt and manganese-based olivine materials have been studied because of their higher operating potential, but lot of research efforts are still required before commercialization [16].

### 1.4.2 ANODE MATERIALS

The classification of anode materials for LIBs in not based on their structure, but on the energy storage mechanism (**Figure 1.11**). The operating potential of these materials lies above that of lithium reduction in order to avoid potentially harmful deposition of lithium metal. Therefore, enhancements in specific energy are usually achieved by increasing the specific capacity of anode materials. Indeed, active materials for negative electrodes usually display larger specific capacities than that of cathode materials.

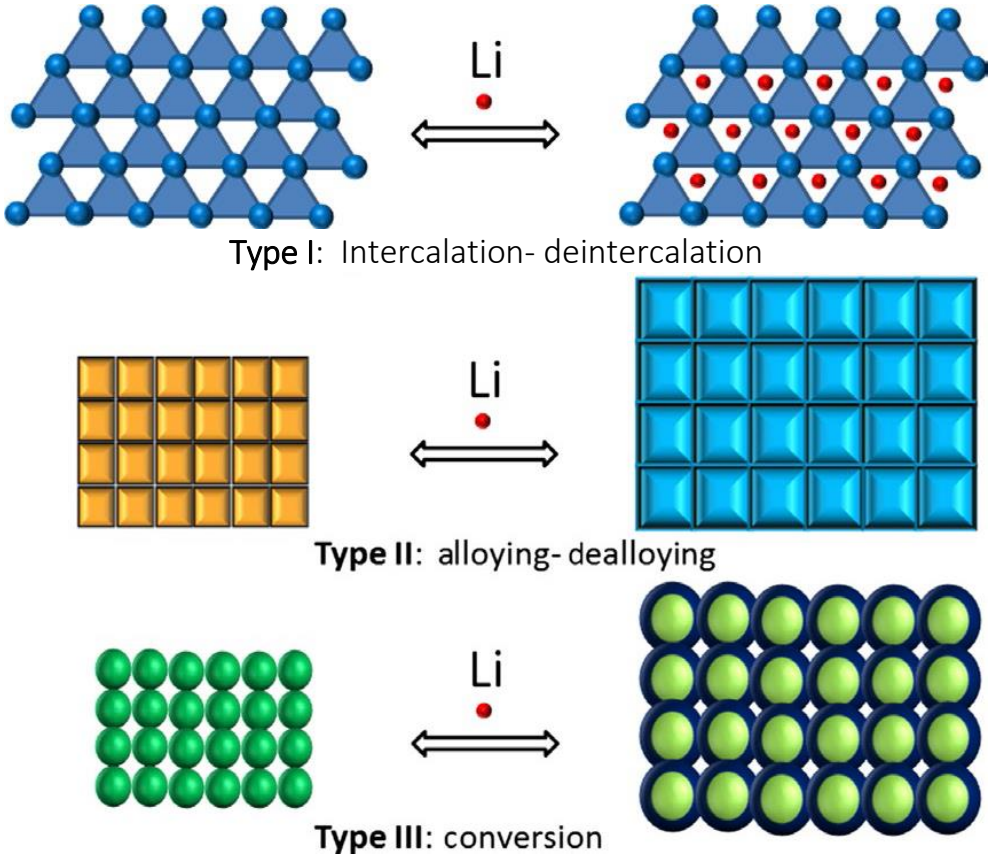


**Figure 1.11** Schematic of different mechanisms for reversible storage of lithium ions in anode materials. Adapted from [11].

### 1.4.2.1 INTERCALATION REACTION MATERIALS

Graphitic materials have been used as anodes since the early commercialization of LIBs and nowadays are still the most largely employed negative electrode materials in secondary lithium-ion batteries [24]. Natural

and artificial graphites are composed of layers of ordered carbon atoms. Lithium-ions are intercalated/de-intercalated in between the layers during charge and discharge, and their charge is stabilized by injection of electrons from the external circuit. The intercalation of lithium ions is a stepwise process that occurs between 0.5 V to less than 25 mV *vs*. $Li^+/Li$. The typical potential profiles of graphite are shown in **Figure 1.11 a**. As already discussed, the formation of a stable SEI layer is essential for safe operation of graphite-based electrodes, in absence of which decomposition of the electrolyte and eventually graphite exfoliation occurs [25,26] (**Figure 1.11 b**). After SEI layer formation, these materials usually deliver a practical specific capacity of 360 mAh $g^{-1}$ at low current regime.

The major drawback of graphitic electrodes comes from the risk of electrodeposition of metallic lithium onto the electrode surface during charge at high current rates or low temperatures [27]. This process, known as lithium dendrite growth, can lead to hazardous cell failure. In fact, growing dendrites can pierce the electrode separators and, upon contact with the positive cathode, internally short circuit the cell.

Another carbon-based material alternative to graphite is hard carbon (HC). The degree of graphitization is used to distinguish between these materials, being graphites the more ordered material, whereas HCs the less ordered ones [28,29]. HCs can accommodate more charge in spite of more abundant lithium-ion intercalation sites but on the other hand, they generally show a lower Coulombic efficiency during the initial cycle. HCs are good candidates for future applications in electric vehicles and stationary energy storage.

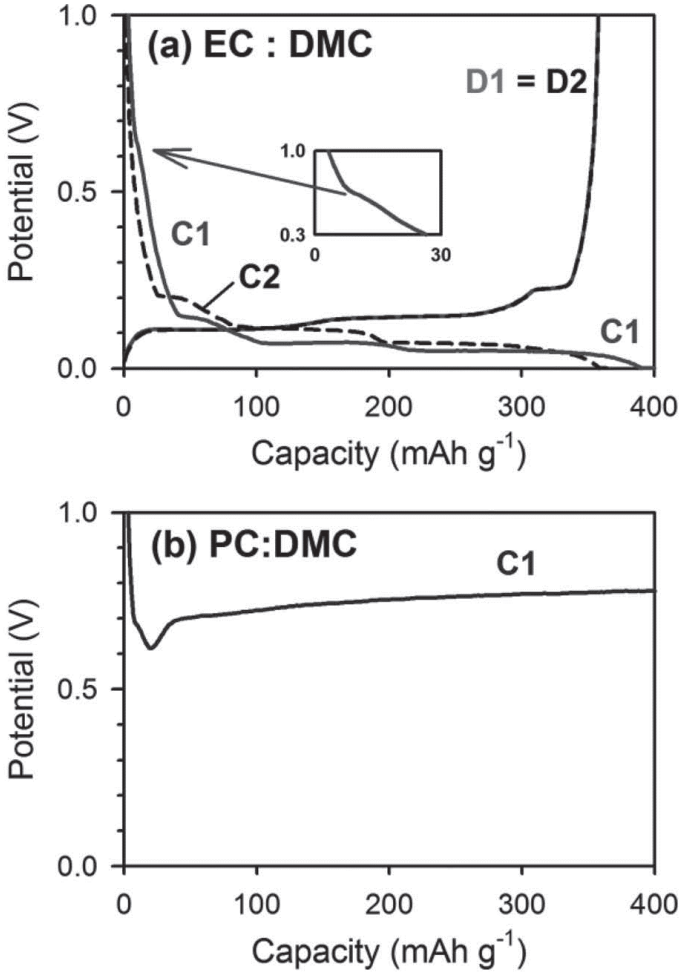


**Figure 1.11** Typical charge (lithiation) and discharge (delithiation) profiles of natural graphites with 1.15 M $LiPF_6$ in 3:7 X :dimethyl carbonate (DMC) as an electrolyte where X = ethylene carbonate (EC) for (**a**) or propylene carbonate (PC) for (**b**). The arrow in (**a**) indicates formation of the solid-electrolyte interface (SEI) layer caused by decomposition of EC. C = charge; D = discharge; number after C or D = cycle number. The profile of D2 is completely overlapped with that of D1. Reproduced with permission from [2].

The only non-carbon-based example in the family of intercalation materials is lithium titanate oxide ($Li_4Ti_5O_{12}$) [30]. Its high operating potential (1.5 V *vs*. $Li^+/Li$), which lies above the decomposition potential of common electrolytes, leads to very high efficiency during the first cycle since SEI layer formation does no occurs; in addition, the risk of dendritic growth is strongly reduced. This property combined with the very limited volume change upon lithium intercalation allows very fast rate of charge and discharge. On the other hand, the low specific capacity of $Li_4Ti_5O_{12}$ (175 mAh $g^{-1}$) is the main drawback of this anode material.

### 1.4.2.2 CONVERSION REACTION MATERIALS

Various transition metal oxides can work as anode materials via conversion reactions [31,32]. These materials possess very high specific capacity values with respect to graphite, in some cases approaching 1000 mAh $g^{-1}$, but suffer from very large volume changes that detrimentally effects their cycle life. Moreover, the generally high operating potential along with the low coulombic efficiencies make these materials unsuitable for practical applications at present.

### 1.4.2.3 ALLOYING REACTION MATERIALS

Metalloid elements such as silicon and germanium or metals like tin can alloy with lithium, thus resulting in high energy density anode materials [33].

The most attractive characteristics of alloy anodes are the extremely high specific capacity (up to 4000 mAh $g^{-1}$ for $Li_{4.4}Si$) and the low operating potential (0.4 V vs. $Li^+/Li$ for $Li_{4.4}Si$). However, large volume changes occur during reversible charge/discharge and lead to fragmentation of the composite electrodes. The advanced solutions for volume change issues are the reduction of particle size to nanometer scale and the introduction of buffer phase between the particles. These materials have great potential for all kind applications, from portable electronics to large-scale storage but a great deal of research is still required before their successful commercialization.

### 1.4.3 SEPARATORS

The main role of separators is to prevent the direct contact between electrodes in a cell, thus avoiding internal shortcuts. Standard separators for LIBs are porous materials that can incorporate sufficient amounts of liquid electrolyte to guarantee lithium-ion conductivity between the electrodes. For high energy and power density, separators must be thin to reduce internal cell resistance. At present, commercial separators for lithium-ion cells are nominally less than 50 μm in thickness. In addition, for longevity, chemical and electrochemical stability is required to prevent degradation and loss of mechanical properties. Good wettability in the electrolyte is obviously needed to reduce resistance to lithium-ion conductivity. Standard separators for LIBs are microporous polymeric materials based on polyolefin, such as polyethylene (PE), polypropylene (PP), or multi-layered

blends of such [34–36]. **Figure 1.12** shows the microporous structure of a commercially available separator for LIBs produced by Celgard®.

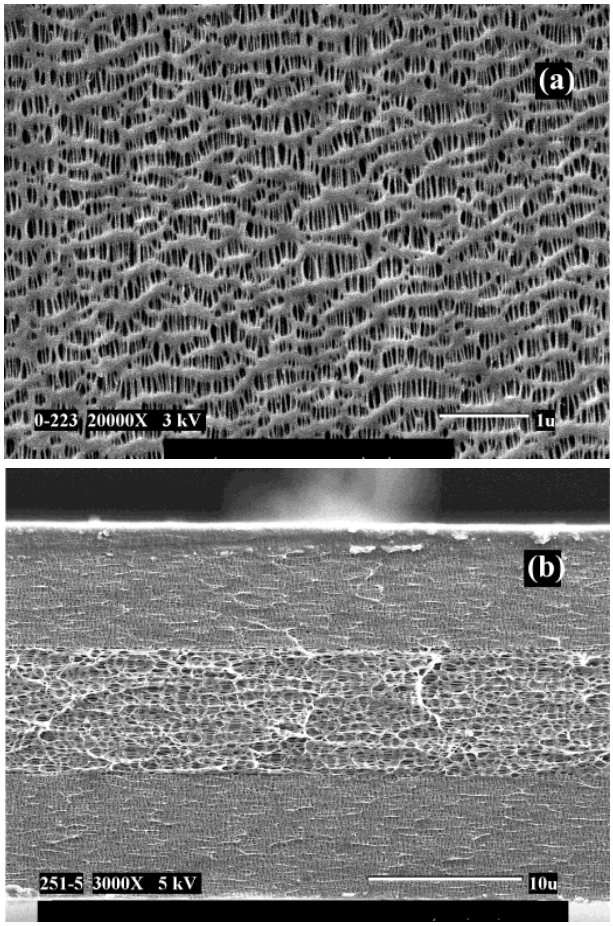


**Figure 1.12** Scanning electron micrographs of Celgard® 2325 (PP/PE/PP) separator used in lithium-ion batteries: (a) surface image and (b) cross-section image. Reproduced with permission from [34].

Polyolefin-based separators exhibit excellent chemical stability and mechanical properties, a thickness lower than 30 μm and an average pore size below 1 μm. When a LIB is accidentally overcharged or abused, heat is generated that can seriously affect safety and lead to hazardous consequences, i.e. decomposition of the liquid electrolyte and ignition of the gas produced. In case of "thermal runaway" of LIBs, polymeric separator can provide an internal margin of safety. In fact, separator pores collapse near the melting point of the polymeric material, thus drastically increasing the cell impedance, and interrupting battery operation by shutting down the external current flow. Commercially available trilayer PP/PE/PP separators (Celgard® 2320 and 2325) are good examples of shutdown materials. Additionally, in case of melting of the PE internal layer, the external PP layers continue to offer mechanical stability due to the difference between the melting temperature of PE and PP. The development of novel separator materials is closely connected with that of electrolyte materials and will be thoroughly discussed in the next paragraphs.

## 1.4.4. ELECTROLYTES

### 1.4.4.1 NON-AQUEOUS LIQUID ELECTROLYTES

Non-aqueous electrolytes for LIB applications are composed of lithium-ion salts dissolved in organic carbonates. The key properties of electrolyte solutions are high dielectric permittivity (to dissolve the salts), low viscosity (to facilitate lithium-ion transport), and good interfacial stability with both

the electrodes [15,37]. Ideally, the electrochemical stability window (ESW) of an electrolyte should be wider than the potential range defined by the working electrodes of the battery; otherwise, the electrolyte would undergo degradation via reduction and/or oxidation reactions. Since the absence of a single carbonate-based solvent capable to meet all the aforementioned requirements, mixtures of solvents of either high dielectric permittivity or low viscosity are commonly used. Standard electrolytes formulations for LIBs comprise ethylene carbonate (EC), due to its essential SEI forming ability and high dielectric permittivity, mixed with low viscosity linear carbonate esters, the most commonly used of which are dimethyl carbonate (DMC), diethyl carbonate (DEC), and ethylmethyl carbonate (EMC) [37]. **Table 1.1** summarize the most important physical-chemical properties of common organic carbonates. Ionic conductivities of such electrolytes may exceed $10^{-2}$ S $cm^{-1}$ at ambient temperature and support cell operation in the range of –30 to 60 °C. Above these temperatures, liquid electrolytes do not assure safe operation because of volatility of the organic components. Temperature limitations are a serious drawback for liquid electrolytes, in fact internal temperatures of large size battery packs can increase easily to 40-50 °C, even under normal operation conditions [2]. Hence, flammability of volatile components of the electrolyte can result in unwanted fires and explosions of LIBs. Electrochemical reaction with the electrodes are other causes of electrolyte degradation. Although ester carbonates are prone to reduction at low potential (< 0.5 V *vs*. $Li^+/Li$), this issue is avoided by the formation of the SEI layer that kinetically hinder sustained reductions.

**Table 1. Organic Carbonates and Esters as Electrolyte Solvents**

| Solvent name | Structural formula | Melting point (°C) | Boiling point (°C) | Viscosity (cP) | Dielectric constant, **ε** |
|---|---|---|---|---|---|
| Ethylene carbonate, EC | 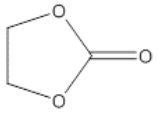 | 36 | 248 | 1.9 (at 40°C) | 98.6 (at 40°C) |
| Propylene carbonate, PC | 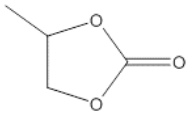 | -49 | 242 | 2.5 | 64.9 |
| Dimethyl carbonate, DMC | 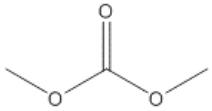 | 4.2 | 91 | 0.59 | 3.1 |
| Diethyl carbonate, DEC | 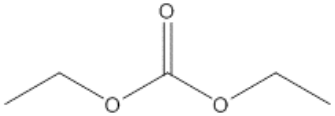 | -74.3 | 126 | 0.75 | 2.8 |
| Ethyl methyl carbonate, EMC | 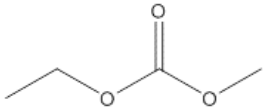 | -53 | 110 | 0.65 | 2.9 |

On the other hand, resistance to oxidation of carbonates is only satisfactory with conventional 4 V cathode materials. Most of the high voltage cathode materials, developed to increase energy density of the battery, operate at potential above the anodic stability limit of common organic carbonates. Thus, efforts are being made to replace, at least partially, these carbonate-based components to achieve improvements over the state-of-the-art [37].

### 1.4.4.2 ALTERNATIVE LIQUID SOLVENTS FOR LIBS

Alkyl sulfones have been investigated because of their high dielectric permittivity, low flammability and excellent anodic stability [38–41]. Nevertheless, sulfones are unsuitable for practical application in LIBs because of their inability to form protective SEI layers on graphitic anodes and their generally high viscosities. Sulfoxide-based solvents were also discarded for a number of reasons, mainly poor SEI forming properties combined with even lower anodic stability compared to alkyl sulfones [42].
Electrolytes based on acetonitrile (ACN) combine good dielectric permittivity and low viscosity, resulting in high ionic conductivities. On the other hand, the narrow electrochemical stability window of ACN strongly limits its application in LIBs field. In recent years, several other nitriles have been intensively studied in order to increase their stability limits, di-nitriles with short alkyl chains revealed increased thermal and electrochemical stability but their ability to form efficient SEI layers has yet to be proved [43–46]. Finally, phosphorus-based solvents have been proposed because of their

exceptional flame-retardant, but once again these solvents have been found to be unable to form protective SEI layer [47,48]. To date, alternative solvents capable to replace conventional organic carbonate have yet to be developed [15,37].

### 1.4.4.3 SALTS

The fundamental requirements of a salt for LIBs can be summarized as follows: it should not react with other cell components, it should be readily soluble in aprotic solvents, ions of the salt should be highly mobile, anions should be stable against oxidative as well as thermal decomposition [15,37]. Lithium hexafluorophosphate ($LiPF_6$) in 1M concentration is the most commonly employed salt in commercial electrolyte solutions. The success of $LiPF_6$ with respect to other lithium salts, such as $LiAsF_6$, $LiClO_4$ or $LiBF_4$, is due to the combination series of well-balanced properties rather than achievement of outstanding performance [15]. For example, in the commonly used solvent mixtures, it has lower ionic conductivity than $LiAsF_6$, lower thermal stability than most of the other salts, and lower anodic stability than $LiClO_4$. However, each one of the other proposed salts is affected by serious drawbacks that preclude its widespread application. $LiClO_4$ was found to strongly oxidize the other electrolyte components and to react violently with them at high temperature or under high current rates [49,50]. $LiAsF_6$ was discarded due to toxicity concerns [51]. $LiBF_4$ was initially considered due to its lower toxicity and higher safety with respect to other

candidates but the moderated ion conductivities achieved with $LiBF_4$ have been the major obstacle to its application [52].

Among novel lithium salts candidates (**Figure 1.13**), lithium bis(trifluoromethanesulfonyl)imide (LiTFSI), firstly reported in 1984, showed a high dissociation level owing to the strong electron withdrawing group ($SO_2CF_3$) and because its improved safety, thermal stability, and good conductivity, it has quickly attracted much attentions [53–55]. Despite of these advantages, the severe corrosion of aluminum current collectors caused by LiTFSI has made its application impossible in liquid electrolyte based LIBs so far. Similar issues with Al-corrosion were reported for the analogous lithium bis(pentafluoroethanesulfonyl)imide (LiBETI).

Finally, particular attention was paid to lithium bis(oxalato)borate (LiBOB), this salt is anodically stable up to 4.3 V vs. $Li^+/Li$, it can form a protective SEI layer on the surface of graphite and it was found to be fully compatible with Al current collector, however the ionic conductivity of LiBOB solutions in carbonate based solvents were found slightly lower than that of conventional salts and therefore its practical use is still debated [56–58].

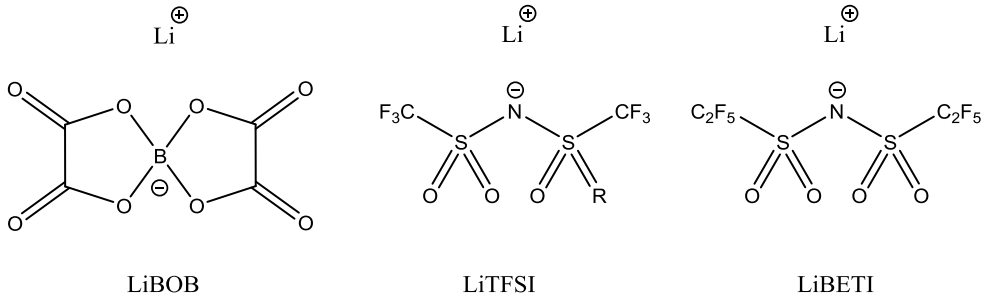


**Figure 1.13** Novel lithium salts structures

### 1.4.4.5 ROOM TEMPERATURE IONIC LIQUIDS

Room temperature ionic liquids (RTILs) are salts consisting of a bulky, asymmetric organic cation and an inorganic anion. Usually, their melting point is below or close to ambient temperature [37]. RTILs have several advantages over organic solvents: high chemical and thermally stability, non-flammability, negligible vapor pressure and, in some cases, high electrochemical stability and hydrophobicity. These properties make them attractive candidates for applications as electrolytes in lithium batteries.

Heterocyclic quaternary ammonium compounds, such as imidazolium, pyrrolidinium, and piperidinium, are the most popular cations. Anions are usually selected among conventional lithium salts negative counter-ions. Anions usually have a major role in determining not only the melting temperature, but also the electrochemical stability of the resulting RTILs. The most electrochemically stable anions ($PF_6^-$ and $BF_4^-$) always result in high temperature melting salts, while the more "plasticizing" $TFSI^-$ anion usually reacts at high potentials (e.g., corrosion toward aluminum current collector or simply electrochemical oxidation). Recent reviews cover extensively the last literature findings related to RTILs as electrolytes for LIBs [37,59] (**Figure 1.14**)

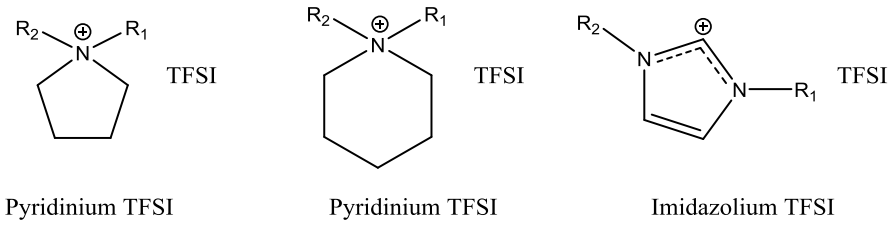


**Figure 1.14** Novel room-temperature ionic liquids structures

## 1.5 POLYMER ELECTROLYTES

To date, safety issues of conventional liquid electrolytes based on organic carbonates are probably the major drawback of LIBs. For example, the operating temperature range of LIBs is strongly limited by the volatility of organic carbonates. The internal temperature of large-size battery packs can exceed 50 °C and, consequently, thermal stability of the electrolyte is a critical parameter to take in account. In addition, the flammability of liquid solvents has led to accidents of flaming and explosions of batteries in the past. Finally, liquid carbonates are not fully compatible with high energy density electrodes, such as high voltage cathodes, since their instability at high potentials. As the majority of new applications for LIBs requires even stricter safety margin, the replacement of liquid carbonates with safer counterparts is essential for the development of next-gen LIBs. Polymer electrolytes have been proposed as an alternative to liquid electrolytes [60]. Since the discovery of ionic conductivity of alkali metal ions in poly(ethylene oxide) [61], the interest of the scientific community has grown around this

new class of materials. Their promising advantages over conventional liquid electrolytes include intrinsic thermal and electrochemical stability, non-flammability and non-toxicity. Finally, these electrolytes systems have the potential to be multifunctional, as materials showing sufficient mechanical strength can also play the role of electrodes separators in addition to ion conductive media. A large number of polymer electrolyte systems have been proposed based on polyethylene oxide, polypropylene oxide, polyacrylonitrile, polymethylmethacrylate, polyvinylchloride, polyvinylidenefluoride, polysiloxane and polyphosphazene. Along with the above-mentioned homopolymers, other microstructures have been investigated like statistical, block or grafted copolymers. In addition, different macromolecular architectures such as linear, comb-like, branched, networked and functionalized polymers were proposed as potential candidates. Extensive reviews on this topic can be found in several literature reports [62–67]. Because of the large number of examples, it is convenient to group polymer electrolytes in two main categories:

(1) Solid polymer electrolytes (SPEs)
(2) Gel polymer electrolytes (GPEs)

The former category includes mixtures of lithium salts in high-molecular-weight polymers. In these systems, a Lewis base contained in the polymer host is responsible for lithium-ion solvation [66]. Generally, SPEs can be produced in thin films with good mechanical properties. The latter category of polymer electrolytes is obtained by the incorporation of large amounts of conventional liquid electrolytes into a polymer matrix. In this case, the solvation is mainly owed to the solvent and the polymer may not participate

at all in solvating the ions. GPEs are characterized by higher ionic conductivities at ambient temperature, but reduced mechanical robustness.

### 1.5.1 SOLID POLYMER ELECTROLYTES

Ionic conductivity of alkali metal ions, such as lithium-ion, in poly(ethylene oxide) (PEO) was firstly demonstrated by Fenton *et al* [61]. Four decades after this discovery, the majority of research works performed on SPEs still focus on this system and its structural variation. PEO is a polyether compound with a chemical structure of H-(O-$CH_2$-$CH_2$)$_n$-OH. Depending on the molecular weight, this polymer is also known as poly(ethylene glycol) (PEG). Normally, PEO is the polymer with a molecular weight above 35000 g $mol^{-1}$, whereas PEG refers to oligomers of ethylene oxide with a molecular weight below 35000 g $mol^{-1}$. A number of pioneering scientific works were devoted to the study of the lithium transport mechanism in PEO-based systems. According to these studies, lithium ions are complexed by partial negative charges on the oxygen atoms belonging to the repeating unit. Then, PEO chains can wrap around lithium-ions, thus forming stable multi-nuclear coordination complexes [68], whereas the anions also reside in near proximity of the ion-polymer complex (**Figure 1.15**). The lithium-ion conductivity mechanism in PEO is associated with segmental motion of the polymer chain, along with hopping of lithium ions between the coordination sites.

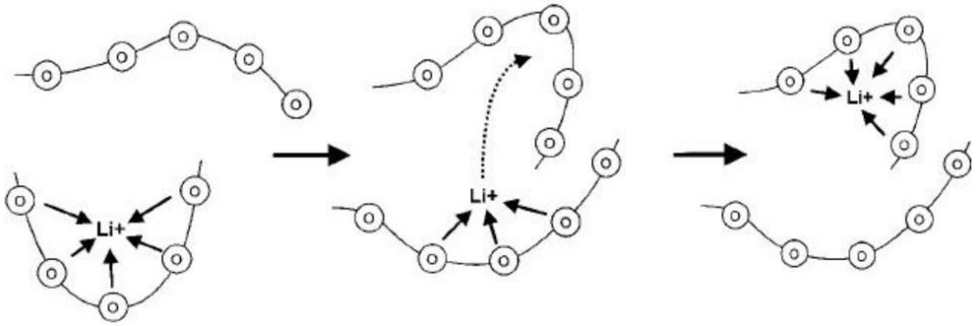


**Figure 1.15** Schematic representation of the coordination site of lithium ions in PEO and its ion conducting mechanism. Reproduced with permission from [62]

Therefore, ion conductivity in PEO cannot occur below the glass transition temperature of the polymer. Moreover, it is generally accepted that fast ion conduction can exclusively occur in the amorphous phase of the polymer, the crystalline domains being almost ionic insulating. Since PEO is a semi-crystalline material, strategies for increasing its ionic conductivity have been mainly focused on breaking the crystallinity of the polymer. Another drawback of PEO is the loss of dimensional stability above the melting temperature of its crystalline phase, which is around 60 °C.

The use of lithium salts with large anions like BOB [69], imidazole [70] and TFSI [71] was reported to suppress effectively the crystallinity and increase the ionic conductivity; unfortunately, it significantly increases the glass transition temperature of PEO, reducing the mobility of EO segments [72].

Interesting results were obtained by introducing ceramic fillers, thus forming composite SPEs. Inorganic fillers such as $Al_2O_3$ [73], $SiO_2$ [74], MgO [75] showed to hinder the crystalline phase formation by specific

interactions of the surface groups of the ceramic particles with the polymer chain. To date, these electrolytes showed ionic conductivity values that range between $10^{-5}$ and $10^{-4}$ S $cm^{-1}$ at temperatures between 40 and 100 °C, thus excluding ambient temperature application. In the high temperature range, the ionic conductivity strongly increases, thus admitting practical application. Metal organic frameworks (MOFs) as filler also provide hybrid properties and enhance the ionic conductivity and interfacial properties of solid polymer electrolytes [76].

Along with inorganic filler, the use of bio-derived filler was also investigated. The main advantage deriving with these materials is their low cost and environmental compatibility. Cellulose nanocrystals [77], chitin [78], and cyclodextrins [79] have been used as the reinforcing phase in PEO matrices.

Another simple way to improve the percentage of amorphous phase in PEO is to blend it with other polymers. The blending method may serve to improve ionic conductivities and dimensional stability of polymer electrolytes. Moreover, preparation of blends is generally an easily up-scalable process, particularly suitable for practical application. Several examples are present in literature including blends of PEO with poly(methacrylic acid), poly[bis-(methoxyethoxyethoxide)phosphazene], poly(2-vinylpyridine), poly(vinylidene fluoride), polyethylenimine, poly(oligo-(oxyethylene)oxyterephthaloyl, poly(dimethyl siloxane), and networked cellulose [80–83].

Block copolymers have been proposed as solid-state electrolytes, in which two or more different structural units are combined to achieve the

two antagonistic properties of high mechanical strength and satisfactory ionic conductivity [84,85]. Although the oligoether linkages of PEO are difficult to replace in order to achieve good ionic conductivity, a wide range of options is available among high $T_g$ polymers to guarantee structural integrity. Wang et al. [86] used pedant ethylene-oxide units attached to a polystyrene (PS) backbone that was later combined with styrene units to form an ion-conducting block copolymer. This solution led to micro-phase separation, in which the EO-rich phase formed a conductive pathway for lithium-ions. A similar approach was demonstrated by Niitani et al. [87], in which a methyl methacrylate backbone was used to attach the pendant ethylene-oxide units. Although in both cases room temperature ionic conductivity did not exceed $10^{-4}$ S $cm^{-1}$, mechanically robust copolymers were obtained with the ability to hinder effectively lithium dendrite growth. Other examples of block copolymer electrolytes include the use of poly(butyl methacrylate) [88], poly(lauryl methacrylate) [89], poly(n-hexadecyl methacrylate) [90], poly(benzyl methacrylate) [91], and poly(methacrylic acid) [92].

Another approach to induce phase separation between the PEO rich-phase and the structural phase was to graft long side-chains of poly(dimethyl siloxane) to the polymer backbone [93], interesting ionic conductivity values were obtained, but at the cost of mechanical properties, thus almost completely vanish the advantages of the block architecture.

With the aim of dismantling the crystalline structure of PEO, the grafting strategy has also been employed to attached PEG chains to a series of organic and inorganic polymers, such as poly(methacrylic acid) [72],

polyphosphazenes [94–97], polysiloxane [98–100] and boron-containing macromolecules [101,102].

Hyperbranched polymers have received much attention due to their unique macromolecular structures. Compared to linear polymers, hyperbranched systems can hinder the crystallization of polymer chain more easily, which leads to enlargement of the amorphous phase. Therefore, PEO-based hyperbranched polymers were employed as hosts for polymer electrolytes. Lee el al. [103] investigated a series of hyperbranched PEO polymers based on glycerol that showed a 100-fold increase in the ionic conductivity below 50 °C compared to linear PEO. Niitani et al. [104] synthesized a hyperbranched copolymer based on polystyrene and poly(oligoethylene oxide)methacrylate via controlled polymerization techniques, and blend it with different lithium salts (LiBETI, LiTFSI, $LiClO_4$, $LiPF_6$, and $LiBF_4$). The SPE containing LiBETI exhibited high ionic conductivities of $10^{-4}$ S $cm^{-1}$ at 30 °C.

### 1.5.2 GEL POLYMER ELECTROLYTES

Despite almost three decades of investigation, PEO-based solid polymer electrolytes with practical application at ambient are still an unachieved challenge. Hence, research efforts have been focused on gel polymer electrolytes [63]. Attempts have been made to improve the ionic conductivity of PEO by adding low molecular weight plasticizer and conventional aprotic solvents. PEO-based polymer matrixes can be swollen in conventional electrolytes, and due to the good soaking properties of PEO,

adsorb high weight percent of the electrolyte. As previously mentioned, in such systems, salt solvation is mainly carried out by the solvent molecules and the polymer matrix may not participate at all in solvating the salt. In addition, the transport mechanism in GPEs is generally owed to the conventional liquid electrolyte rather than to the interaction with the polymer backbone. The polymer matrix serves mainly to provide dimensional integrity, and the ether linkage is no longer the sole choice of building block for its chemical structure. A number of alternative polymers have been proposed and tested, such as polyacrylonitrile, polymethylmethacrylate, polyvinylchloride, polyvinylidenefluoride and polysiloxanes [63]. Generally, the concomitant consequence of the low polymer content in GPEs is the poorer mechanical strength as compared with pure SPEs, and either chemical or physical cross-linking is frequently necessary for the dimensional stability of such gel materials.

Poly(acrylonitrile) (PAN) based electrolytes offer a homogenous, hybrid electrolyte film in which the salt and the plasticizer are molecularly dispersed. Watanabe et al. [105] used a combination of plasticizers EC and PC to plasticize PAN and complexed with $LiClO_4$. They concluded that the PAN host is inactive in the ionic transport mechanism but acts as a matrix for structural stability. PAN-based gels were found to have lithium ion transference numbers exceeding 0.5 because of the absence of oxygen atoms in the PAN matrix [106]. PAN based electrolytes were prepared by encapsulating Li-salt solutions obtained by dissolving $LiN(CF_3SO_2)_2$, $LiAsF_6$, $LiCF_3SO_3$ and $LiPF_6$ in a plasticizer mixture of EC and PC [107]. Cyclic voltammetry studies revealed that the electrolytes have an inherent

oxidation stability window exceeding 5 V vs $Li^+/Li$. These electrolytes exhibited high ionic conductivity and high lithium transference number. However, their application in rechargeable lithium polymer batteries is hindered and is attributed to the instability at the lithium metal electrode interface. It has been found that Li ions strongly interact with the C≡N groups of PAN [108]. At a concentration as low as 5% of $Li^+$ ions, because of the high intensity of the characteristic vibration of the C≡N group of PAN, it is very difficult to observe the interaction between ions and molecules. Despite several advantages of PAN-based electrolytes, like high ionic conductivity of the order of $10^{-3}$ S $cm^{-1}$ at 20 °C, wide electrochemical stability of 4.5 V and Li-transference number around 0.6, their poor compatibility with Li metal anode offsets from practical applications. Other studies clearly revealed that the Li electrode undergoes serious passivation when in contact with PAN-based electrolytes, affects cyclability and eventually leads to safety hazards [109].

In 1985, Iijima and Toyoguchi found that poly(methyl methacrylate) (PMMA) could be used as a gelling agent [63]. Later, Appetecchi et al. [110] focused their attention on MMA gel electrolytes with different plasticizers. Authors concluded that the electrochemical stability window depends on the polymer host and lithium salt complexes. Although better scalability has been obtained with PMMA when compared to PAN, voltammetric results and efficiency tests revealed that a consistent fraction of lithium is lost upon cycling and, thus, a large excess of lithium would be required eventually to assure an acceptable life to the battery. The rheological and electrochemical properties of PMMA-$LiClO_4$/PC membrane were obtained by Bohnke et al.

[111]. In low concentrations of PMMA, the gelatinized electrolyte was considered as a liquid electrolyte caged in a polymer matrix. The addition of PMMA in various proportions increased the viscosity of the macromolecular solution. On the contrary, the conductivity was considerably reduced upon PMMA addition. However, the room temperature conductivity remained unvaried, viz. close to the conductivity of liquid electrolytes. DSC data established the thermal stability of these membranes between 110 and 240 °C. A model that emphasized the importance of PC and/or PMMA-lithium solvation effect of ion-pairing and the cross linking action of cations at high PMMA concentration has also been reported [112]. The 20 wt % of PMMA gels was considered as a liquid electrolyte encaged in an inert polymer matrix. On the other hand, a very strong interaction between the polymeric chains and the ionic species was observed when the concentration of PMMA was increased to 45 wt % the gel. The DSC, NMR, electrical conductivity studies have been made by Stallworth et al. [113] for gel electrolytes synthesized from PMMA, EC, PC and various lithium salts ($LiClO_4$, $LiAsF_6$, $LiN(CF_3SO_2)_2$). DSC analysis revealed that gel electrolytes exhibit single glass transition temperature. These results are in accordance with those reported for PAN electrolytes [114]. Vondrak et al. [115] prepared PMMA gel electrolytes with PC as plasticizer and complexed with salts of various perchlorates of different cation sizes including lithium. The gel electrolyte, which possesses lithium as cation exhibited maximum conductivity and was attributed to its smaller ionic radii. Even though it has many favorable merits, the poor mechanical strength of plasticized PMMA offsets these electrolytes from practical applications.

Sukeshini et al. [116] complexed poly(vinyl chloride) (PVC) with lithium bis(trimethyl sulfonyl) imide (LiTFSI) and plasticized with dibutyl phthalate (DBP) and dioctyl adipate (DOA). The ionic conductivity of the membranes was increased considerably when the content of PVC was decreased. The electrochemical stability domains close to 4.0 V at 60 °C, established by cyclic voltammetry using Ni-ultra microelectrodes, was limited in the cathodic side by Li deposition and stripping processes and in the anodic side by the oxidation of the polymer. The efficiency of the lithium stripping followed by the deposition was found to be poor and was attributed to the reaction of dibutyl phthalate or dioctyl adipate with Li. Membranes based on PVC showed ionic conductivity in the order of $10^{-3}$ S $cm^{-1}$ at ambient conditions. However, the compatibility towards the lithium metal anode was not satisfactory enough for any direct application in practical lithium battery.

By virtue of its attractive properties, poly(vinylidene fluoride) - PVDF has been chosen as a polymer host for lithium battery applications. PVdF based polymer electrolytes poses high anodic stability due to the presence of strong electron-withdrawing functional groups (–C–F) and the polymer itself has a dielectric constant (ε = 8.4) that helps for greater dissolution of lithium salts and, subsequently, supports high concentration of charge carriers. Tsuchida et al. [117] examined the plasticized PVdF gel electrolytes and they found that viscosity plays a major role in influencing the conductivity rather than the dielectric constant of the plasticizer. A novel polymer electrolyte comprising of PVdF-EC-PC and a lithium salt ($LiCF_3SO_3$, $LiPF_6$ or $LiN(SO_2CF_3)_2$) was prepared by thermal extrusion method [118]. The mechanical strength of the polymer electrolyte film varied widely and depended on the PVdF

content. The viscosity of the medium and the concentration of charge carriers, which are directly related to the weight ratio of PVdF-EC-PC and the kind of Li salt studied, mainly influenced the conductivity of the electrolyte. Although, PVdF-based electrolytes offer excellent electrochemical properties, this fluorinated polymer is not stable when in contact with lithium metal, leading to poor interfacial properties between lithium and fluorine.

The compatibility study of Li metal anode with PVdF-EC-PC-imide polymer electrolyte revealed that these electrolytes may have good shelf life at room temperature. In addition, the cyclic voltammetry studies suggested that PVdF electrolytes are more suitable for primary than secondary batteries when Li metal is employed as anode [118]. A rechargeable all-plastic battery was fabricated with PVdF-PC-$LiClO_4$ membrane as electrolyte using a poly acetylene film as an active electrode material. This battery system has been found to be feasible as small power source in low current electronic devices. However, problems associated with the rather limited ionic conductivity of polymer electrolytes, the degradation of battery performance and adhesion between the acetylene films and polymer electrolyte are to be rectified [119].

## REFERENCES

[1] J.-M. Tarascon, M. Armand, Issues and challenges facing rechargeable lithium batteries, Nature. 414 (2001) 359–367. doi:10.1038/35104644.

[2] T.-H. Kim, J.-S. Park, S.K. Chang, S. Choi, J.H. Ryu, H.-K. Song, The Current Move of Lithium Ion Batteries Towards the Next Phase, Adv. Energy Mater. 2 (2012) 860–872. doi:10.1002/aenm.201200028.

[3] A. Yoshino, The Birth of the Lithium-Ion Battery, Angew. Chem. Int. Ed. 51 (2012) 5798–5800. doi:10.1002/anie.201105006.

[4] J.B. Goodenough, K.-S. Park, The Li-Ion Rechargeable Battery: A Perspective, J. Am. Chem. Soc. 135 (2013) 1167–1176. doi:10.1021/ja3091438.

[5] H.D. Yoo, E. Markevich, G. Salitra, D. Sharon, D. Aurbach, On the challenge of developing advanced technologies for electrochemical energy storage and conversion, Mater. Today. 17 (2014) 110–121. doi:10.1016/j.mattod.2014.02.014.

[6] G.L. Soloveichik, Battery Technologies for Large-Scale Stationary Energy Storage, Annu. Rev. Chem. Biomol. Eng. 2 (2011) 503–527. doi:10.1146/annurev-chembioeng-061010-114116.

[7] http://www.bp.com/content/dam/bp/pdf/energy-economics/statistical-review-2015/bp-statistical-review-of-world-energy-2015-full-report.pdf, accessed february 2016, (n.d.).

[8] https://www.ipcc.ch/pdf/assessment-report/ar5/syr/SYR_AR5_FINAL_full_wcover.pdf, accessed february 2016, (n.d.).

[9] O. Morton, Solar energy: A new day dawning?: Silicon Valley sunrise, Nature. 443 (2006) 19–22. doi:10.1038/443019a.

[10] M. Lei, L. Shiyan, J. Chuanwen, L. Hongling, Z. Yan, A review on the forecasting of wind speed and generated power, Renew. Sustain. Energy Rev. 13 (2009) 915–920. doi:10.1016/j.rser.2008.02.002.

[11] D. Deng, Li-ion batteries: basics, progress, and challenges, Energy Sci. Eng. 3 (2015) 385–418. doi:10.1002/ese3.95.

[12] B. Scrosati, History of lithium batteries, J. Solid State Electrochem. 15 (2011) 1623–1630. doi:10.1007/s10008-011-1386-8.

[13] L. Jabbour, R. Bongiovanni, D. Chaussy, C. Gerbaldi, D. Beneventi, Cellulose-based Li-ion batteries: a review, Cellulose. 20 (2013) 1523–1545. doi:10.1007/s10570-013-9973-8.

[14] R. Fong, U. von Sacken, J.R. Dahn, Studies of Lithium Intercalation into Carbons Using Nonaqueous Electrochemical Cells, J. Electrochem. Soc. 137 (1990) 2009–2013. doi:10.1149/1.2086855.

[15] K. Xu, Nonaqueous Liquid Electrolytes for Lithium-Based Rechargeable Batteries, Chem. Rev. 104 (2004) 4303–4418. doi:10.1021/cr030203g.

[16] M.S. Whittingham, Lithium Batteries and Cathode Materials, Chem. Rev. 104 (2004) 4271–4302. doi:10.1021/cr020731c.

[17] K. Mizushima, P.C. Jones, P.J. Wiseman, J.B. Goodenough, LixCoO2 (0<x<-1): A new cathode material for batteries of high energy density, Mater. Res. Bull. 15 (1980) 783–789. doi:10.1016/0025-5408(80)90012-4.

[18] J.R. Dahn, U. von Sacken, C.A. Michal, Structure and electrochemistry of Li1±yNiO2 and a new Li2NiO2 phase with the Ni (OH)2 structure, Solid State Ion. 44 (1990) 87–97. doi:10.1016/0167-2738(90)90049-W.

[19] J.W. Fergus, Recent developments in cathode materials for lithium ion batteries, J. Power Sources. 195 (2010) 939–954. doi:10.1016/j.jpowsour.2009.08.089.

[20] M.M. Thackeray, W.I.F. David, P.G. Bruce, J.B. Goodenough, Lithium insertion into manganese spinels, Mater. Res. Bull. 18 (1983) 461–472. doi:10.1016/0025-5408(83)90138-1.

[21] E. Rossen, C.D.W. Jones, J.R. Dahn, Structure and electrochemistry of LixMnyNi1−yO2, Solid State Ion. 57 (1992) 311–318. doi:10.1016/0167-2738(92)90164-K.

[22] W.-J. Zhang, Structure and performance of LiFePO4 cathode materials: A review, J. Power Sources. 196 (2011) 2962–2970. doi:10.1016/j.jpowsour.2010.11.113.

[23] A. Yamada, S.C. Chung, K. Hinokuma, Optimized LiFePO4 for Lithium Battery Cathodes, J. Electrochem. Soc. 148 (2001) A224–A229. doi:10.1149/1.1348257.

[24] J.O. Besenhard, M. Winter, J. Yang, W. Biberacher, Filming mechanism of lithium-carbon anodes in organic and inorganic electrolytes, J. Power Sources. 54 (1995) 228–231. doi:10.1016/0378-7753(94)02073-C.

[25] A.N. Dey, B.P. Sullivan, The Electrochemical Decomposition of Propylene Carbonate on Graphite, J. Electrochem. Soc. 117 (1970) 222–224. doi:10.1149/1.2407470.

[26] H.F. Xiang, C.H. Chen, J. Zhang, K. Amine, Temperature effect on the graphite exfoliation in propylene carbonate based electrolytes, J. Power Sources. 195 (2010) 604–609. doi:10.1016/j.jpowsour.2009.07.036.

[27] M. Winter, J.O. Besenhard, Lithiated Carbons, in: -Ing Claus Daniel, J.O. Besenhard (Eds.), Handb. Battery Mater., Wiley-VCH Verlag GmbH & Co. KGaA, 2011: pp. 433–478. http://onlinelibrary.wiley.com/doi/10.1002/9783527637188.ch15/summary (accessed February 17, 2016).

[28] K. Sato, M. Noguchi, A. Demachi, N. Oki, M. Endo, A Mechanism of Lithium Storage in Disordered Carbons, Science. 264 (1994) 556–558. doi:10.1126/science.264.5158.556.

[29] J.R. Dahn, T. Zheng, Y. Liu, J.S. Xue, Mechanisms for Lithium Insertion in Carbonaceous Materials, Science. 270 (1995) 590–593. doi:10.1126/science.270.5236.590.

[30] K. Zaghib, M. Simoneau, M. Armand, M. Gauthier, Electrochemical study of Li4Ti5O12 as negative electrode for Li-ion polymer rechargeable batteries, J. Power Sources. 81–82 (1999) 300–305. doi:10.1016/S0378-7753(99)00209-8.

[31] J. Cabana, L. Monconduit, D. Larcher, M.R. Palacín, Beyond intercalation-based Li-ion batteries: the state of the art and challenges of electrode materials reacting through conversion reactions, Adv. Mater. Deerfield Beach Fla. 22 (2010) E170–192. doi:10.1002/adma.201000717.

[32] Y.F. Zhukovskii, E.A. Kotomin, P. Balaya, J. Maier, Enhanced interfacial lithium storage in nanocomposites of transition metals with LiF and Li2O: Comparison of DFT calculations and experimental studies, Solid State Sci. 10 (2008) 491–495. doi:10.1016/j.solidstatesciences.2007.12.030.

[33] C.-M. Park, J.-H. Kim, H. Kim, H.-J. Sohn, Li-alloy based anode materials for Li secondary batteries, Chem. Soc. Rev. 39 (2010) 3115–3141. doi:10.1039/B919877F.

[34] P. Arora, Z.J. Zhang, Battery separators, Chem. Rev. 104 (2004) 4419–4462.

[35] R. Spotnitz, Separators for Lithium-Ion Batteries, in: -Ing Claus Daniel, J.O. Besenhard (Eds.), Handb. Battery Mater., Wiley-VCH Verlag GmbH & Co. KGaA, 2011: pp. 693–717. http://onlinelibrary.wiley.com/doi/10.1002/9783527637188.ch20/summary (accessed February 17, 2016).

[36] S.S. Zhang, A review on the separators of liquid electrolyte Li-ion batteries, J. Power Sources. 164 (2007) 351–364. doi:10.1016/j.jpowsour.2006.10.065.

[37] K. Xu, Electrolytes and Interphases in Li-Ion Batteries and Beyond, Chem. Rev. 114 (2014) 11503–11618. doi:10.1021/cr500003w.

[38] S.-Y. Lee, K. Ueno, C.A. Angell, Lithium Salt Solutions in Mixed Sulfone and Sulfone-Carbonate Solvents: A Walden Plot Analysis of the Maximally Conductive Compositions, J. Phys. Chem. C. 116 (2012) 23915–23920. doi:10.1021/jp3067519.

[39] L. Xue, K. Ueno, S.-Y. Lee, C.A. Angell, Enhanced performance of sulfone-based electrolytes at lithium ion battery electrodes, including the LiNi0.5Mn1.5O4 high voltage cathode, J. Power Sources. 262 (2014) 123–128. doi:10.1016/j.jpowsour.2014.03.099.

[40] X.-G. Sun, C. Austen Angell, New sulfone electrolytes: Part II. Cyclo alkyl group containing sulfones, Solid State Ion. 175 (2004) 257–260. doi:10.1016/j.ssi.2003.11.035.

[41] X.-G. Sun, C.A. Angell, New sulfone electrolytes for rechargeable lithium batteries.: Part I. Oligoether-containing sulfones, Electrochem. Commun. 7 (2005) 261–266. doi:10.1016/j.elecom.2005.01.010.

[42] Y. Yamada, Y. Takazawa, K. Miyazaki, T. Abe, Electrochemical Lithium Intercalation into Graphite in Dimethyl Sulfoxide-Based Electrolytes: Effect of Solvation Structure of Lithium Ion, J. Phys. Chem. C. 114 (2010) 11680–11685. doi:10.1021/jp1037427.

[43] H. Duncan, N. Salem, Y. Abu-Lebdeh, Electrolyte Formulations Based on Dinitrile Solvents for High Voltage Li-Ion Batteries, J. Electrochem. Soc. 160 (2013) A838–A848. doi:10.1149/2.088306jes.

[44] Y. Abu-Lebdeh, I. Davidson, High-Voltage Electrolytes Based on Adiponitrile for Li-Ion Batteries, J. Electrochem. Soc. 156 (2009) A60–A65. doi:10.1149/1.3023084.

[45] A.J. Gmitter, I. Plitz, G.G. Amatucci, High Concentration Dinitrile, 3-Alkoxypropionitrile, and Linear Carbonate Electrolytes Enabled by Vinylene and Monofluoroethylene Carbonate Additives, J. Electrochem. Soc. 159 (2012) A370–A379. doi:10.1149/2.016204jes.

[46] Q. Wang, S.M. Zakeeruddin, I. Exnar, M. Grätzel, 3-Methoxypropionitrile-Based Novel Electrolytes for High-Power Li-Ion Batteries with Nanocrystalline Li4Ti5 O 12 Anode, J. Electrochem. Soc. 151 (2004) A1598–A1603. doi:10.1149/1.1789372.

[47] S. Dalavi, M. Xu, B. Ravdel, L. Zhou, B.L. Lucht, Nonflammable Electrolytes for Lithium-Ion Batteries Containing Dimethyl Methylphosphonate, J. Electrochem. Soc. 157 (2010) A1113–A1120. doi:10.1149/1.3473828.

[48] Z. Jin, L. Wu, Z. Song, K. Yan, H. Zhan, Z. Li, A New Class of Phosphates as Co-Solvents for Nonflammable Lithium Ion Batteries Electrolytes, ECS Electrochem. Lett. 1 (2012) A55–A58. doi:10.1149/2.007203eel.

[49] G.H. Newman, R.W. Francis, L.H. Gaines, B.M.L. Rao, Hazard Investigations of LiClO4 / Dioxolane Electrolyte, J. Electrochem. Soc. 127 (1980) 2025–2027. doi:10.1149/1.2130056.

[50] R. Jasinski, S. Carroll, Thermal Stability of a Propylene Carbonate Electrolyte, J. Electrochem. Soc. 117 (1970) 218–219. doi:10.1149/1.2407468.

[51] K.M. Abraham, J.L. Goldman, D.L. Natwig, Characterization of Ether Electrolytes for Rechargeable Lithium Cells, J. Electrochem. Soc. 129 (1982) 2404–2409. doi:10.1149/1.2123556.

[52] M. Ue, Mobility and Ionic Association of Lithium and Quaternary Ammonium Salts in Propylene Carbonate and γ-Butyrolactone, J. Electrochem. Soc. 141 (1994) 3336–3342. doi:10.1149/1.2059336.

[53] L.J. Krause, W. Lamanna, J. Summerfield, M. Engle, G. Korba, R. Loch, et al., Corrosion of aluminum at high voltages in non-aqueous electrolytes containing perfluoroalkylsulfonyl imides; new lithium salts for lithium-ion cells, J. Power Sources. 68 (1997) 320–325. doi:10.1016/S0378-7753(97)02517-2.

[54] J. Foropoulos, D.D. DesMarteau, Synthesis, properties, and reactions of bis((trifluoromethyl)sulfonyl) imide, (CF3SO2)2NH, Inorg. Chem. 23 (1984) 3720–3723. doi:10.1021/ic00191a011.

[55] L.A. Dominey, V.R. Koch, T.J. Blakley, Thermally stable lithium salts for polymer electrolytes, Electrochimica Acta. 37 (1992) 1551–1554. doi:10.1016/0013-4686(92)80109-Y.

[56] K. Xu, S. Zhang, T.R. Jow, Formation of the Graphite/Electrolyte Interface by Lithium Bis(oxalato)borate, Electrochem. Solid-State Lett. 6 (2003) A117–A120. doi:10.1149/1.1568173.

[57] K. Xu, S. Zhang, B.A. Poese, T.R. Jow, Lithium Bis(oxalato)borate Stabilizes Graphite Anode in Propylene Carbonate, Electrochem. Solid-State Lett. 5 (2002) A259–A262. doi:10.1149/1.1510322.

[58] K. Xu, S. Zhang, T.R. Jow, W. Xu, C.A. Angell, LiBOB as Salt for Lithium-Ion Batteries:A Possible Solution for High Temperature Operation, Electrochem. Solid-State Lett. 5 (2002) A26–A29. doi:10.1149/1.1426042.

[59] I. Osada, H. de Vries, B. Scrosati, S. Passerini, Ionic-Liquid-Based Polymer Electrolytes for Battery Applications, Angew. Chem. Int. Ed. 55 (2016) 500–513. doi:10.1002/anie.201504971.

[60] M. Armand, The history of polymer electrolytes, Solid State Ion. 69 (1994) 309–319. doi:10.1016/0167-2738(94)90419-7.

[61] D.E. Fenton, J.M. Parker, P.V. Wright, Complexes of alkali metal ions with poly(ethylene oxide), Polymer. 14 (1973) 589. doi:10.1016/0032-3861(73)90146-8.

[62] W.H. Meyer, Polymer electrolytes for lithium-ion batteries, Adv. Mater. Deerfield Beach Fla. 10 (1998) 439–448. doi:10.1002/(SICI)1521-4095(199804)10:6<439::AID-ADMA439>3.0.CO;2-I.

[63] J.Y. Song, Y.Y. Wang, C.C. Wan, Review of gel-type polymer electrolytes for lithium-ion batteries, J. Power Sources. 77 (1999) 183–197. doi:10.1016/S0378-7753(98)00193-1.

[64] E. Quartarone, P. Mustarelli, Electrolytes for solid-state lithium rechargeable batteries: recent advances and perspectives, Chem. Soc. Rev. 40 (2011) 2525–2540. doi:10.1039/C0CS00081G.

[65] D.T.H. Jr, N.P. Balsara, Polymer Electrolytes, Annu. Rev. Mater. Res. 43 (2013) 503–525. doi:10.1146/annurev-matsci-071312-121705.

[66] D. Golodnitsky, E. Strauss, E. Peled, S. Greenbaum, Review—On Order and Disorder in Polymer Electrolytes, J. Electrochem. Soc. 162 (2015) A2551–A2566. doi:10.1149/2.0161514jes.

[67] A.S. Shaplov, R. Marcilla, D. Mecerreyes, Recent Advances in Innovative Polymer Electrolytes based on Poly(ionic liquid)s, Electrochimica Acta. 175 (2015) 18–34. doi:10.1016/j.electacta.2015.03.038.

[68] P.G. Bruce, Ion–polyether coordination complexes: crystalline ionic conductors for clean energy storage, Dalton Trans. (2006) 1365–1369. doi:10.1039/B517247K.

[69] G.B. Appetecchi, D. Zane, B. Scrosati, PEO-Based Electrolyte Membranes Based on LiBC4 O 8 Salt, J. Electrochem. Soc. 151 (2004) A1369–A1374. doi:10.1149/1.1774488.

[70] L. Niedzicki, M. Kasprzyk, K. Kuziak, G.Z. Żukowska, M. Armand, M. Bukowska, et al., Modern generation of polymer electrolytes based on lithium conductive imidazole salts, J. Power Sources. 192 (2009) 612–617. doi:10.1016/j.jpowsour.2009.03.050.

[71] N.P. Young, D. Devaux, R. Khurana, G.W. Coates, N.P. Balsara, Investigating polypropylene-poly(ethylene oxide)-polypropylene triblock copolymers as solid polymer electrolytes for lithium batteries, Solid State Ion. 263 (2014) 87–94. doi:10.1016/j.ssi.2014.05.012.

[72] Z. Xue, D. He, X. Xie, Poly(ethylene oxide)-based electrolytes for lithium-ion batteries, J. Mater. Chem. A. 3 (2015) 19218–19253. doi:10.1039/C5TA03471J.

[73] W. Krawiec, L.G. Scanlon Jr., J.P. Fellner, R.A. Vaia, S. Vasudevan, E.P. Giannelis, Polymer nanocomposites: a new strategy for synthesizing solid electrolytes for rechargeable lithium batteries, J. Power Sources. 54 (1995) 310–315. doi:10.1016/0378-7753(94)02090-P.

[74] M. Wetjen, M.A. Navarra, S. Panero, S. Passerini, B. Scrosati, J. Hassoun, Composite Poly(ethylene oxide) Electrolytes Plasticized by N-Alkyl-N-butylpyrrolidinium Bis(trifluoromethanesulfonyl)imide for Lithium Batteries, ChemSusChem. 6 (2013) 1037–1043. doi:10.1002/cssc.201300105.

[75] B. Kumar, S.J. Rodrigues, L.G. Scanlon, Ionic Conductivity of Polymer-Ceramic Composites, J. Electrochem. Soc. 148 (2001) A1191–A1195. doi:10.1149/1.1403729.

[76] C. Yuan, J. Li, P. Han, Y. Lai, Z. Zhang, J. Liu, Enhanced electrochemical performance of poly(ethylene oxide) based composite polymer electrolyte by incorporation of nano-sized metal-organic framework, J. Power Sources. 240 (2013) 653–658. doi:10.1016/j.jpowsour.2013.05.030.

[77] M.A.S. Azizi Samir, F. Alloin, J.-Y. Sanchez, A. Dufresne, Cellulose nanocrystals reinforced poly(oxyethylene), Polymer. 45 (2004) 4149–4157. doi:10.1016/j.polymer.2004.03.094.

[78] N. Angulakhsmi, S. Thomas, J.R. Nair, R. Bongiovanni, C. Gerbaldi, A.M. Stephan, Cycling profile of innovative nanochitin-incorporated poly (ethylene oxide) based electrolytes for lithium batteries, J. Power Sources. 228 (2013) 294–299. doi:10.1016/j.jpowsour.2012.11.007.

[79] L.-Y. Yang, D.-X. Wei, M. Xu, Y.-F. Yao, Q. Chen, Transferring Lithium Ions in Nanochannels: A PEO/Li+ Solid Polymer Electrolyte Design, Angew. Chem. Int. Ed. 53 (2014) 3631–3635. doi:10.1002/anie.201307423.

[80] S. Wang, K. Min, Solid polymer electrolytes of blends of polyurethane and polyether modified polysiloxane and their ionic conductivity, Polymer. 51 (2010) 2621–2628. doi:10.1016/j.polymer.2010.04.038.

[81] C.H. Park, Y.-K. Sun, D.-W. Kim, Blended polymer electrolytes based on poly(lithium 4-styrene sulfonate) for the rechargeable lithium polymer batteries, Electrochimica Acta. 50 (2004) 375–378. doi:10.1016/j.electacta.2004.01.110.

[82] T. Aoki, A. Konno, T. Fujinami, Lithium ion conductivity of blend polymer electrolytes based on borate polymers containing fluoroalkane dicarboxylate and poly(ethylene oxide), Electrochimica Acta. 50 (2004) 301–304. doi:10.1016/j.electacta.2003.12.067.

[83] Z. Wen, T. Itoh, Y. Ichikawa, M. Kubo, O. Yamamoto, Blend-based polymer electrolytes of poly(ethylene oxide) and hyperbranched poly[bis(triethylene glycol)benzoate] with terminal acetyl groups, Solid State Ion. 134 (2000) 281–289. doi:10.1016/S0167-2738(00)00707-4.

[84] M. Singh, O. Odusanya, G.M. Wilmes, H.B. Eitouni, E.D. Gomez, A.J. Patel, et al., Effect of Molecular Weight on the Mechanical and Electrical Properties of Block Copolymer Electrolytes, Macromolecules. 40 (2007) 4578–4585. doi:10.1021/ma0629541.

[85] A. Panday, S. Mullin, E.D. Gomez, N. Wanakule, V.L. Chen, A. Hexemer, et al., Effect of Molecular Weight and Salt Concentration on Conductivity of Block Copolymer Electrolytes, Macromolecules. 42 (2009) 4632–4637. doi:10.1021/ma900451e.

[86] C. Wang, T. Sakai, O. Watanabe, K. Hirahara, T. Nakanishi, All Solid-State Lithium-Polymer Battery Using a Self-Cross-Linking Polymer Electrolyte, J. Electrochem. Soc. 150 (2003) A1166–A1170. doi:10.1149/1.1593652.

[87] T. Niitani, M. Shimada, K. Kawamura, K. Dokko, Y.-H. Rho, K. Kanamura, Synthesis of Li + Ion Conductive PEO-PSt Block Copolymer Electrolyte with Microphase Separation Structure, Electrochem. Solid-State Lett. 8 (2005) A385–A388. doi:10.1149/1.1940491.

[88] P.E. Trapa, B. Huang, Y.-Y. Won, D.R. Sadoway, A.M. Mayes, Block Copolymer Electrolytes Synthesized by Atom Transfer Radical Polymerization for Solid-State, Thin-Film Lithium Batteries, Electrochem. Solid-State Lett. 5 (2002) A85–A88. doi:10.1149/1.1461996.

[89] P.P. Soo, B. Huang, Y.-I. Jang, Y.-M. Chiang, D.R. Sadoway, A.M. Mayes, Rubbery Block Copolymer Electrolytes for Solid-State Rechargeable Lithium Batteries, J. Electrochem. Soc. 146 (1999) 32–37. doi:10.1149/1.1391560.

[90] P. Gavelin, R. Ljungbäck, P. Jannasch, B. Wesslen, Amphiphilic solid polymer electrolytes, Solid State Ion. 147 (2002) 325–332. doi:10.1016/S0167-2738(02)00020-6.

[91] P. Isken, M. Winter, S. Passerini, A. Lex-Balducci, Methacrylate based gel polymer electrolyte for lithium-ion batteries, J. Power Sources. 225 (2013) 157–162. doi:10.1016/j.jpowsour.2012.09.098.

[92] N. Yuca, H. Zhao, X. Song, M.F. Dogdu, W. Yuan, Y. Fu, et al., A Systematic Investigation of Polymer Binder Flexibility on the Electrode Performance of Lithium-Ion Batteries, ACS Appl. Mater. Interfaces. 6 (2014) 17111–17118. doi:10.1021/am504736y.

[93] P.E. Trapa, Y.-Y. Won, S.C. Mui, E.A. Olivetti, B. Huang, D.R. Sadoway, et al., Rubbery Graft Copolymer Electrolytes for Solid-State, Thin-Film Lithium Batteries, J. Electrochem. Soc. 152 (2005) A1–A5. doi:10.1149/1.1824032.

[94] S.-T. Fei, H.R. Allcock, Methoxyethoxyethoxyphosphazenes as ionic conductive fire retardant additives for lithium battery systems, J. Power Sources. 195 (2010) 2082–2088. doi:10.1016/j.jpowsour.2009.09.043.

[95] D.K. Lee, H.R. Allcock, The effects of cations and anions on the ionic conductivity of poly[bis(2-(2-methoxyethoxy)ethoxy)phosphazene] doped with lithium and magnesium salts of trifluoromethanesulfonate and bis(trifluoromethanesulfonyl)imidate, Solid State Ion. 181 (2010) 1721–1726. doi:10.1016/j.ssi.2010.09.051.

[96] G. Nazri, D.M. MacArthur, J.F. Ogara, Polyphosphazene electrolytes for lithium batteries, Chem. Mater. 1 (1989) 370–374. doi:10.1021/cm00003a019.

[97] P.M. Blonsky, D.F. Shriver, P. Austin, H.R. Allcock, Complex formation and ionic conductivity of polyphosphazene solid electrolytes, Solid State Ion. 18 (1986) 258–264. doi:10.1016/0167-2738(86)90123-2.

[98] L.J. Lyons, B.A. Southworth, D. Stam, C.-H. Yuan, R. West, Polymer electrolytes based on polysilane comb polymers, Solid State Ion. 91 (1996) 169–173. doi:10.1016/S0167-2738(96)83016-5.

[99] D. Fish, I.M. Khan, J. Smid, Conductivity of solid complexes of lithium perchlorate with poly{[ω-methoxyhexa(oxyethylene)ethoxy]methylsiloxane}, Makromol. Chem. Rapid Commun. 7 (1986) 115–120. doi:10.1002/marc.1986.030070303.

[100] D. Fish, I.M. Khan, E. Wu, J. Smid, Polymer electrolyte complexes of LiClO4 and comb polymers of siloxane with oligo-oxyethylene side chains, Br. Polym. J. 20 (1988) 281–288. doi:10.1002/pi.4980200320.

[101] M.A. Mehta, T. Fujinami, Li<SUP>+</SUP> Transference Number Enhancement in Polymer Electrolytes by Incorporation of Anion Trapping Boroxine Rings into the Polymer Host, Chem. Lett. 26 (1997) 915–916. doi:10.1246/cl.1997.915.

[102] Y. Aihara, J. Kuratomi, T. Bando, T. Iguchi, H. Yoshida, T. Ono, et al., Investigation on solvent-free solid polymer electrolytes for advanced lithium batteries and their performance, J. Power Sources. 114 (2003) 96–104. doi:10.1016/S0378-7753(02)00529-3.

[103] S.-I. Lee, M. Schömer, H. Peng, K.A. Page, D. Wilms, H. Frey, et al., Correlations between Ion Conductivity and Polymer Dynamics in Hyperbranched Poly(ethylene oxide) Electrolytes for Lithium-Ion Batteries, Chem. Mater. 23 (2011) 2685–2688. doi:10.1021/cm103696g.

[104] T. Niitani, M. Amaike, H. Nakano, K. Dokko, K. Kanamura, Star-Shaped Polymer Electrolyte with Microphase Separation Structure for All-Solid-State

Lithium Batteries, J. Electrochem. Soc. 156 (2009) A577–A583. doi:10.1149/1.3129245.

[105] M. Watanabe, M. Kanba, K. Nagaoka, I. Shinohara, Ionic conductivity of hybrid films based on polyacrylonitrile and their battery application, J. Appl. Polym. Sci. 27 (1982) 4191–4198. doi:10.1002/app.1982.070271110.

[106] G.B. Appetecchi, B. Scrosati, A lithium ion polymer battery, Electrochimica Acta. 43 (1998) 1105–1107. doi:10.1016/S0013-4686(97)10117-7.

[107] H.S. Choe, B.G. Carroll, D.M. Pasquariello, K.M. Abraham, Characterization of Some Polyacrylonitrile-Based Electrolytes, Chem. Mater. 9 (1997) 369–379. doi:10.1021/cm9604120.

[108] Z. Wang, B. Huang, H. Huang, R. Xue, L. Chen, F. Wang, A Vibrational Spectroscopic Study on the Interaction Between Lithium Salt and Ethylene Carbonate Plasticizer for PAN-Based Electrolytes, J. Electrochem. Soc. 143 (1996) 1510–1514. doi:10.1149/1.1836671.

[109] B. Scrosati, Lithium Rocking Chair Batteries: An Old Concept?, J. Electrochem. Soc. 139 (1992) 2776–2781. doi:10.1149/1.2068978.

[110] G.B. Appetecchi, F. Croce, B. Scrosati, Kinetics and stability of the lithium electrode in poly(methylmethacrylate)-based gel electrolytes, Electrochimica Acta. 40 (1995) 991–997. doi:10.1016/0013-4686(94)00345-2.

[111] O. Bohnke, C. Rousselot, P.A. Gillet, C. Truche, Gel Electrolyte for Solid-State Electrochromic Cell, J. Electrochem. Soc. 139 (1992) 1862–1865. doi:10.1149/1.2069512.

[112] O. Bohnke, G. Frand, M. Rezrazi, C. Rousselot, C. Truche, Fast ion transport in new lithium electrolytes gelled with PMMA. 2. Influence of lithium salt concentration, Solid State Ion. 66 (1993) 105–112. doi:10.1016/0167-2738(93)90033-Y.

[113] P.E. Stallworth, S.G. Greenbaum, F. Croce, S. Slane, M. Salomon, Lithium-7 NMR and ionic conductivity studies of gel electrolytes based on

poly(methylmethacrylate), Electrochimica Acta. 40 (1995) 2137–2141. doi:10.1016/0013-4686(95)00153-6.

[114] F. Croce, S.D. Brown, S.G. Greenbaum, S.M. Slane, M. Salomon, Lithium-7 NMR and ionic conductivity studies of gel electrolytes based on polyacrylonitrile, Chem. Mater. 5 (1993) 1268–1272. doi:10.1021/cm00033a014.

[115] J. Vondrák, M. Sedlaříková, J. Velická, B. Klápště, V. Novák, J. Reiter, Gel polymer electrolytes based on PMMA, Electrochimica Acta. 46 (2001) 2047–2048. doi:10.1016/S0013-4686(01)00413-3.

[116] A. Mary Sukeshini, A. Nishimoto, M. Watanabe, Transport and electrochemical characterization of plasticized poly(vinyl chloride) solid electrolytes, Solid State Ion. 86–88, Part 1 (1996) 385–393. doi:10.1016/0167-2738(96)00156-7.

[117] E. Tsuchida, H. Ohno, K. Tsunemi, Conduction of lithium ions in polyvinylidene fluoride and its derivatives—I, Electrochimica Acta. 28 (1983) 591–595. doi:10.1016/0013-4686(83)85049-X.

[118] Z. Jiang, B. Carroll, K.M. Abraham, Studies of some poly(vinylidene fluoride) electrolytes, Electrochimica Acta. 42 (1997) 2667–2677. doi:10.1016/S0013-4686(97)00005-4.

[119] T. Nagatomo, C. Ichikawa, O. Omoto, All-Plastic Batteries with Polyacetylene Electrodes, J. Electrochem. Soc. 134 (1987) 305–308. doi:10.1149/1.2100451.

# CHAPTER TWO

## *Multipurpose polymer electrolyte encompassing room temperature ionic liquids*

### 2.1. INTRODUCTION

The discovery of ionic conductivity of alkali metal ions in poly(ethylene oxide) (PEO) by Fenton *et al* [1] started an intensive branch of research on this material as a promising solid polymer electrolyte. However, at ambient temperature the ionic conductivity of lithium salt complexes in PEO is limited due to the semi-crystalline nature of PEO. Crystalline regions in PEO are not readily available for ion transport, and ion conduction is therefore limited to the amorphous phase. Several attempts have been made to improve the ionic conductivity of PEO, including the introduction of inorganic fillers [2], the use of specifically designed counter-ions [3], the chemical functionalization of its polymeric chains [4], the design of interpenetrating cross-linked networks [5], etc.

In recent years, room-temperature ionic liquids (RTILs) have been intensively investigated [6,7] due to their excellent properties such as non-volatility, non-flammability, and ionic conductivity up to 1 mS $cm^{-1}$. These properties make ionic liquids very attractive for application electrolytes in lithium batteries.

Recently, the combination of high molecular weight PEO, lithium bis (trifluoromethansulfonyl)imide (LiTFSI) and an ionic liquids (N-methyl-N-butylpyrrolidinium bis(trifluoromethansulfonyl)imide) has been explored as a polymer-based electrolyte in lithium ion batteries[8]. The aforementioned components were mixed and processed at elevated temperatures under dry conditions. By this process, ternary composites PEO/RTIL/LiTFSI with high ionic conductivity were obtained in the form of thin films. No solvent was used in the process. However, the increase in conductivity (compared to binary systems PEO/Li salt) was still limited, as the mechanical stability of the composites was poor when the content of ionic liquid exceeded a certain limit. It has been reported that for ternary composites PEO/RTIL/LiTFSI this limit is in the range of 10/1/1 (by mole). At higher contents of ionic liquid, soft and sticky gels are obtained which are difficult to process on an industrial scale. Until today, this represented a serious limitation to the practical use of ionic liquids in PEO based electrolytes.

In this chapter, a solution to this problem is proposed: a highly conductive PEO-based polymer electrolyte was prepared via a direct UV induced crosslinking in the presence of a lithium salt and an imidazolium-based RTIL. Elastomeric, resistant, and self-standing polymer electrolyte (SPE) membranes were obtained and characterized in terms of their ionic

conductivity, electrochemical stability, mechanical properties, thermal and interfacial stability. In this study, without using any solvents a cross-linked polymer matrix was elaborated within a few minutes. Significantly, the feasibility of using such material in LIBs at different temperatures was established, also thanks to a suitable in situ polymerization procedure directly on the surface of the electrode films, fundamental to obtain an intimate interfacial adhesion. The process is simple, eco-friendly, and even adaptable to battery-processing methods to achieve better interfaces. In addition, the simplicity of the proposed process and the wide availability of the materials used make this system very promising and ready to be industrially scaled up following the main principles of green chemistry.

## 2.2. EXPERIMENTAL SECTION

### 2.2.1 MATERIALS

All starting materials and reagents were purchased from commercial suppliers and used without any further purification. PEO (average $M_w \approx 10^6$, Sigma-Aldrich) was vacuum dried overnight at 50 °C before use. Lithium bis(trifluoromethane sulfonyl) imide salt (LiTFSI, 99.9% purity, battery grade, Solvionic) and 1-ethyl-3-methylimidazolium-bis(trifluoromethyl-sulfonyl) imide (EMI-TFSI, 99.5%, Solvionic) were vacuum dried overnight at 100 °C before use. The free-radical photoinitiator 2-methyl-benzophenone (MBP, ≥99%, Sigma-Aldrich) and lithium metal foils (Li, high-purity lithium foils, Chemetall Foote Corp.) were used as received. Lithium iron phosphate

($LiFePO_4$) was supplied by Lithops s.r.l. All substances were stored in an argon-filled dry glovebox (MBRAUN LABstar) having a humidity content below 1 ppm.

### 2.2.2. PREPARATION OF THE POLYMER ELECTROLYTES

An optimal PEO:EMI-TFSI:LiTFSI polymer electrolyte composition was selected, which is 45:45:10 in weight ratio. Before arriving to the reported formulation, several tests were performed to understand the fundamental aspects of polymer electrolytes to decide the quantity and type of photoinitiator as well as the suitable molecular weight of PEO depending on the easiness in processing, solubility of salt, ionic mobility in terms of [EO]/[Li] ratio, and mechanical integrity. MBP was selected as the photo-cross-linker with superior solubility and optimum cross-linking properties in the 5% w/w ratio with respect to the PEO content. The ternary polymer electrolyte was prepared adapting an existent literature protocol first proposed by Rupp et al [9]. Initially, a homogeneous solution of EMITFSI, lithium salt and photoinitiator was prepared by mixing the components at 50 °C for 1 h. Subsequently, PEO and the latter solution were blended in a mortar to promote homogeneous mixing; the mixture was left at 120 °C for 2 h under inert atmosphere. Then, the mixture was sandwiched between two Mylar sheets and reduced into a thin film by a hot press at 90 °C at 50 bar for 15 min. Without removing the Mylar sheets, the film was UV cured for 3 min per side under a xenon arc lamp (Helios Italquartz, 45 mW $cm^{-2}$). Before any further use, the obtained polymer electrolyte films (thickness of 90 ± 5 µm, measured using Thickness Gages Series 547 equipped with an

ABSOLUTE Digimatic Indicator from Mitutoyo) were dried overnight under high vacuum at 45 °C. All the above reported procedures were carried out in an environmentally controlled dry room (10 $m^2$, RH < 2 ± 1% at 20 °C) manufactured by Soimar.

### 2.2.3 CHARACTERISATION OF THE POLYMER ELECTROLYTES

The physical-chemical characterization techniques used in this chapter are described in the Appendix.

### 2.2.4. FABRICATION AND CHARACTERIZATION OF LIBS

Laboratory-scale lithium cells were tested in terms of galvanostatic charge/discharge cycling at different current rates with an Arbin Instrument Testing System model BT-2000. Potential cut offs are given in section 2.3. Cell assembly was performed inside the dry glovebox. A two-electrode electrochemical test cell model ECC-Std (EL-CELL) was assembled using a $LiFePO_4$-based composite working electrode and a lithium metal counter electrode. The $LiFePO_4$-based composite electrode was prepared by casting and successively drying a 1-methyl-2-pyrrolidone (NMP, Sigma-Aldrich) slurry having the composition 88:6:6 w/w in $LiFePO_4$ (active material, Clariant LP2), electronic conductivity enhancer AB50 (Shawinigan Black AB50, Chevron Corp.), and binder PVdF (Solvay Solef 6020). Electrodes were vacuum dried for 5 h at 120 °C before use. The cell was assembled by combining a lithium metal anode with an electrode/electrolyte composite prepared by light curing the polymer electrolyte directly onto the $LiFePO_4$ cathode film surface. In a typical preparation, a blend of UV-cured polymer

electrolyte was prepared following the procedure described in section 2.2.2 and placed between the electrode and a Mylar sheet. The mixture was reduced into a film by hot pressing and followed up with a light-induced photopolymerization directly over the electrode film [10]. Then, electrolyte/ electrode disks (area 2.54 $cm^2$) were cut from the sheet and dried under vacuum overnight at 70 °C prior to cell assembly.

## 2.3. RESULTS AND DISCUSSION

### 2.3.1. CHARACTERIZATION OF THE POLYMER ELECTROLYTES

The precursor mixture comprising PEO, RTIL, LiTFSI and the hydrogen abstraction photoinitiator (MBP), after hot pressing and UV light exposure, formed a transparent, self-standing, and non-tacky polymer electrolyte membrane, as shown in **Figure 2.1**. Under UV excitation, MBP may abstract protons from methylene groups thus generating free radicals on the PEO chains [9]. Then a free radical may combine with another one from the same chain or a neighbor chain, thus creating a crosslinking point (see also the sketched picture of **Figure 2.1**).

Polymer electrolytes composed of PEO and Li salts typically use [EO]/[Li] mole ratio as a parameter to increase the mobile Li cation content; in our selected formulation, an [EO] to [Li] ratio of 30:1 was considered as optimal.

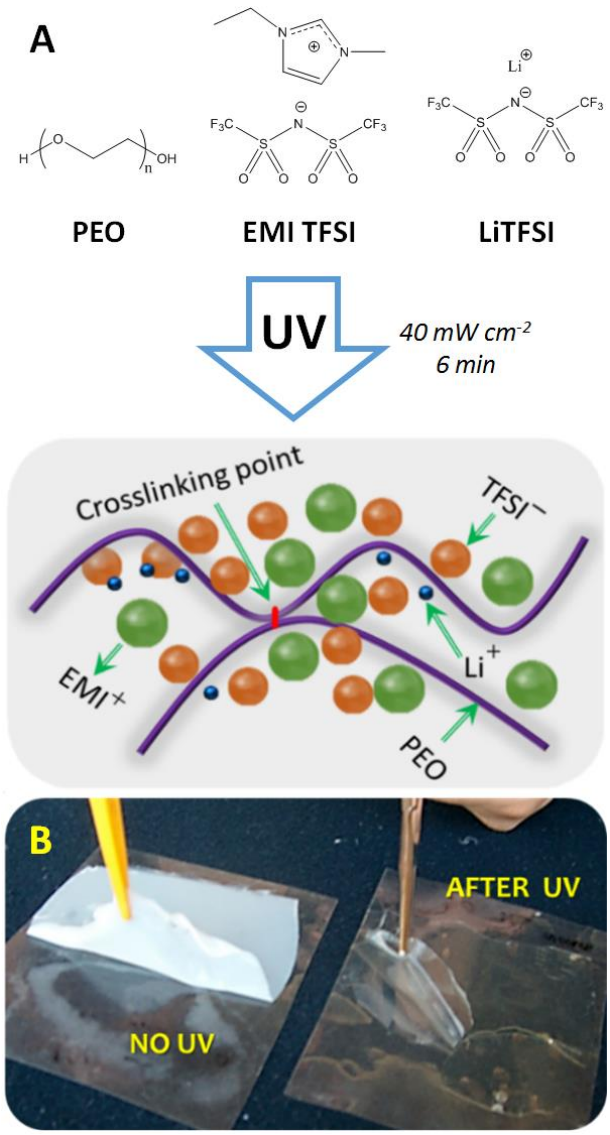


**Figure 2.1 (a)** Sketched representation of the UV process along with the components used in this study and the hypothesized interlinking of PEO polymer chains encompassing imidazolium-based RTIL. **(b)** The real aspect of the polymer electrolyte formed after UV exposure , which is almost transparent, tack free, flexible and easy to manage.

The mechanical robustness of the cross-linked polymer electrolyte is shown in **Figure 2.2 (a)**, where the remarkable elasticity is demonstrated. It is impressive to note that the sample was easily stretchable and highly flexible, as demonstrated by the ability to retain its original shape and size after the stress was released. FESEM analysis was conducted to characterize the morphology of the photocured polymer films. A representative top view is shown in **Figure 2.2 (b)**; the surface of the cross-linked polymer presents a uniform wrinkled texture, resulting from the fabrication method adopted. The bright and dark areas in the image belong to amorphous PEO domains alternated to some residual ordered (semicrystalline) domains, respectively; the wrinkled texture derives from the formation of cross-linking domains between the polymer chains under conditions of compressive stress applied by the rigid support [11]. Once the stress is removed the chains may tend to come back to their normal state (stress release), but the subsequent cross-linking process induced by the UV light help the matrix to freeze in a wrinkled form. In the present case, the surface morphology appears to be highly regular, thus confirming a good blending between the components of the ternary mixture. A similar precursor mixture processed without a UV irradiation step generated a non-uniform and hardly homogeneous membrane; refer to the inset of **Figure 2.2 (b)**.

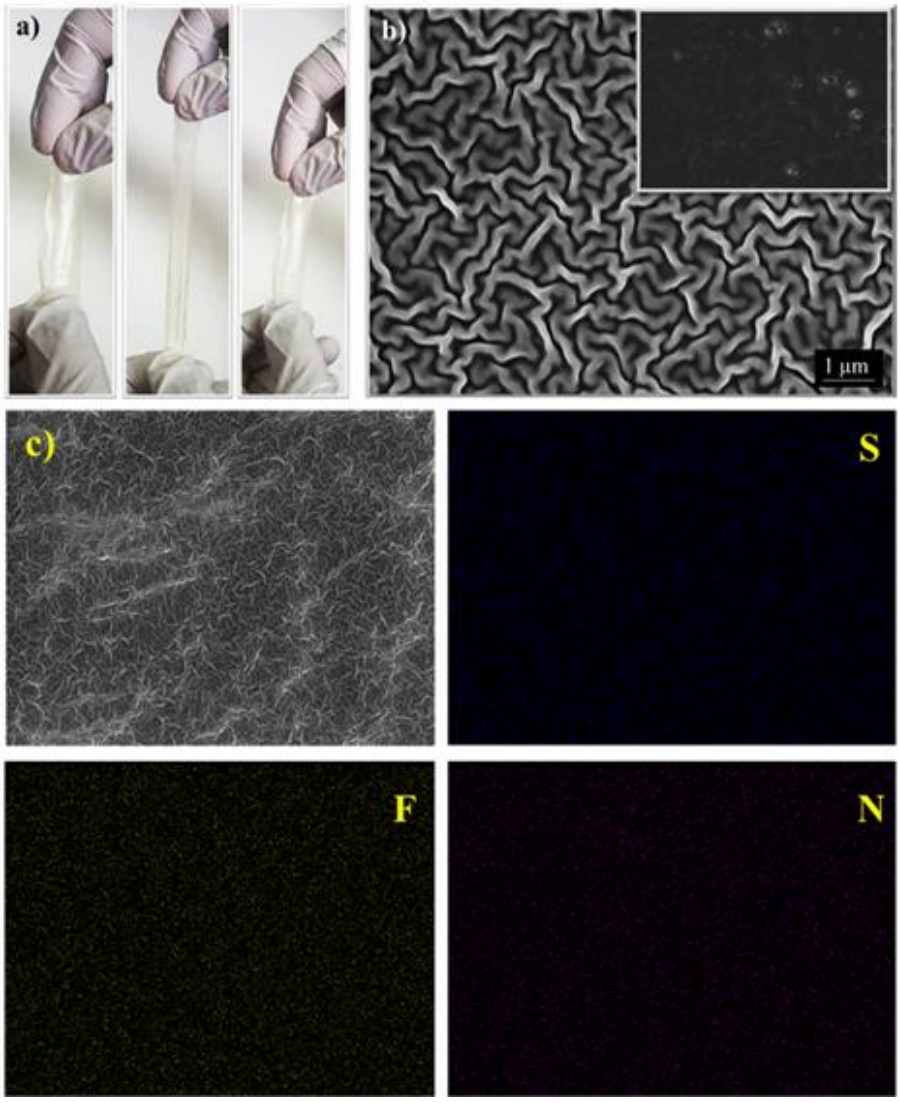


**Figure 2.2** a) Appearance of the light-cured crosslinked polymer electrolyte sample upon manual elongation, b) FESEM analysis at high magnification of the sample surface, c) focus on the area (30 µm × 30 µm) of the image where EDX analysis was carried out, along with the following images in which S, F and N indicate the distribution of sulphur, fluorine and nitrogen, respectively, of $TFSI^-$ anion in the selected area of the sample.

On the contrary, the cross-linking produced by UV irradiation allows the incorporation of the same amount of RTIL and salt, leading to a material with dramatically different morphological characteristics in terms of homogeneity and robustness. Moreover, the UV-cured PEO-based network was able to retain efficiently the RTIL without any leakage. Furthermore, the EDX analysis shown in **Figure 2.2 (c)** confirmed the homogeneous distribution of S, N, and F elements present in the $TFSI^-$ anion, which is an indirect indication that the prepared polymer electrolyte is highly homogeneous.

Gel content studies guaranteed that the UV irradiation on the sample for overall 6 min was sufficient to form a well-crosslinked film with high reproducibility. Indeed, the insoluble fraction of the samples was found to be higher than 95% with respect to the total PEO content after 18 h of extraction in $CHCl_3$. This confirms that all PEO chains incorporated in the polymer matrix are in the cross-linked form.

Mechanical properties were evaluated by tensile analysis; typical force (N) – elongation (mm) curves for both UV-irradiated and non-irradiated samples are shown in **Figure 2.3**. They reveal that the average Young's modulus *E* of the polymer electrolyte before UV irradiation (0.4 ± 0.05 MPa) was higher than the SPE membrane after UV irradiation (0.2 ± 0.05 MPa). Moreover, the UV irradiated polymer electrolytes showed higher tensile resistance $R_{max}$ (1.45 ± 0.05 MPa) than the non-irradiated one (0.6 ± 0.15 MPa). It can be also drawn from **Figure 2.3** that the overall area under stress/strain curve of UV irradiated polymer electrolyte was much higher than the one not exposed to UV light, which makes the material tougher. If

one considers that 45 wt% of ionic liquid was incorporated in the SPE membrane, these are highly satisfying values.

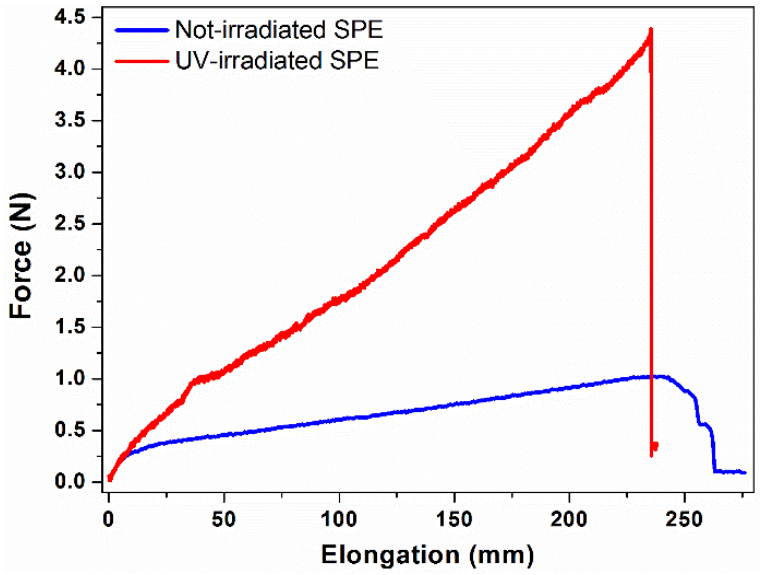


**Figure 2.3** Mechanical measurements carried out on UV irradiated and non-irradiated SPEs at ambient temperature by traction test.

The results of the thermogravimetric study are shown in **Figure 2.4 (a)**. As a reference, all the components of the SPE were tested separately. EMI-TFSI was thermally stable up to 450 °C and shows a one-step degradation process. PEO and LiTFSI decomposed at slightly lower temperature (around 400 °C) again with a well-defined single step process. The resulting crosslinked polymer electrolyte showed a two-step degradation process: the first one, occurred at around 400 °C, corresponds to the decomposition of the PEO matrix and embedded lithium salt. The second step corresponds to

EMI-TFSI degradation and occurred around 450 °C. The first dip before reaching 100 °C was ascribed to the loss of humidity that might be absorbed during the handling of the sample for testing. Overall, the sample showed a thermal stability up to 375 °C under inert conditions, and such a remarkable result is particularly interesting for application in energy storage and conversion devices with increased safety. The plasticizing effect of EMI-TFSI on the polymer electrolyte was studied by DSC, the results of which are shown in **Figure 2.4 (b)**. The glass transition of the polymer electrolyte occurs at −56 °C. Interestingly, the melting of the crystalline phase of PEO occurred at about 20 °C, which was a much lower temperature than the standard PEO melting. The shift may occur due to several reasons, such as the addition of lithium salt, addition of EMI-TFSI, and most importantly the crosslinking reaction, which only allow restricted movement of the –EO– chains to reorganise themselves to form crystallites. Even though the interlinking between the chains was not uniform, the crystallites formed by the reactions could be smaller, which may reflect in lowering the melting of crystalline peaks. Moreover, the starting point of broadening peak could be an indication of just PEO chain rearrangement rather than melting. Another possibility might be the melting of some excess LiTFSI-EMI-TFSI phase as reported by Shin *et al*. [8] Overall, the degree of crystallinity was effectively minimised to nearly fully amorphous state by addition of Li salt, RTIL and UV-induced crosslinking process.

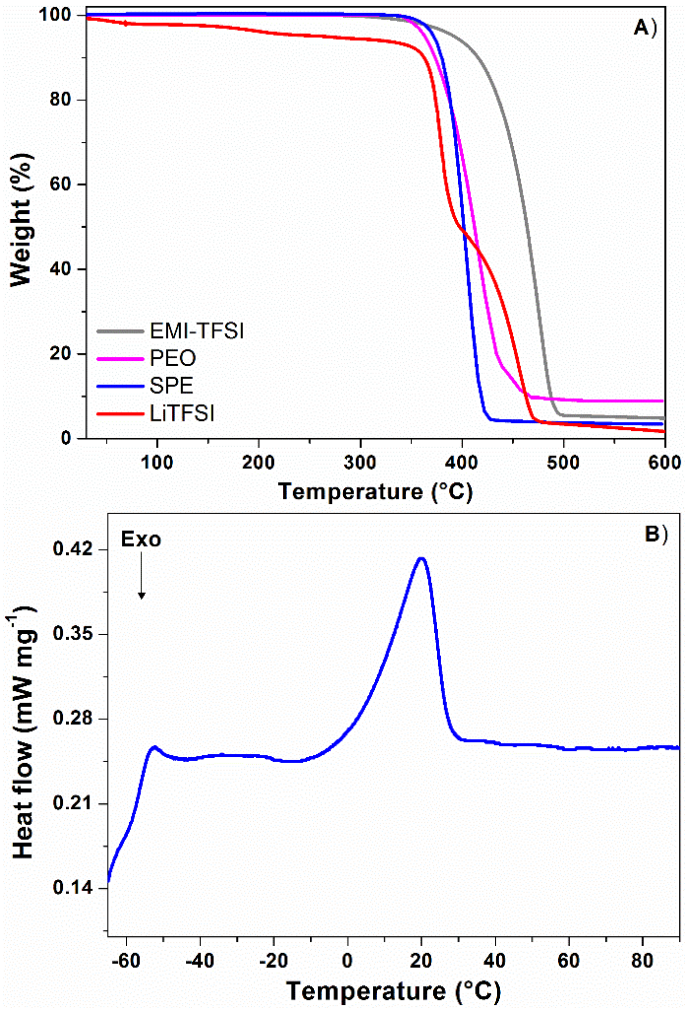


**Figure 2.4.** Thermal characteristics of the materials: a) TGA profiles and b) DSC traces.

XRD was used to get a further confirmation of the fundamental role of the photocuring step in reducing the overall crystallinity of the PEO-based polymer electrolyte to nearly fully amorphous state (see **Figure 2.5**). Pristine

PEO showed intense characteristic peaks corresponding to the crystalline characteristics of the polymer matrix. The addition of EMI-TFSI, LiTFSI along with the UV-induced photo-polymerization process greatly reduced the intensity of the peaks along with almost negligible reflections (peaks at 2θ = 37 and 44° were due to the aluminium sample holder), thus indicating an almost completely amorphous polymer electrolyte. Indeed, the small peaks present on the broad peak of SPE between 15 and 25° is in agreement with the DSC graphs obtained for the same sample.

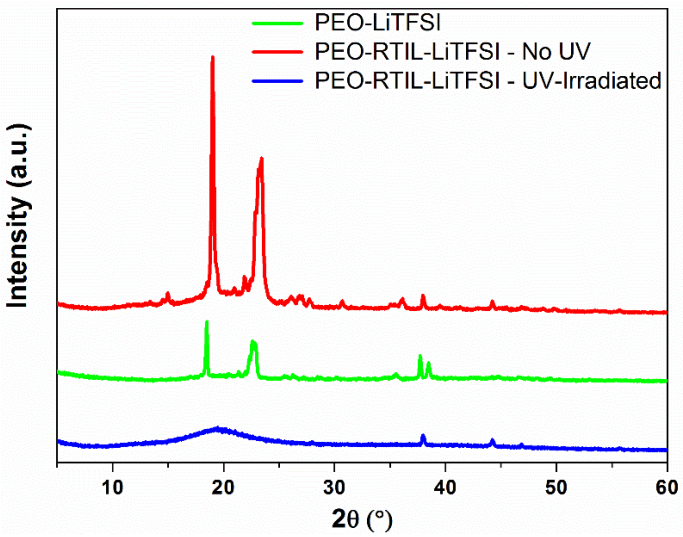


**Figure 2.5.** X-ray diffraction (XRD) analysis of the different samples.

The ionic conductivity of solid polymer electrolytes at ambient temperature is usually two to three orders of magnitude lower than that of a liquid electrolyte, thus precluding their practical application in standard

LIBs. It is well known that PEO crystallization reduces ionic conductivity [12]. To overcome this issue, EMI-TFSI was incorporated into the polymer matrix. The ionic conductivity of the polymer electrolyte in the temperature interval between 20 and 80 °C is shown in **Figure 2.6**. At 20 °C the σ value is equal to $2.5\times10^{-4}$ S $cm^{-1}$. This result is of particular interest as is sufficiently high to allow ambient temperature operation of Li-ion cells. It exceeds $10^{-3}$ S $cm^{-1}$ already at 50 °C. The Vogel-Tamman-Fulcher (VTF) [13] behaviour of the SPE was verified fitting the conductivity data with respect to temperature. The R-square value confirms the quality of the fitting. The value of activation energy was found to be 8.23 kJ $mol^{-1}$. This result is in good accordance with the DSC study discussed in the previous paragraph. Beneficial effects coming from the incorporation of EMI-TFSI in the polymer matrix are observed, including its plasticizing effect, which reduces the crystalline degree of PEO and provides a high mobility phase for $Li^+$ ions to be transported through the SPE [14]. Despite increasing the ionic conductivity, the incorporation of ionic liquids usually leads to loss of mechanical stability. The UV crosslinking process allows preparing stable polymer electrolyte having both high ionic conductivity and excellent mechanical properties. Although different mixture of PEO, lithium salts and RTILs have been proposed in the past years, the ambient temperature conductivity herein presented is of particular interest since it matches values obtained with higher amount of lithium salts or even exceed values obtained with higher amount of RTIL [15].

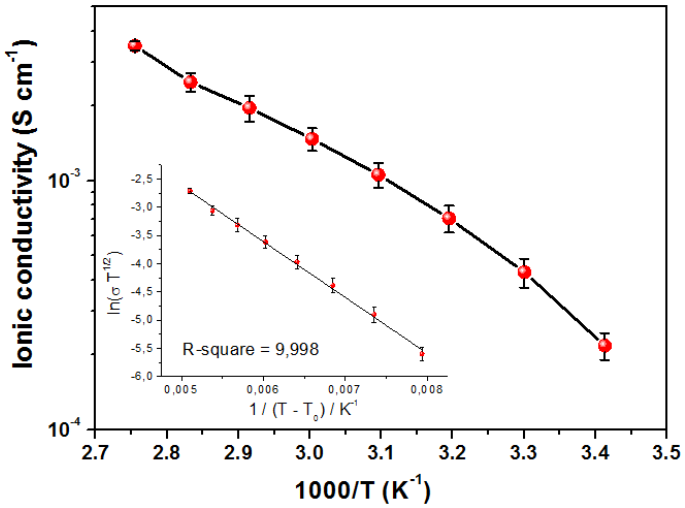


**Figure 2.6.** Arrhenius plot for ionic conductivity as a function of temperature of the polymer electrolyte membrane (in the inset, the fitting by means of the VTF equation). Data obtained by impedance spectroscopy.

An appropriate assessment of the ionic conduction in polymer electrolytes and its influence on the other electrochemical properties can be derived from lithium ion transport behaviour. The lithium transference number, $t_{Li+}$, is a key factor in the optimisation of electrolytes encompassing RTIL and Li salt for Li and Li-ion battery; in fact, high $t_{Li+}$ guarantees high power density. As typically observed when using polymer electrolyte systems encompassing RTIL and salts [16], $t_{Li+}$ of the polymer electrolyte membrane is not very high (note that the calculated mole ratio of $Li^+/EMI^+$ in the proposed system equals to 0.3:1 in the present system). It results in 0.165 at 55 °C, which is in good agreement with recent literature reports [16,17].

### 2.3.2 EVALUATION OF THE PERFORMANCES IN ALL-SOLID LITHIUM POLYMER CELL

A secondary lithium-based battery typically operates between 0.02 and 4.2 V vs. $Li^+/Li$; therefore, the ESW of the electrolyte must be wider than the operating potential in order to assure high Coulombic efficiencies and long stable cycling. The electrochemical stability limits of the polymer electrolyte were evaluated by cyclic voltammetry and the results are shown in **Figure 2.7**. Despite a shoulder centred at 4.2 V vs. $Li^+/Li$ is clearly visible in the CV, the main anodic breakdown potential of the polymer occurs at above 4.6 V vs. $Li^+/Li$, as indicated by a steep increase in the anodic current exceeding the current threshold of 0.01 mA $cm^{-2}$. This is also supported by literature finding for similar systems encompassing EMI-based RTILs[18,19]. Above this potential, the electrolyte starts to decompose by oxidative irreversible reactions. Upon cathodic scan towards more negative potential values, a small cathodic current that do not exceed the current threshold is observed; this event is most likely associated with reduction of the electron deficient C2 carbon of the imidazolium ring[15]; the multistep decomposition of some impurity traces in EMI-TFSI (used as received) may not be excluded. However, this phenomenon is neglectable due to the solid character of the electrolyte. The interpretations on both anodic and cathodic behaviours are supported by the following findings: (i) the irreversibility of the peaks, and (ii) the trend of the second sweep cycle where the gradual disappearance of the events are detected (e.g., the 4.2 V shoulder peak in the second anodic scan). An overall good cathodic electrochemical stability is indicated by the lithium plating/stripping, which is clearly evident at around 0 V vs. $Li^+/Li$. The

most important information that can be resumed from ESW test are: (i) the presence of a well-defined lithium deposition/stripping couple of peaks confirms both the proper working of the solid polymer electrolyte in lithium cell as well as the presence of a porous and ion transporting interface, (ii) the safe operation of the system under standard working conditions, since the anodic breakdown occurs at potential higher than 4 V versus Li, (iii) the purity of the entire system demonstrated by the very flat plateau in the stability region [20].

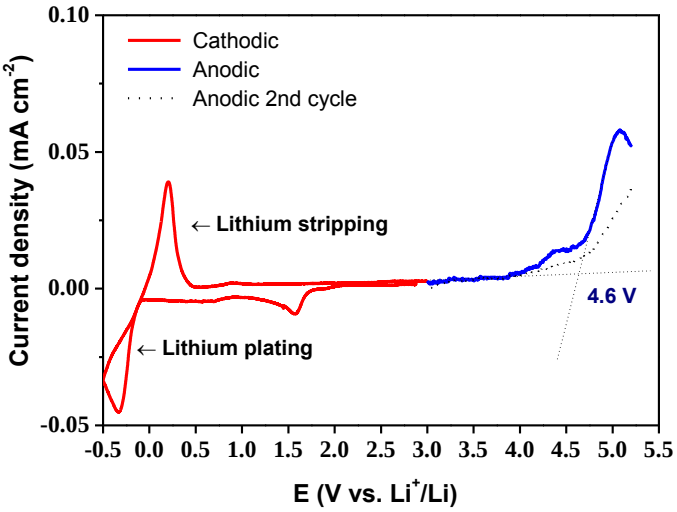


**Figure 7.** Electrochemical stability window (ESW) of the polymer electrolyte at ambient temperature; potential scan rate of 0.1 mV $s^{-1}$.

In view of practical applications, the polymer electrolyte membrane was assembled in a lab-scale all-solid-state lithium polymer cell, and its electrochemical behaviour was investigated by means of galvanostatic

charge/discharge cycling as a function of the cycle number at ambient temperature. The cell was assembled by combining a lithium metal anode with an electrode-electrolyte composite prepared by light-curing the polymer electrolyte directly onto the $LiFePO_4$ cathode surface, a rapid and easily scalable procedure detailed in Section 2.2.4. One major drawback related to the use of solid polymer electrolytes is the unsufficient contact between the active materials of the electrode and the polymer matrix. The hot-press step here adopted, instead, is fundamental to obtain a good penetration of the polymer electrolyte precursors into the composite cathode. In fact, the melted PEO/RTIL blend is likely to fill the porosity of the electrode, thus ensuring good wetting of the active material particles. A very thin (≈30 μm thickness) and mechanically robust polymer electrolyte film with excellent adhesion to the electrode surface is then obtained after the subsequent direct photopolymerization procedure. Moreover, the crosslinked polymer matrix is able to effectively retain the RTIL, thus no leakage is guaranteed (confirmed by conductivity measurements in which the bulk resistance of the electrolyte was stable after several thermal cycles as well as 15 days of storage at 55 °C).

FESEM images taken after cracking the sample are given in **Figure 2.8**. Particularly at higher magnifications, it can be clearly observed that the electrolyte layer creates a conformal coating by following the contours of the electrode particles. This results in improved active area at the interface between the electrode and the polymer electrolyte, correspondingly reflecting in improved specific energy and specific power of the cell[21]. The oriented crosslinked polymer electrolyte morphology is clearly evident on

top of the electrode along with the optimum interface and interpenetration between the electrode active material particles and the electrolyte.

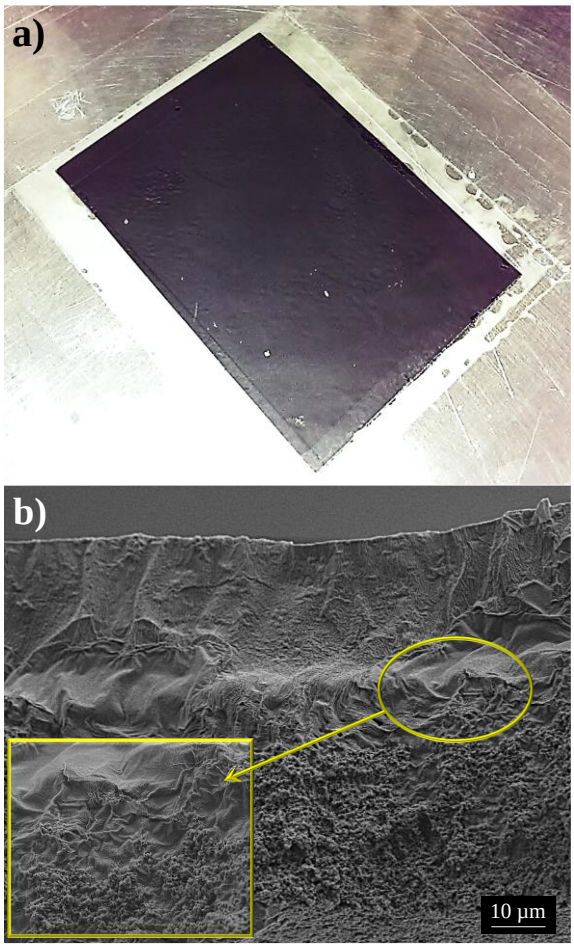


**Figure 2.8.** a) Photograph of a freshly prepared self-supporting multiphase electrode/electrolyte composite obtained by direct hot-pressing and *in situ* photopolymerization of the polymer electrolyte on top of the $LiFePO_4$ composite electrode; b) Cross-sectional FESEM images illustrating the morphology of the multiphase electrode/electrolyte composite at different degree of magnification.

The response of the cell is shown in **Figure 2.9**. Constant current charge/discharge profiles extracted from cycling tests carried out at increasing cycling rates at mild temperature (55 °C) are shown in plot (A) of **Figure 2.9**. They reflect the good properties of the newly elaborated system, showing definite flat potential plateaus both on charge and on discharge related to the typical biphasic $Li^+$ extraction/insertion mechanism in $LiFePO_4$. This is well in agreement with the characteristics of the selected active material: at about 3.5 V vs. $Li^+/Li$ upon charge (i.e., $Li^+$ de-insertion from the $LiFePO_4$ structure) and at about 3.35 V vs. $Li^+/Li$ upon discharge (i.e., $Li^+$ insertion into the $FePO_4$ structure), with a steep potential increase/decay at its end [22]. The polarization was found to be very limited even at 0.2C rate. This fact accounts for an efficient redox reaction kinetics, due to both limited internal resistance at the electrode/electrolyte interface and limited cell overpotential contributions. In general, the material shows a good cycling stability at each of the tested current regimes, as for the good overlapping of the charge/discharge curves, accounting for a charge coefficient (charge capacity/following discharge capacity) very close to unity. The maximum specific capacity values obtained by the $LiFePO_4$/electrolyte composite developed in this chapter (see plot B of **Figure 2.9**) are about 143 and 132 mAh $g^{-1}$ at 0.1C and 0.2C, respectively. Noteworthy, the newly developed polymer electrolyte demonstrate the ability to be reversibly cycled at 20 °C as well (again exploiting the direct *in situ* polymerization, see plots A and B in **Figure 2.10**), still retaining stable response at each of the selected current densities.

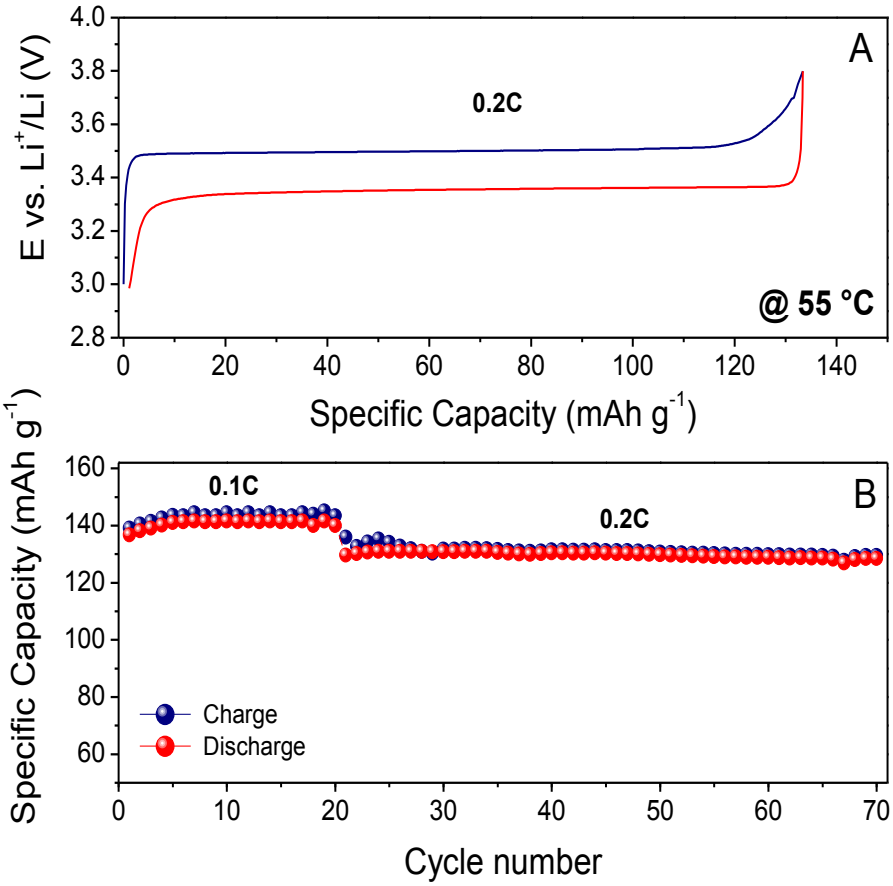


**Figure 2.9**. Cycling behavior of the solid polymer lithium cell assembled by contacting the $LiFePO_4$-based electrode/polymer electrolyte with a lithium metal anode in the 3.0 – 3.8 V *vs.* $Li^+/Li$ range at different temperatures: a) constant current charge/discharge potential *vs.* specific capacity profiles extracted from cycle 70 at 0.2C rate and b) specific capacity *vs.* cycle number plot at different C rates at 55 °C.

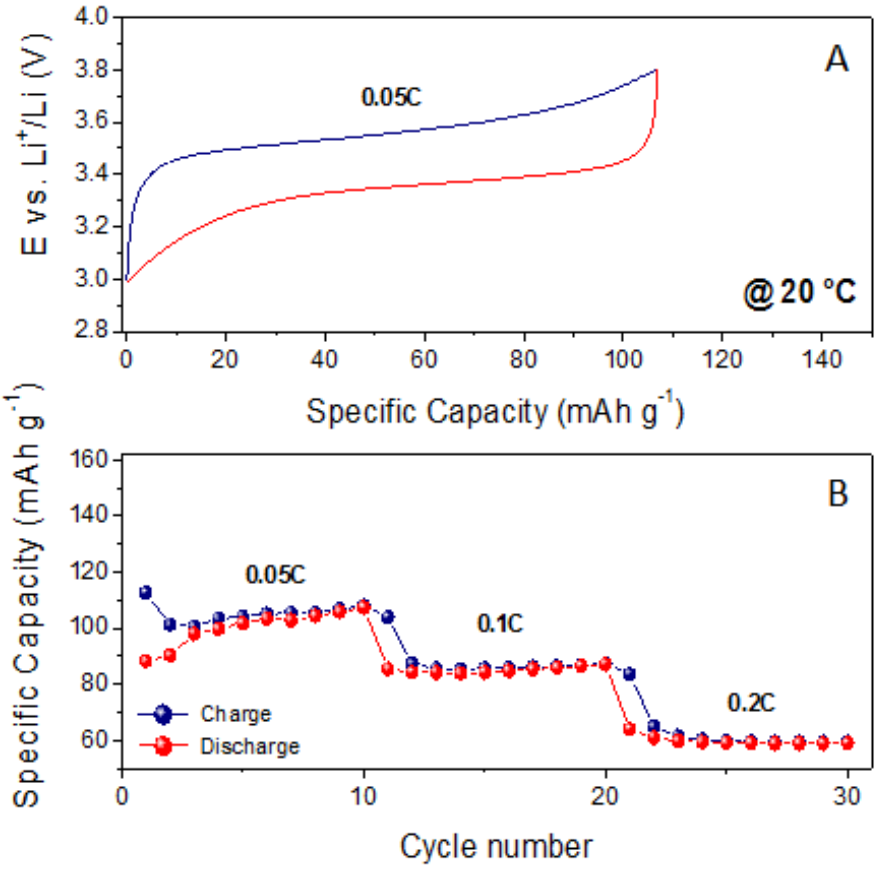


**Figure 2.10**. Cycling behavior of the solid polymer lithium cell assembled by contacting the $LiFePO_4$-based electrode/polymer electrolyte with a lithium metal anode in the 3.0 – 3.8 V *vs.* $Li^+/Li$ range at different temperatures: a) constant current charge/discharge potential *vs.* specific capacity profiles extracted from cycle 10 at 0.05C rate and b) specific capacity *vs.* cycle number plot at different C rates at 20 °C,

Note that the same commercial $LiFePO_4$ material tested in the same cell assembled in the same Lab conditions using a standard liquid electrolyte can provide about 157 and 145 mAh $g^{-1}$ at the same current regimes. Overall,

although the specific capacity obtained is slightly lower than that obtained for the same $LiFePO_4$ cathode material at the same currents in liquid electrolyte, the polymer cell shows good capacity retention exceeding 91%. This is a convincing indication of a good interfacial contact between the electrodes and the electrolyte separator, arising from the fabrication procedure adopted. Nevertheless, full specific capacity was not obtained, even at low current regime, which indicates that the full wetting of the active material surface was not achieved; such an issue might be solved by optimizing the polymer electrolyte formulation and fabrication procedure, or even developing three-dimensional porous solid electrolyte with high surface area thus allowing the increase of the interface region. The rate capability of the lithium metal polymer cell is also excellent. Good performance at high current rate may be ascribed to the efficient ionic conduction in the polymer-coated separator and the favorable interfacial charge transport between the electrodes and the electrolyte in the cell. The sum of these phenomena, along with the simple, fast and ecofriendly preparation procedure allow to realize the optimum conditions for the newly elaborated material to act as solid polymer electrolyte in LIBs.

## 2.4. CONCLUSIONS

In summary, in this chapter an innovative polymer electrolyte membrane for quasi-solid state energy storage devices was introduced, obtained by a unique, rapid, economic, easily up-scalable and environmentally friendly two-step process including a photo-curing step. Compared to other

techniques, the production process here proposed appears highly advantageous due to its ease and rapidity in processing. No solvents are employed at any stages of the processing; moreover the materials used can be eventually recycled thus making the whole process environmentally benign. This novel fabrication method could reduce the manufacturing cost and simplify the fabrication process. Moreover, it is worth to be noted that the newly developed preparation method has led to an international patent recently published [23]. The new configuration adopted for the production of multiphase electrolyte/electrolyte assembly consisted in the direct formation of the SPE on top of the $LiFePO_4$ composite positive electrode surface by hot pressing followed by UV-induced crosslinking. The characterization and obtained results demonstrated an enhanced adhesion of the polymer electrolyte to the active electrode materials. The lab-scale lithium polymer cell assembled showed stable charge/discharge characteristics without any capacity fading even at 0.2C current regime. This process plays a critical role in improving the wettability and electrolyte retention, the interfacial adhesion between the electrode active material and the separator and the cycle performance of the resulting lithium polymer cell assembly. Due to the intimate contact between the electrode material grains and the polymer electrolyte matrix, the interface does not create problems arising by insufficient contact. Thus, the cell produced by hot pressing combined with UV light-induced crosslinking holds a great potential to be used in high-performance, versatile and cost-effective LIBs.

Finally, the versatile use of these membranes for other applications such as DSSCs makes this process a strong tool to prepare universal membranes

with multipurpose feature [24]. Although further efforts are necessary to reduce the contact resistance, we have successfully indicated the adaptability of UV polymerisation of PEO to industrial manufacturing process of all-solid-state energy production and storage devices.

## REFERENCES


[1] D.E. Fenton, J.M. Parker, P.V. Wright, Complexes of alkali metal ions with poly(ethylene oxide), Polymer. 14 (1973) 589. doi:10.1016/0032-3861(73)90146-8.

[2] Y. Dkhissi, F. Huang, Y.-B. Cheng, R.A. Caruso, Quasi-Solid-State Dye-Sensitized Solar Cells on Plastic Substrates, J. Phys. Chem. C. 118 (2014) 16366–16374. doi:10.1021/jp408844q.

[3] K. Onishi, S. Sewa, K. Asaka, N. Fujiwara, K. Oguro, The effects of counter ions on characterization and performance of a solid polymer electrolyte actuator, Electrochimica Acta. 46 (2001) 1233–1241. doi:10.1016/S0013-4686(00)00695-2.

[4] J. Rolland, J. Brassinne, J.-P. Bourgeois, E. Poggi, A. Vlad, J.-F. Gohy, Chemically anchored liquid-PEO based block copolymer electrolytes for solid-state lithium-ion batteries, J. Mater. Chem. A. 2 (2014) 11839–11846. doi:10.1039/C4TA02327G.

[5] P.-L. Kuo, C.-A. Wu, C.-Y. Lu, C.-H. Tsao, C.-H. Hsu, S.-S. Hou, High Performance of Transferring Lithium Ion for Polyacrylonitrile-Interpenetrating Crosslinked Polyoxyethylene Network as Gel Polymer Electrolyte, ACS Appl. Mater. Interfaces. 6 (2014) 3156–3162. doi:10.1021/am404248b.

[6] S. Zhang, J. Sun, X. Zhang, J. Xin, Q. Miao, J. Wang, Ionic liquid-based green processes for energy production, Chem. Soc. Rev. 43 (2014) 7838–7869. doi:10.1039/C3CS60409H.

[7] D.R. MacFarlane, N. Tachikawa, M. Forsyth, J.M. Pringle, P.C. Howlett, G.D. Elliott, et al., Energy applications of ionic liquids, Energy Environ. Sci. 7 (2013) 232–250. doi:10.1039/C3EE42099J.

[8] J.-H. Shin, W.A. Henderson, S. Passerini, Ionic liquids to the rescue? Overcoming the ionic conductivity limitations of polymer electrolytes, Electrochem. Commun. 5 (2003) 1016–1020. doi:10.1016/j.elecom.2003.09.017.

[9] B. Rupp, M. Schmuck, A. Balducci, M. Winter, W. Kern, Polymer electrolyte for lithium batteries based on photochemically crosslinked poly(ethylene oxide) and ionic liquid, Eur. Polym. J. 44 (2008) 2986–2990. doi:10.1016/j.eurpolymj.2008.06.022.

[10] C. Gerbaldi, M. Destro, J.R. Nair, S. Ferrari, I. Quinzeni, E. Quartarone, High-rate V2O5-based Li-ion thin film polymer cell with outstanding long-term cyclability, Nano Energy. 2 (2013) 1279–1286. doi:10.1016/j.nanoen.2013.06.007.

[11] L. He, C. Tang, X. Xu, P. Jiang, W.-M. Lau, F. Chen, et al., Hyperthermal hydrogen induced cross-linking and fabrication of nano-wrinkle patterns in ultrathin polymer films, Surf. Coat. Technol. 261 (2015) 311–317. doi:10.1016/j.surfcoat.2014.11.013.

[12] Z. Xue, D. He, X. Xie, Poly(ethylene oxide)-based electrolytes for lithium-ion batteries, J. Mater. Chem. A. 3 (2015) 19218–19253. doi:10.1039/C5TA03471J.

[13] G.S. Fulcher, Analysis of Recent Measurements of the Viscosity of Glasses.—Ii1, J. Am. Ceram. Soc. 8 (1925) 789–794. doi:10.1111/j.1151-2916.1925.tb18582.x.

[14] S.K. Chaurasia, R.K. Singh, S. Chandra, Ionic liquid assisted modification in ionic conductivity, phase transition temperature and crystallization kinetics behaviour of polymer poly(ethylene oxide), Solid State Ion. 262 (2014) 790–794. doi:10.1016/j.ssi.2013.09.048.

[15] J.-W. Choi, G. Cheruvally, Y.-H. Kim, J.-K. Kim, J. Manuel, P. Raghavan, et al., Poly(ethylene oxide)-based polymer electrolyte incorporating room-temperature ionic liquid for lithium batteries, Solid State Ion. 178 (2007) 1235–1241. doi:10.1016/j.ssi.2007.06.006.

[16] S. Ferrari, E. Quartarone, P. Mustarelli, A. Magistris, M. Fagnoni, S. Protti, et al., Lithium ion conducting PVdF-HFP composite gel electrolytes based on N-methoxyethyl-N-methylpyrrolidinium bis(trifluoromethanesulfonyl)-imide ionic liquid, J. Power Sources. 195 (2010) 559–566. doi:10.1016/j.jpowsour.2009.08.015.

[17] C. Liu, X. Ma, F. Xu, L. Zheng, H. Zhang, W. Feng, et al., Ionic liquid electrolyte of lithium bis(fluorosulfonyl)imide/N-methyl-N-propylpiperidinium bis(fluorosulfonyl)imide for Li/natural graphite cells: Effect of concentration of lithium salt on the physicochemical and electrochemical properties, Electrochimica Acta. 149 (2014) 370–385. doi:10.1016/j.electacta.2014.10.048.

[18] H. Matsumoto, H. Sakaebe, K. Tatsumi, Preparation of room temperature ionic liquids based on aliphatic onium cations and asymmetric amide anions and their electrochemical properties as a lithium battery electrolyte, J. Power Sources. 146 (2005) 45–50. doi:10.1016/j.jpowsour.2005.03.103.

[19] G.H. Lane, Electrochemical reduction mechanisms and stabilities of some cation types used in ionic liquids and other organic salts, Electrochimica Acta. 83 (2012) 513–528. doi:10.1016/j.electacta.2012.08.046.

[20] A. Chiappone, J.R. Nair, C. Gerbaldi, L. Jabbour, R. Bongiovanni, E. Zeno, et al., Microfibrillated cellulose as reinforcement for Li-ion battery polymer

electrolytes with excellent mechanical stability, J. Power Sources. 196 (2011) 10280–10288. doi:10.1016/j.jpowsour.2011.07.015.

[21] J.R. Nair, M. Destro, C. Gerbaldi, R. Bongiovanni, N. Penazzi, Novel multiphase electrode/electrolyte composites for next generation of flexible polymeric Li-ion cells, J. Appl. Electrochem. 43 (2012) 137–145. doi:10.1007/s10800-012-0492-3.

[22] F. Di Lupo, G. Meligrana, C. Gerbaldi, S. Bodoardo, N. Penazzi, Surfactant-assisted mild solvothermal synthesis of nanostructured LiFePO4/C cathodes evidencing ultrafast rate capability, Electrochimica Acta. 156 (2015) 188–198. doi:10.1016/j.electacta.2015.01.048.

[23] Polymer electrolyte membranes and process for the production thereof, n.d. http://www.google.com/patents/WO2015104727A1 (accessed March 7, 2016).

[24] J.R. Nair, L. Porcarelli, F. Bella, C. Gerbaldi, Newly Elaborated Multipurpose Polymer Electrolyte Encompassing RTILs for Smart Energy-Efficient Devices, ACS Appl. Mater. Interfaces. 7 (2015) 12961–12971. doi:10.1021/acsami.5b02729.

# CHAPTER THREE

## *Quasi-solid polymer electrolytes based on high boiling point glyme plasticizers*

### 3.1 INTRODUCTION

In the previous chapter, it was shown that UV-induced cross-linking could be a versatile tool to incorporate large amounts of room temperature ionic liquids (RTILs) in polymer electrolyte membranes with the aim of increasing room-temperature ionic conductivity and, at the same time, retain sufficient mechanical properties due to the crosslinked nature of the network. However, despite the excellent properties of RTILs, such as non-volatility, non-flammability, and intrinsic high ionic conductivity, these materials are known to reduce substantially the lithium-ion transference number. In the solution of a lithium salt in a RTIL, only a small fraction of the total cationic current is carried by lithium-ion, the rest being carried by the positive ion of the RTIL. Indeed, the lithium-ion transference number is an important parameter as it accounts for the fraction of the overall ionic current that is

actually useful for the lithium-ion cell chemistry. Thus, 1-ethyl-3-methylimidazolium-bis(trifluoromethyl-sulfonyl) imide was replaced by tetraethylene glycol dimethyl ether and the results are described in this chapter.

Glymes are well known for complexing with metal-ions through their multiple ether-like oxygen atoms [1]. When a lithium salt is dissolved in glyme-based solvents, the resulting solutions show promising ionic conductivity and $Li^+$ ion transport properties [2,3]. Due to the excellent properties imparted by glymes in the liquid electrolyte, recently they have received plenty of attention for next-generation systems beyond Li-ion, such as lithium sulphur [4] and lithium air rechargeable batteries [5].

Most of the systems referring to glyme-based electrolytes are either blended with thermoplastic materials or directly used in their liquid form. Little work [6] has been devoted to study their possible implementation in a self-standing, softly cross-linked thermoplastic polymer matrix. In the present study, a system based on PEO and tetraglyme was developed, and directly cross-linked in one-pot along with the supporting lithium salt under UV irradiation to retain the solid-like nature and dimensional stability. By concurrent exploitation of photo-induced cross-linking and in situ functionalization procedures, kinetically driven inhibition of the PEO chains crystallization was readily achieved at ambient conditions, leading to polymer electrolytes that possessed solid-like properties without hampering ionic mobility. They were prepared by mixing PEO as the polymer matrix, tetraethylene glycol dimethyl ether (tetraglyme, TEGDME) as the active plasticizer, lithium bistrifluoromethane sulfonimide (LiTFSI) as the source of

$Li^+$ ions and 4-methyl benzophenone (MBP) as the light-induced hydrogen abstraction mediator (photoinitiator). Under UV excitation, MBP may abstract an acidic proton from a methylene group and generate a free radical chain [7]. This free radical may combine with another free radical belonging to the same chain or other –EO– chains to interlink themselves. The final interlinked solid polymer electrolyte (ISPE) films are mechanically robust, highly flexible, homogeneous and largely amorphous. They also exhibit excellent properties in terms of compatibility with the lithium metal electrode and suppression of hazardous dendrite growth. The sum of these characteristics enlighten the striking prospects of the newly developed ISPE as electrolyte separators in both Li-ion and Li metal batteries conceived for high energy and/or power demanding applications, including hybrid vehicles and smart grid storage systems.

## 3.2 EXPERIMENTAL SECTION

### 3.2.1 PREPARATION OF THE QUASI-SOLID POLYMER ELECTROLYTE

The reactive formulations were based on poly(ethylene oxide) (PEO, average Mw 100,000, Sigma-Aldrich) and a high boiling point plasticiser bis[2-(2-methoxyethoxy) ethyl]ether (tetraglyme, TEGDME, Sigma-Aldrich) along with bis(trifluoromethane) sulfonimide lithium salt (LiTFSI, battery grade, Solvionic). The photo-induced hydrogen abstraction facilitator was 4-methylbenzophenone (MBP, Sigma-Aldrich). Calculated amounts of the materials were heat treated at 70 °C for 3 hours. After blending, the resulting

mixture was hot-pressed at 90 °C for 15 min to obtain a homogeneous thin film. The film was later exposed to UV light for 6 min to reticulate the reactive species, thus obtaining the cross-linked ISPE of average thickness 90 ± 10 μm. The solid and non-tacky film was peeled off from the substrate (Mylar sheet), and used for further characterization. The procedure was carried out in the dry room (10 $m^2$, R.H. <2% ± 1 at 20 °C) produced by Soimar (Caluso, Italy).

### 3.2.2 CHARACTERISATION OF THE POLYMER ELECTROLYTES.

The physico-chemical characterization techniques used for sample characterisation are described in the Appendix.

### 3.2.3 PREPARATION OF ELECTRODE-ELECTROLYTE COMPOSITES

Electrodes were prepared from a slurry that contains $TiO_2$ (Hombicat-100) or $LiFePO_4$ (Clariant-LP2), carbon black and PVdF in the 70:20:10 weight ratio, respectively. The slurry was deposited over a Cu (or Al) current collector foil and later dried overnight (120 °C). In a typical preparation procedure, appropriate amounts of PEO, tetraglyme, LiTFSI and MBP were mixed at 70 °C and mechanically grinded to obtain a viscous paste-like mixture. This mixture was later deposited over a composite electrode film, and hot pressed (20 bar, 90 °C) for 15 min to obtain a uniform coating over the electrode surface. This setup was exposed to UV light for 6 min to obtain

a cross-linked polymer electrolyte system. Then, electrolyte/electrode disks (area 2.54 $cm^2$) were cut from the sheet and dried under vacuum overnight at 40 °C prior to cell assembly. The electrodes we used in the present case are not pressed/calendared prior to pre-polymer deposition, which can help in retaining some pores/voids for the electrolyte components to accommodate while overall processing.

## 3.3 RESULTS AND DISCUSSION

### 3.3.1 PHYSICAL – CHEMICAL CHARACTERIZATION

A schematic representation of the preparation procedure, along with the materials used, is shown in **Figure 3.1**. In the same Figure, the aspect is shown of the ISPE formed after UV exposure (right top), which is almost transparent, tack free, flexible and easy to handle. On the right bottom side of **Figure 3.1**, the possibility of interlinking of polymer chains is hypothesized, with the in situ oligomer formation and plausible grafting of TEGDME molecules onto the long PEO chains upon 6 min of UV irradiation (intensity on the surface of the sample of 40 mW $cm^{-2}$).

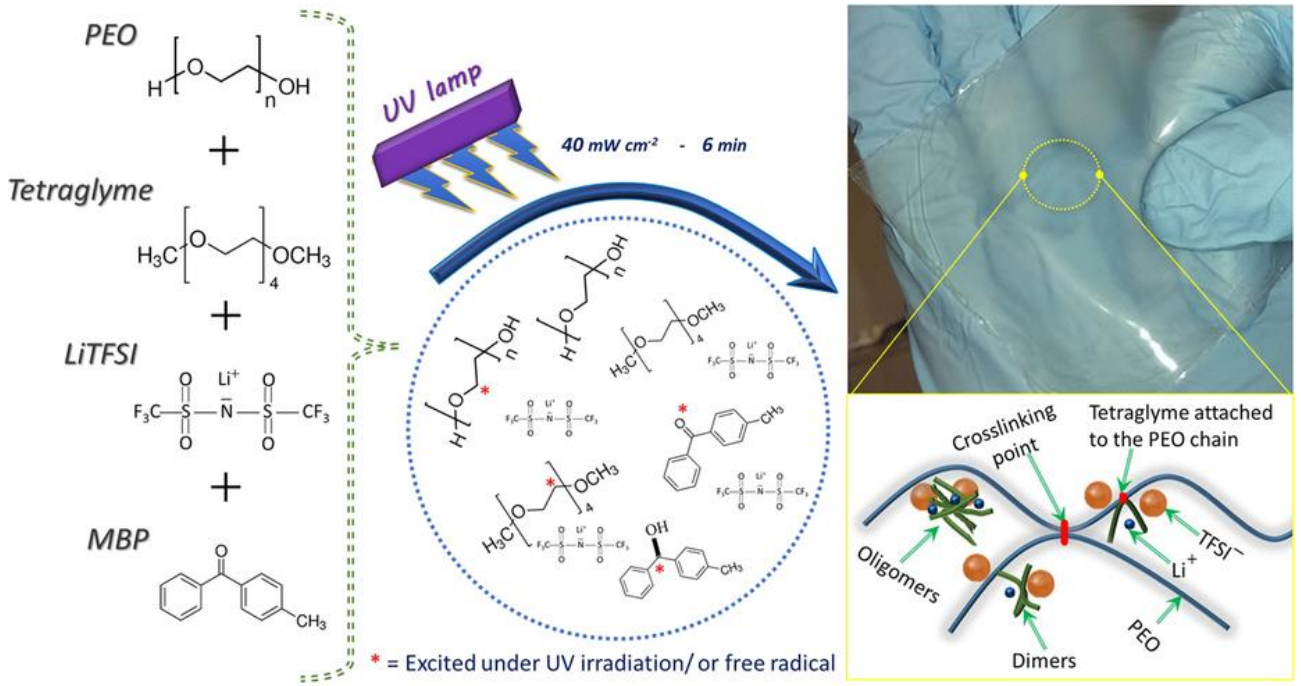


**Figure 3.1**. Sketched representation of ISPE preparation along with used materials, and plausible illustration (right bottom) of interconnected PEO chains with hypothesized branched clusters of tetraglyme oligomers; on the top right, the real aspect of a freshly prepared ISPE.

The overall characteristics and composition of the different samples under study are listed in **Table 3.1**, including the glass transition temperature ($T_g$) values and the gel content (insoluble fraction after cross-linking) against the corresponding –EO– to Li ratio.

**Table 3.1. Composition of ISPEs, along with their $T_g$ and gel-content values.**

| | LiTFSI$^{\Psi}$ | PEO$^{\Psi}$ | TEGDME$^{\Psi}$ | $T_g^{\S}$ | Gel$^{\Psi}$ | EO:Li |
|---|---|---|---|---|---|---|
| PTL-1 | 10 | 41.3 | 41.2 | −34 | 42 ± 2 | 54:1 |
| PTL-2 | 15 | 38.8 | 38.7 | −38 | 39 ± 2 | 35:1 |
| PTL-3 | 20 | 36.3 | 36.2 | −44 | 37 ± 3 | 23:1 |

MBP content is 7.5 wt. % of the total weight of materials. $^{\Psi}$units in wt. %. $^{\S}$unit in °C.

High-resolution FESEM analysis at 50K magnification of sample PTL-1, is shown in **Figure 3.2 (a–d**). It shows the characteristics of a soft, cross-linked polymer electrolyte with rather high degree of amorphous nature. The micrographs are well in agreement with the results obtained by Schulze et al. [8], who used a one-pot synthetic strategy based on polymerization-induced phase separation to generate nanostructured polymer electrolytes that exhibited an unprecedented combination of high modulus and ionic conductivity. In the present case, phase separation is not possible as the material is made of similar –EO– based backbones. Indeed, viscosity as well as polymerization induced aggregation and-to a certain extent - rearrangement of the PEO chains could be possible.

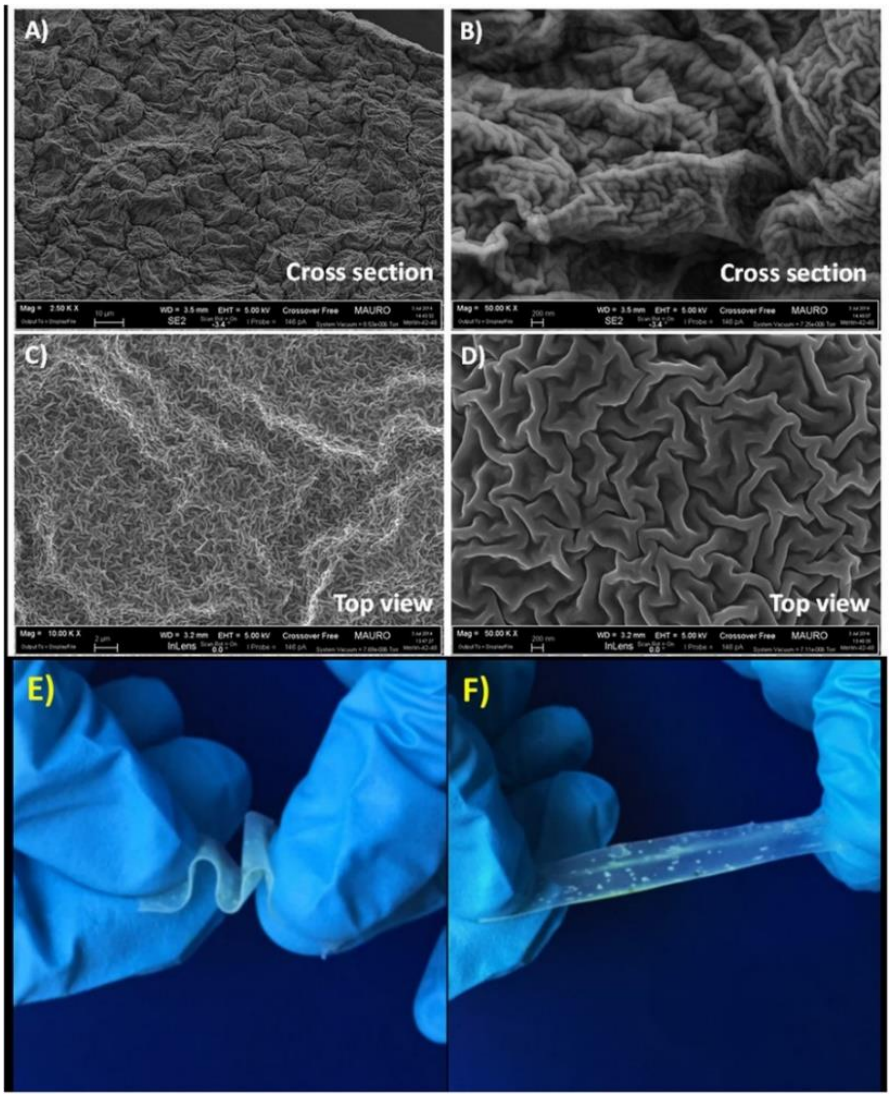


**Figure 3.2.** Micrographs showing the overall morphology of sample PTL-1: cross-section under secondary electron mode (a,b) and top view (c,d), at different magnifications; (e,f) shown the images of the sample PTL-1 (at 25 °C) under stretch and bend mode, demonstrating the mechanical integrity and excellent elasticity.

The photopolymerisation was carried out after keeping the highly viscous reactive mixture under conditions of mechanical stress (90 °C, pressed at 20 bar) between two Mylar foils [9]. In particular, micrographs clearly evidence the exceptional homogeneity of the sample, a characteristic wrinkled structure is repeated on the polymer membrane with no noticeable presence of pores or voids. Moreover, the images showed in **Figure 3.2 (e,f)** demonstrate that the obtained ISPE is stretchable and highly elastic (once the stress is released, it can go back to the previous shape). These results all together confirm that the proposed electrolyte is soft, weakly cross-linked, flexible, and shape retaining at ambient conditions.

The differential scanning calorimetry (DSC) values are tabulated in **Table 3.1**, and the respective profiles are shown in **Figure 3.3**. Both the glass transition and the melting temperatures were determined for all the samples. $T_g$ values vary between –34 and –44 °C. As expected, the amount of salt noticeably influences the $T_g$ of the ISPEs prepared with 1:1 tetraglyme to PEO ratio. Generally, low $T_g$ values account for a moderately enhanced segmental motion of the –EO– moieties in the polymer matrix, which is facilitated by low crystallinity. Moreover, a noticeable change in the peak associated with the melting of the crystalline region is clearly evidenced: an increase in LiTFSI content reduces the intensity of the melting peak, which also results broadened. As noted in **Table 3.1**, an increase in salt content reduces the [EO]/[Li] ratio from 54:1 to 23:1. Thus, an increased amount of $Li^+$ ions is available for the coordination with PEO chains, thus reducing the tendency of forming crystalline phases. Moreover, the cross-linking effect further reduces the mobility of the PEO main chains. Overall, a relationship

is present between the phase transition temperature and the salt content: the higher is the salt content; the lower is the transition temperature. This is expected as for the typical coordination effect by lithium salt, which weakly decreases the $T_g$ [10].

Furthermore, ISPEs in all cases exhibit crystalline melting peaks near room temperature during the heating cycle of the DSC analysis. This may be attributed to low cross-linking density ($7.7 \times 10^3$ mol $m^{-3}$ for PTL-1, calculated at 0 °C), which allows the long enough –EO– chains to rearrange and crystallize in the matrix [11]. It is worth noting that the melting points of these newly elaborated polymer electrolytes are well below the typical PEO-based electrolytes when tested by means of DSC [10,12]. If one calculates the number of MBP molecules per –EO– moieties, the latter exceeds 46 ± 3 per each photoinitiator molecule. This ratio is sufficient to enforce the rearrangement of the –EO– moieties to form weak crystalline phases. One cannot neglect the effect of tetraglyme in diluting the number of cross-linking per area, as some of the initiator molecules are actively involved in real-time oligomerization and eventual branching processes. Thus, the effective cross-linking would be lower than the theoretical calculations from mole ratios. Overall, the average cross-linking length obtained in the present study suggests that cross-linking is not sufficient to prevent the PEO crystallization. It can be hypothesized that a higher degree of cross-linking may not be also favoured, as it may induce the low molecular weight tetraglyme and/or its oligomers to squeeze out of the system during thermal stresses. Thus, an optimum cross-linking was selected, which could assure a good mechanical integrity along with good plasticizer retention (leak free).

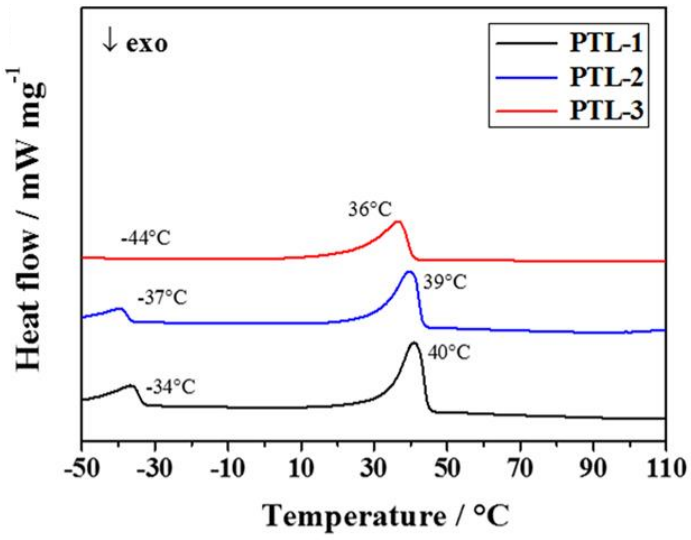


**Figure 3.3** Differential scanning calorimetry (DSC) curves of the ISPEs PTL-1 to PTL-3 containing various amounts of LiTFSI salt.

The thermal gravimetric analysis (TGA) plot is shown in **Figure 3.4**. It shows three main weight losses for all the samples. The first one is associated to tetraglyme loss, the second one to PEO decomposition and the last one to lithium salt decomposition. The first dip before 100 °C indicates the loss of humidity that may be absorbed during the handling of the sample for testing. Taking into account the experimental errors related to the measurement and the sample preparation, the overall weight loss is consistent with the polymer electrolyte composition. According to the differential thermal analysis (shown in dotted lines), the weight loss occurs

for all the samples above 190 °C, the major contributor being tetraglyme [11]. Higher amounts of LiTFSI reduce the thermal stability of the polymer matrix, which is clearly visible in the differential curves (shift of the peak from 218 to 195 °C). This could be the general trend observed for tetraglyme kind of plasticizers that show the tendency to decompose in reaction with fluorinated anions [1].

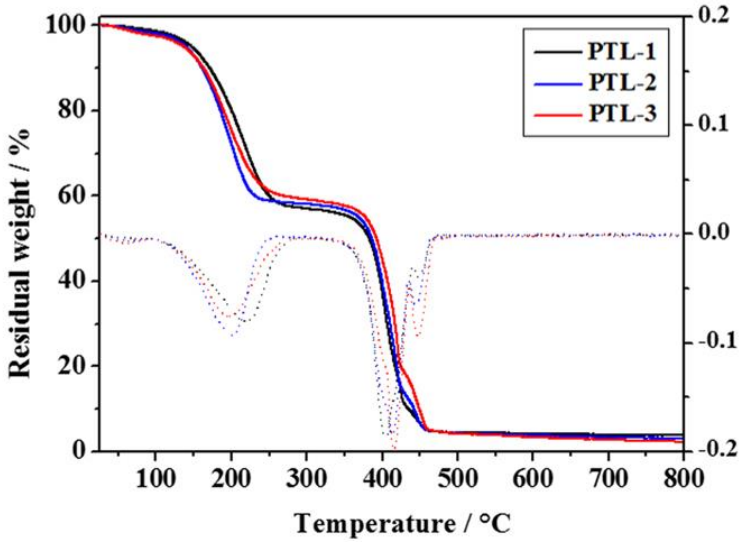


**Figure 3.4** Thermogravimetric analysis (TGA) of the same series of ISPEs along with related differential curves (dotted lines of same colour code). Taking into account the experimental errors related to the measurement and the sample preparation, all weight losses are consistent with the polymer electrolyte compositions.

Thus, both DSC and TGA profiles show that no unusual phase changes or weight losses occur in the temperature range between 25 and 150 °C, which makes the material thermally stable and useful as a polymer electrolyte under standard operating conditions in real battery configuration.

Dynamic mechanical thermal analysis (DMTA) were performed. Sample PTL-1 was considered as the representative for all the samples prepared and the resulting profiles (both modulus and loss modulus) are shown in **Figure 3.5 (a,b)**. It clearly indicates that the material has low $T_g$, which is in agreement with the DSC analysis.

In addition, the calculated cross-linking density ($7.7 \times 10^3$ mol $m^{-3}$, calculated at 0 °C) was found to be comparatively lower than other known systems [13]. This is an indication that the number of cross-linking points between the PEO chains is lower than expected, which allows the long enough –EO– chains to rearrange and crystallize in the matrix.

Tensile tests were carried out on the PTL-1 sample according to ASTM Standard D638; the Young's modulus was found to be 0.3 MPa and maximum force at break was found to be 1.5 MPa. The material can stretch very well under stress (see **Figure 3.6**), as justified by the maximum strain (elongation) of around 17 mm before the membrane was broken.

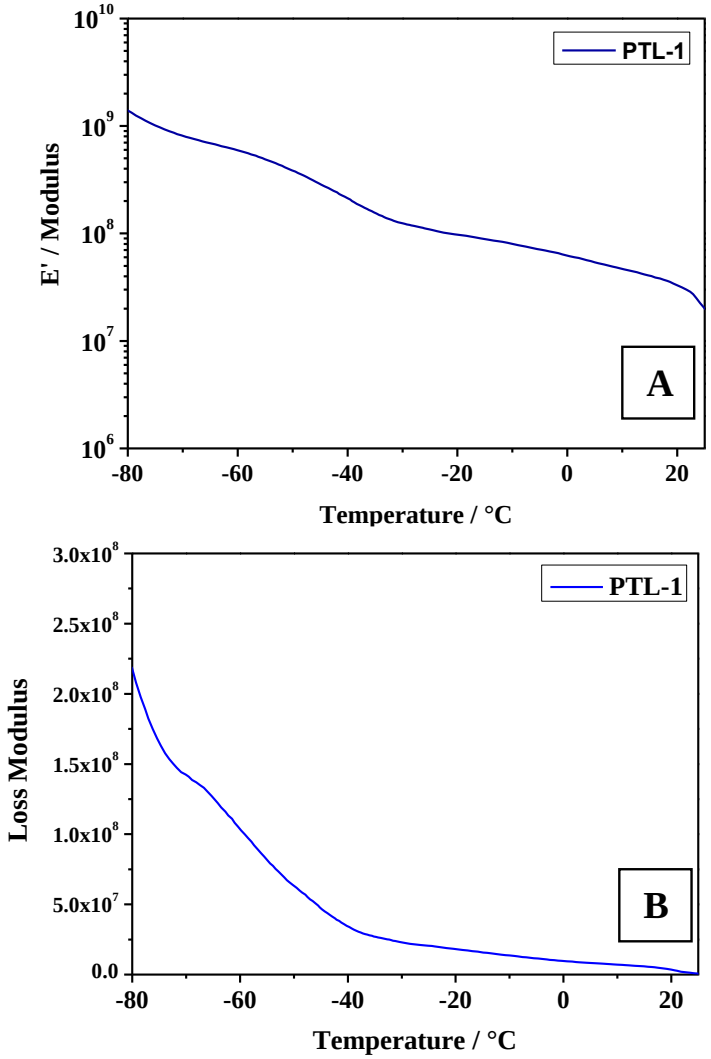


**Figure 3.5** Modulus profile (a) and loss modulus profile (b) of PTL-1 sample, in which the results are shown for DMTA tests carried out between –80 to 30 °C. Above 20 °C, the test failed due to the extra-soft characteristics of the polymer membrane if compared to the applied force from the instrument (10 N).

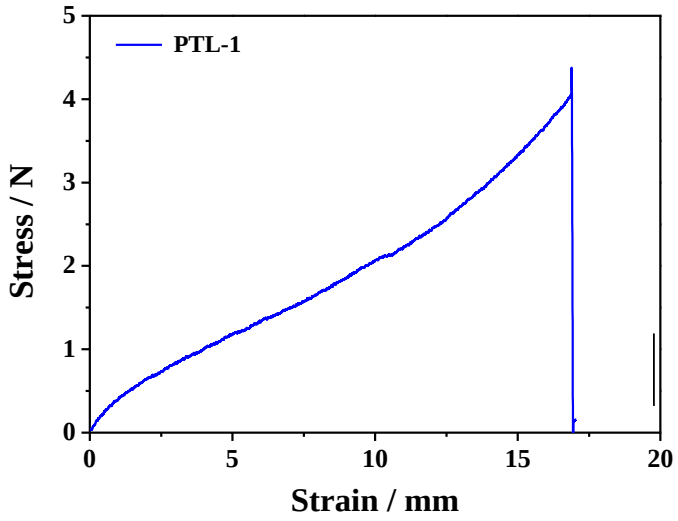


**Figure 3.6.** Tensile tests (reported as Stress/Strain curve) carried out on sample PTL-1 according to ASTM Standard D638, using a Sintech 10/D instrument equipped with an electromechanical extensometer (clip gauge).

The insoluble fraction (gel content) of the cross-linked polymer was determined by extracting with THF for 24 hours using a Soxhlet apparatus. Gel content values between 37 and 42 % were obtained for the crosslinked polymer electrolytes, and are given in **Table 3.1**. These values are generally lower than that obtained in the previous chapter when PEO and room temperature ionic liquids (RTILs) were used.

Indeed, tetraglymes possess accessible protons that can take part in the dehydrogenation reaction under UV irradiation in the presence of the photoinitiator. Thus, tetraglyme molecules may take part in the polymerization reaction to form oligomers or react with the radicals

generated on the PEO backbones. These oligomers formed by tetraglyme may not remain in the polymer matrix, which may account for the lower insoluble fraction of the cross-linked material obtained during extraction with THF.

FTIR studies (**Figure 3.7**) were performed on sample PTL-1 with and without UV curing to unravel any drastic difference induced by the irradiation. The FTIR spectra are identical and no noticeable changes are observed, which confirms that the soft cross-linking strategy does not induce any drastic modification in the polymeric components as well as with respect to the TFSI− anion. Moreover, for comparison purposes, FTIR analysis of liquid TEGDME added with 10 wt. % of LiTFSI was performed and compared to the spectra of PTL-1. Differences were found in the obtained spectra. In general, three kinds of ions can be present in an electrolyte system: free ions, free ions co-existing with ion pairs and aggregates [14]. PTL-1 analyzed after UV-curing was almost absent with the peaks corresponding to aggregates (1236 and 1143 $cm^{-1}$) if compared to the LiTFSI/TEGDME system that contains the same wt. % of lithium salt. As a result, it can be assumed that the electrolyte is enriched with free ions and neutral ion pairs, which can move faster in the polymer matrix.

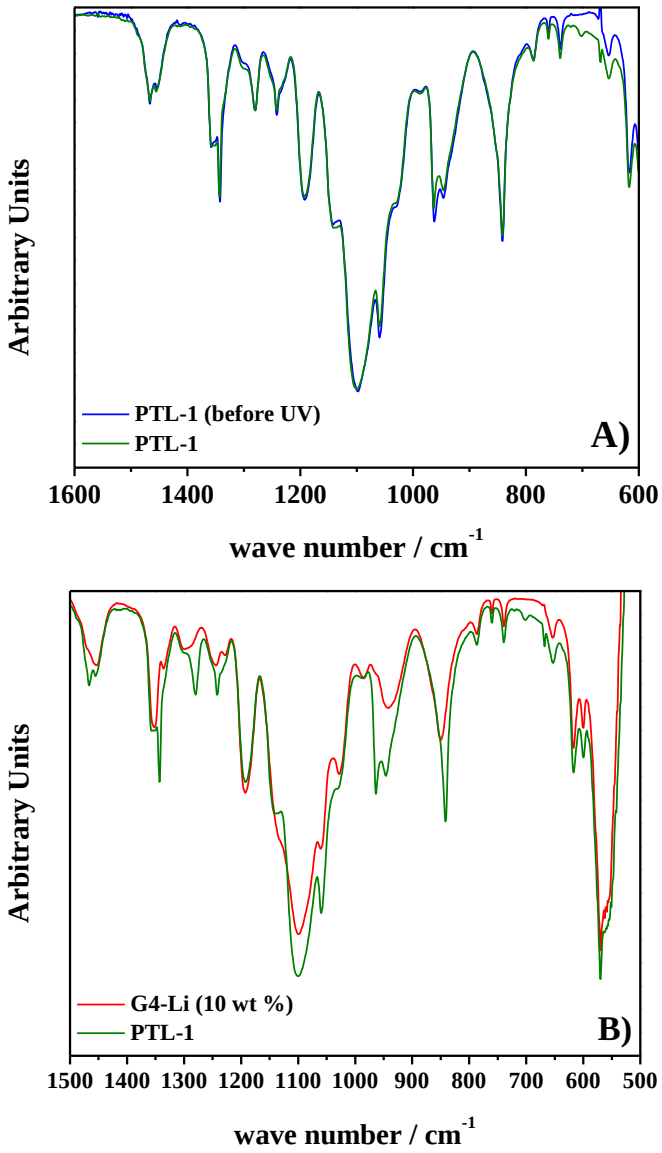


**Figure 3.7** (a) FTIR profiles of PTL-1 before and after UV curing; (b) FTIR profiles of PTL-1 and liquid TEGDME-LiTFSI. The tests were carried out at room temperature.

### 3.3.2. ELECTROCHEMICAL CHARACTERIZATION

Electrochemical impedance spectroscopy (EIS) analysis was carried out between 0 and 85 °C. The Arrhenius plots for all samples are shown in **Figure 3.8 A**. The plots of PTL-1 to PTL-3 demonstrate the influence of the lithium salt when PEO to tetraglyme ratio is 1:1. It is widely accepted that ionic conductivities exceeding 0.1 mS $cm^{-1}$ at room temperature are necessary for an electrolyte to function in real battery configuration. Nevertheless, the crystalline domains of PEO-based polymers restrict the ionic mobility. Recently, Khurana et al. [15] reported a cross-linked –EO– based polymer electrolyte showing an ionic conductivity higher than 0.1 mS $cm^{-1}$ at 25 °C. In the present study, even improved ionic conductivities (0.40 mS $cm^{-1}$ for PTL-3) were achieved for interlinked PEO-based solid polymer electrolytes. The conductivity values increase with an increase in the salt concentration, then reaching the maximum for PTL-3 where the −EO− to Li ratio is 23:1. However, the difference is not huge; indeed, all membranes demonstrate conductivity values ≥0.1 mS $cm^{-1}$ at 25 °C. It was decided not to increase the salt concentration further as for the ion pairing nature of TFSI-based salts, which strongly influences the ionic mobility, probably due to the saturation of the hopping sites [16]. It is worth mentioning that the sample retains good elastic and mechanical integrity under stress. After several days of conductivity tests, which were carried out under 10 N pressure, it was observed that the membrane retains its size and shape without any noticeable damages around the edges. Indeed, the thickness variation after the test was <2%. This is an encouraging result as ISPEs are super soft, low

$T_g$ and highly plasticized. Further, it confirms that no leakage of tetraglyme from the polymer matrix occurs.

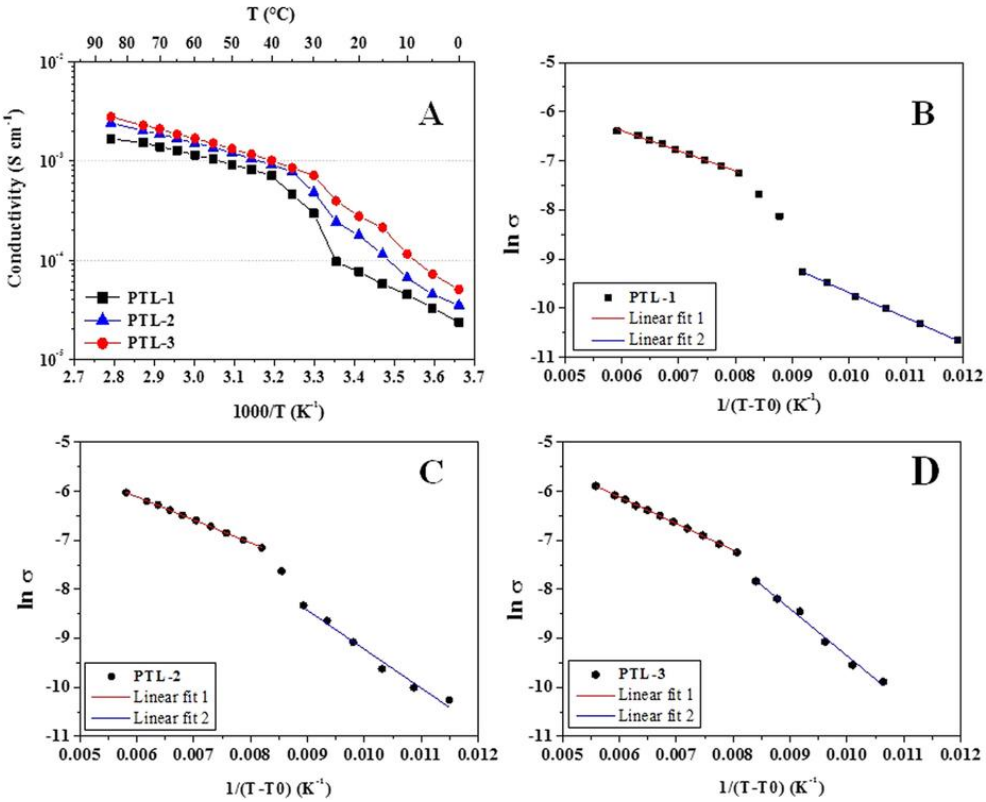


**Figure 3.8.** (A) Arrhenius plot showing the ionic conductivity vs. temperature for ISPEs prepared with various LiTFSI content. (B–D) VTF fitting of the samples PTL-1 to PTL-3.

Generally, for polymer electrolytes the dependence of ionic conductivity upon the temperature is not straightforward. The overall plot that starts from 0 to 85 °C does not exhibit a linear behaviour. Between 0 to 30 °C, the

conductivity increases with Vogel–Tamman–Fulcher (VTF) dependence for all ISPEs. The same behaviour (see **Figure 3.8 B–D**) is observed above the melting point between 35 and 85 °C. The deflection around 30 °C reflects the phase transitions occurring due to the melting of crystalline regions or rearrangement of –EO– moieties, which is in agreement with the behaviour observed by DSC analysis (see **Table 3.2**).

**Table 3.2.** Ionic conductivity (σ, at 25 °C) and related characteristics of ISPEs prepared with different salt content.

| Name | Ea/Ea' # | $t_{Li+}$ | $D_{Li+}$ $ | Σ * |
|---|---|---|---|---|
| PTL-1 | 4.3/3.4 | 0.55 ± 0.06 | $5.6 \times 10^{-6}$ | 0.11 |
| PTL-2 | 6.6/3.9 | 0.48 ± 0.02 | $1.2 \times 10^{-7}$ | 0.24 |
| PTL-3 | 7.9/4.5 | 0.32 ± 0.08 | $2.1 \times 10^{-8}$ | 0.40 |

$E_a$ is the activation energy before deflection (0 to 30 °C). $E_a$' is the activation energy after deflection (35 to 85 °C). $t_{Li+}$ is the lithium transference number; $D_{Li+}$ is the lithium diffusion coefficient. *mS $cm^{-1}$. #kJ $mol^{-1}$. $cm^2$ $s^{-1}$.

The mechanism of ionic conductivity in polymer electrolytes can be understood from activation energy ($E_a$) calculations. $E_a$ was calculated by fitting the conductivity values with VTF equation [1]. The corresponding plots were used to determine the $E_a$ of the electrolyte system. The VTF equation is believed to describe the conduction behaviour of highly concentrated liquid electrolytes and molten salts [17]. As listed in **Table 3.2**, $E_a$ varies from 4.3 to 7.9 kJ $mol^{-1}$, when the data are fitted with VTF equation below the deflection point, in the Arrhenius plot of **Figure 3.8 (a)**. When the

curves are fitted above the deflection point (35–85 °C, $E_{a'}$), values ranging from 3.4–4.5 kJ $mol^{-1}$ are obtained. The values obtained are superior to the data reported in the recent literature [18]. Above 0 °C, the ionic conductivity increases with a VTF-like dependence for all the samples. The discontinuities around 30 °C may be related to thermal transitions, which may include chain rearrangement, dielectric relaxations or melting of crystalline domains, formed by the PEO chains between two cross-linking points. Noteworthy, $E_a$ increases with an increase in the salt concentration, which is ascribed to the formation of ion pairs and increased viscosity of the polymer matrix. Thus, the high ambient temperature conductivity values of the PTL series of electrolytes are predominantly associated with high ionic mobility.

The lithium-ion transference number ($t_{Li+}$) was calculated using the method reported by Evans et al. [19]. An optimum $t_{Li+}$ is necessary for the functioning of a polymer electrolyte in a Li-ion cell. Low $t_{Li+}$ induces the build-up of anion concentration gradients, which may lead to cell polarization at high power rates. Low $t_{Li+}$ may also induce dendrites growth in Li-metal cells, which is one of the major obstacles restricting the widespread intrusion of such batteries into the market[20–23]. In the family of polymer electrolytes under study, sample PTL-1 (**Figure 3.9**) shows the highest transference number (0.55 ± 0.06, **Table 3.2**) at 25 °C. It is worth noting that at higher salt concentrations, $t_{Li+}$ reduces to smaller values, which may be ascribed to the formation of anion pairs or aggregates. Overall, the transport number in the PTL series of samples is comparatively higher than the classical literature data on polymer electrolytes, but it is close to the data obtained for systems that contain tetraglyme as co-solvent [24–26].

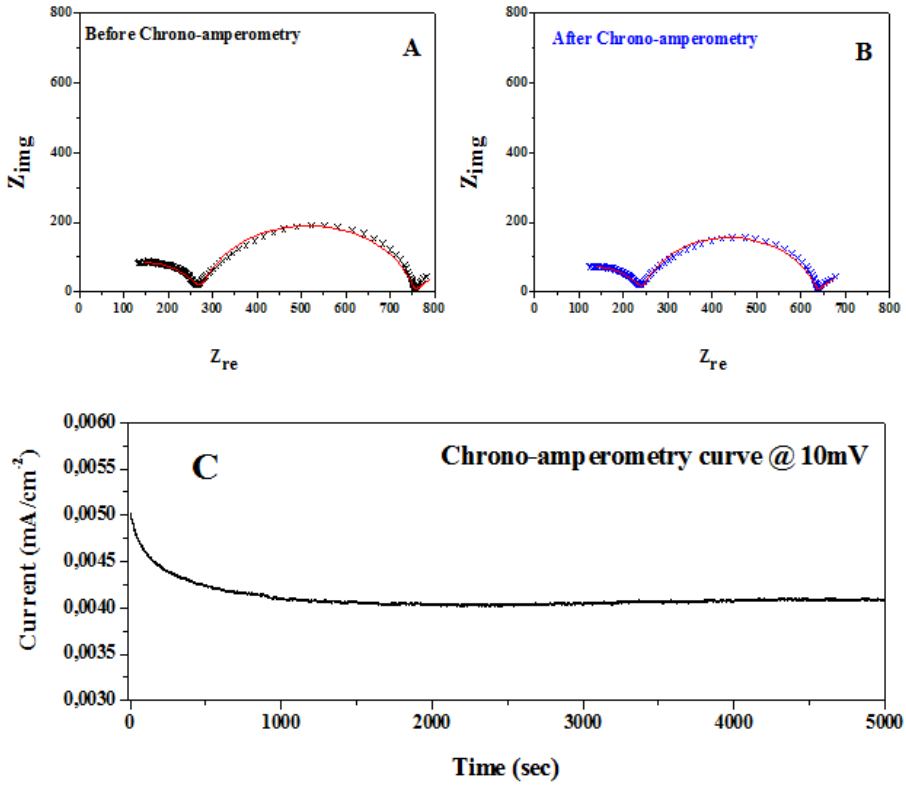


**Figure 3.9. (a,b)** Nyquist plot of a membrane assembled in a symmetric cell (Li/PTL-1/Li) and tested at 20 °C in the frequency range between 2 MHz and 0.1 Hz, before and after the chrono-amperometry test; **(c)** Chrono-amperometry curves obtained for PTL-1 containing cell, tested at 10 mV polarization until obtaining a steady state current under open circuit potential conditions. Tests were carried out for all the samples, but only PTL-1 is showed as the representative.

The reasons for such a high number is the absence of ion pairs, or the presence of more free ions and neutral ion pairs. Moreover, the oligomerisation of tetraglyme moieties weakens the coordination between

$Li^+$ ions and O atom of TEGDME. This facilitates the movement of $Li^+$ ions inside the polymer matrix leading to improved transference number values. It was previously demonstrated by Kriz et al. [26] that tetraglyme can loosen the coordination of $Li^+$ ions with –EO– units of PEO chains, resulting in improved ion mobility, and might also enable $Li^+$ ions to decouple from ion pairs.

The $Li^+$ ion diffusion coefficient ($D_{Li+}$) can fit very well with the previously measured ionic conductivity and transference number. $D_{Li+}$ (see **Table 3.2**) was estimated using the method reported by Ma et al [25]. Typical responses are noted as natural logarithm of potential (V) versus time (t) at 25 °C. The results are in good agreement with the corresponding $t_{Li+}$ values. Moreover, PTL-1 shows the highest value ($5.6 \times 10^{-6}$ $cm^2$ $s^{-1}$), which is at least one order of magnitude higher than the literature reports for similar systems [25,27,28]. The presence of free TFSI ions and neutral ion pairs, which can move faster due to the reduced solvent salt interactions, thereby increase the disorder in the polymer matrix [14]. This result is in agreement with the conductivity, transport number and diffusion coefficient studies as well as supported by FTIR studies.

A deep understanding of the interfacial properties between the lithium metal electrode and the polymer electrolyte is necessary in order to provide more insight over the factors controlling the recharge ability of lithium-based polymer batteries. PTL-1 sample was examined in terms of compatibility (interfacial stability) with the lithium metal electrode. Sample PTL-1 was selected for further characterizations due to the optimal characteristics exhibited during the previously discussed analyses. As shown

in **Figure 3.10**, the PTL-1 based lithium symmetric cell shows stable resistance after few days of testing. Indeed, the resistance increases during the initial days of storage indicating an appropriate formation of a thin solid electrolyte interface (SEI) layer at the surface of the lithium metal electrode [29].

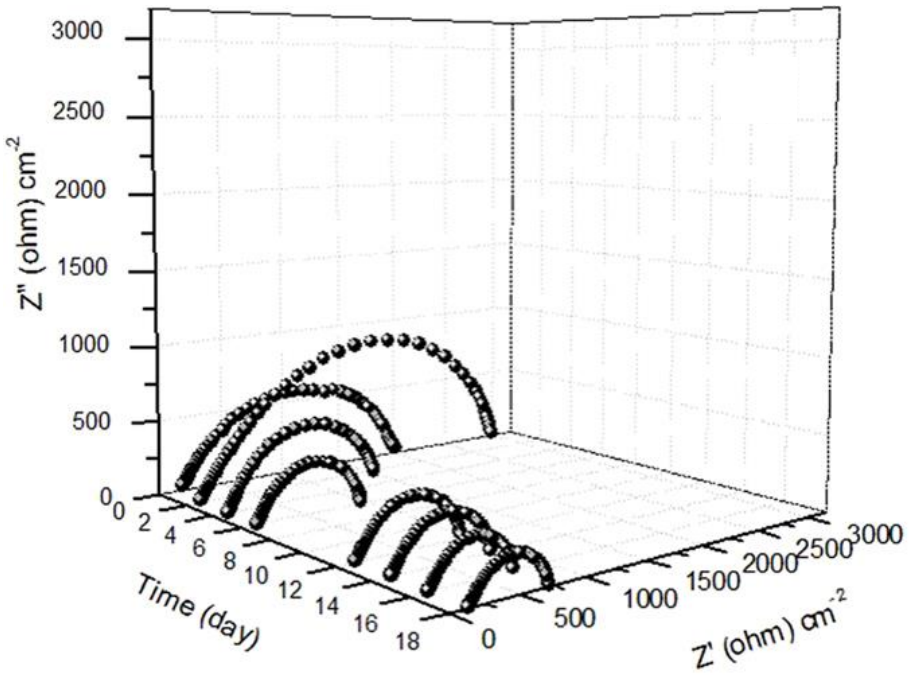


**Figure 3.10** 3D Nyquist plot representing the evolution of the interfacial resistance with time for sample PTL-1, using the Li/PTL-1/Li cell configuration.

The resistance rapidly decreases and stabilizes at around 700 Ω $cm^{-2}$ after about 6 days, accounting for the very stable interfacial characteristics of the

sample. This behaviour is typical of most of the polymer electrolytes, and is clearly related to the initial formation of the SEI layer, its stabilization and, then, the improved contact achieved with time at the interface between the lithium metal electrode and the polymer electrolyte [30,31].

Electrochemical stability window (ESW) is a fundamental parameter that determines the durability and energy output of a lithium cell. **Figure 3.11** shows the electrochemical stability of sample PTL-1 towards anodic oxidation and cathodic reduction reactions. The test was performed at 25 °C. From the cathodic profile, the almost ideally reversible lithium plating and stripping processes are well evidenced. Overall, a wide electrochemical window is accessible for the electrolyte to be safely used between 0 to above 5.2 V vs. $Li/Li^+$. Such a high anodic stability window can be explained by the simultaneous oxidative decomposition of both the TFSI anions, tetraglyme moieties and PEO matrix in the high potential regions [27]. In particular, the presence of tetraglyme in the electrolyte matrix increases the overall oxidation stability [24]. Even though the $CH_2$–$CH_2$–O– chemical moiety is same for both PEO and tetraglyme, the difference may arise from the –$CH_3$ end group of tetraglyme, which avoids the interaction between the electrode surface and the –OH terminal groups of PEO. However, the oxidation stability is anyway superior to the pure PEO-based system, and this is an intriguing aspect of this electrolyte. This value is excellent when one envisages the application with high voltage cathode materials.

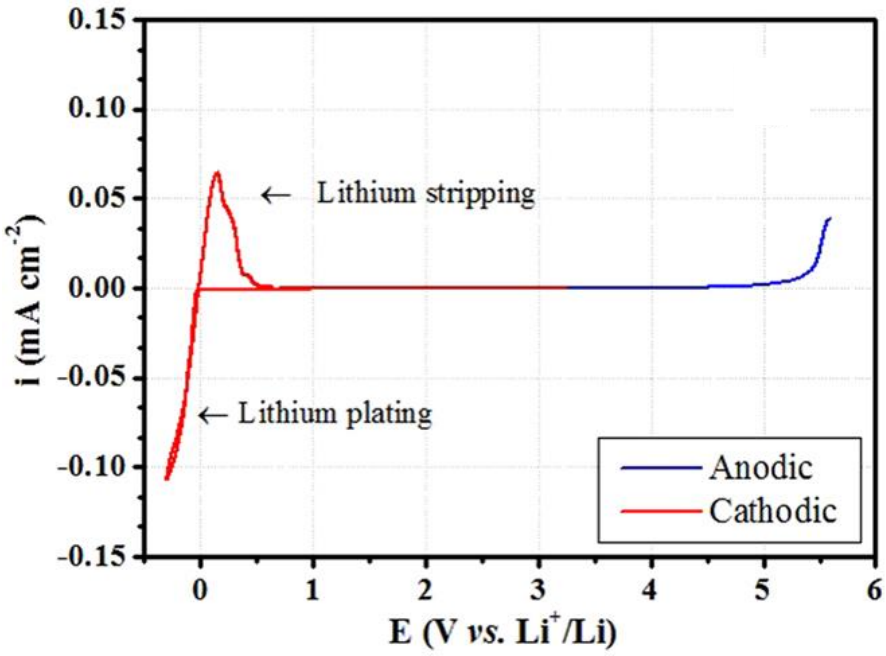


**Figure 3.11** Electrochemical stability window (anodic and cathodic scan) of PTL-1. The tests were performed at 25 °C.

Many researchers developed polymer electrolytes that exhibit ionic conductivity values as high as 0.1 mS $cm^{-1}$ at 25 °C [32,33], but very few investigated the lithium dendrite nucleation and growth resistance in real cell configuration [34]. Inspired by the dendrite studies reported by Balsara et al. [35] and Khurana et al. [15], galvanostatic lithium plating/stripping measurements in symmetric Li/PTL-1/Li cells were performed to determine the lifetime of the assembled lithium metal polymer batteries. Such a test is of utmost importance when very long-term ageing of lithium metal polymer

cells is envisaged [20]. Measurements were performed at 0.1 and 0.3 mA $cm^{-2}$ current densities at 25 °C (3 h Li-plating and 3 h Li-stripping). When the current density was increased from 0.1 to 0.3 mA $cm^{-2}$, a large change in the potential is observed due to the formation of a dendritic short circuit [20] as demonstrated in **Figure 3.12**. Thus, ISPE can be safely used at 0.1 mA $cm^{-2}$, which is assumed as a remarkable value for a quasi-solid electrolyte system operating at ambient temperature.

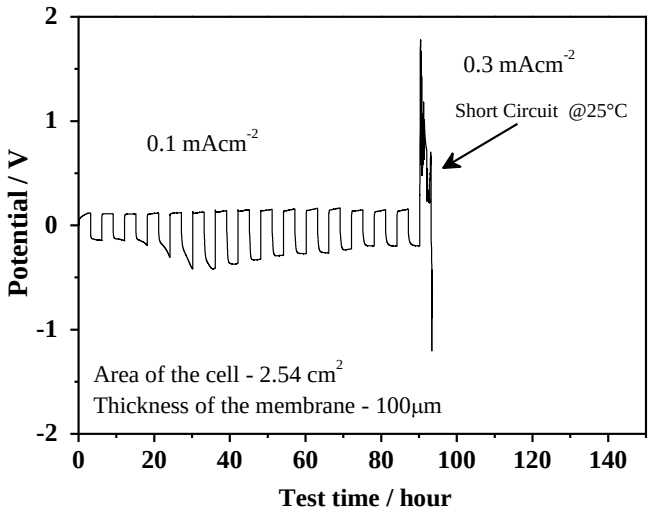


**Figure 3.12.** Galvanostatic cycling curve obtained for Li/PTL-1/Li symmetric cell at fixed current densities of 0.1 mA $cm^{-2}$ and 0.3 mA $cm^{-2}$ at 25 °C.

Prolonged galvanostatic cycling tests were performed (**Figure 3.13**) at 0.1, 0.2 and 0.05 mA $cm^{-2}$ with plating and/or stripping steps lasting for 30 min. This test assures the durability and safe operation of the ISPEs in lithium

metal cells conceived for ambient temperature applications. The total charge carried during the plating / stripping process is not very high, however, one can hypothesise that this is a good indication towards pursuing this path for future studies.

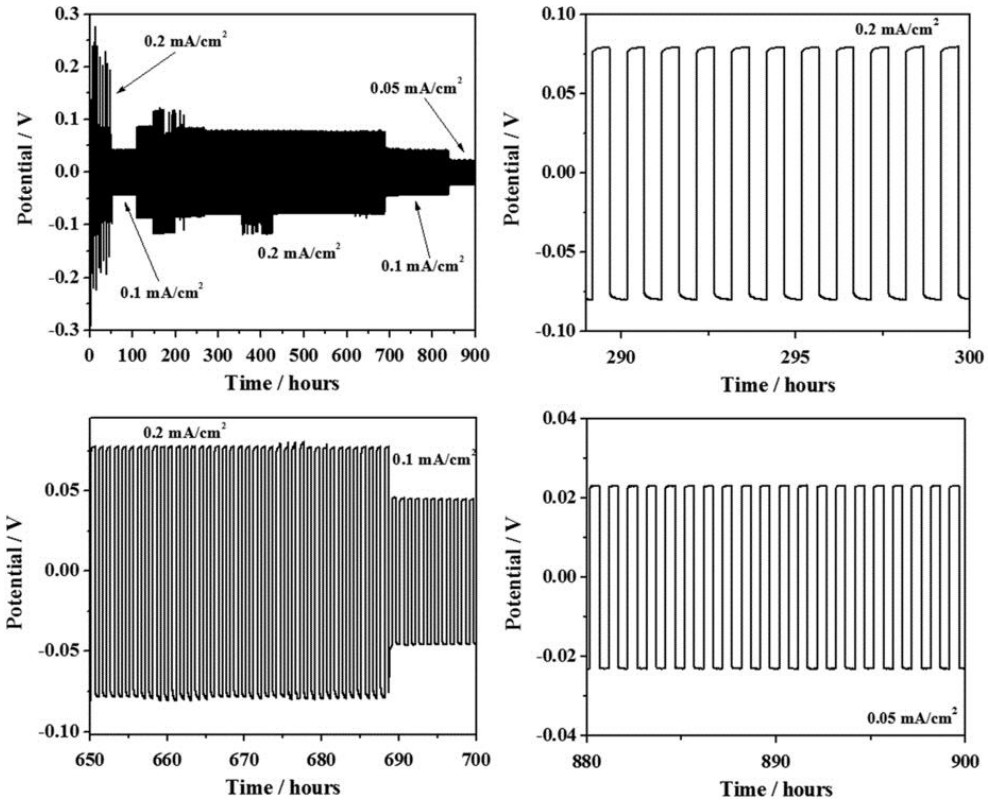


**Figure 3.13.** Potential vs. test time of lithium stripping and plating of a symmetrical lithium cell at various current rates (i.e., 0.05, 0.1, 0.2 mA $cm^{-2}$) at 25 °C.

To demonstrate its practical application, PTL-1 was assembled in a lab-scale all-solid-state Li-polymer cell, and galvanostatically cycled at ambient temperature. The cell was assembled by combining a Li-metal anode with an electrode/electrolyte composite prepared by in situ UV cross-linking the ISPE directly over the $TiO_2$-based working electrode (details in paragraph 3.2). One of the major drawbacks of typical truly solid polymer electrolytes is the insufficient contact between the electrode active materials and the polymer matrix. Thus, the direct cross-linking step over the electrode surface is fundamental to obtain a good electrode/electrolyte interfacial adhesion. The process enables us to obtain a stable and thin (≈30 µm) polymer electrolyte film with uniform distribution over the electrode. The general aspects of the bare electrode, electrolyte and the final aspect of the $TiO_2$-based electrode film are shown in **Figure 3.13 (a,b)**.

The cross-sectional FESEM images, **Figure 3.13 (c)**, show an intimate contact achieved between the active materials and the polymer electrolyte. Particularly at higher magnifications, it can be clearly observed that the electrolyte layer creates a conformal coating by following the contours of the electrode particles. This leads to improved active materials utilisation at the interface between the electrode and the polymer electrolyte, which correspondingly improves the specific energy and power of the cell. The oriented cross-linked polymer electrolyte morphology is observable on top of the electrode **Figure 3.13 (c)**, along with the optimum interface and interpenetration between the electrode active material particles and the electrolyte.

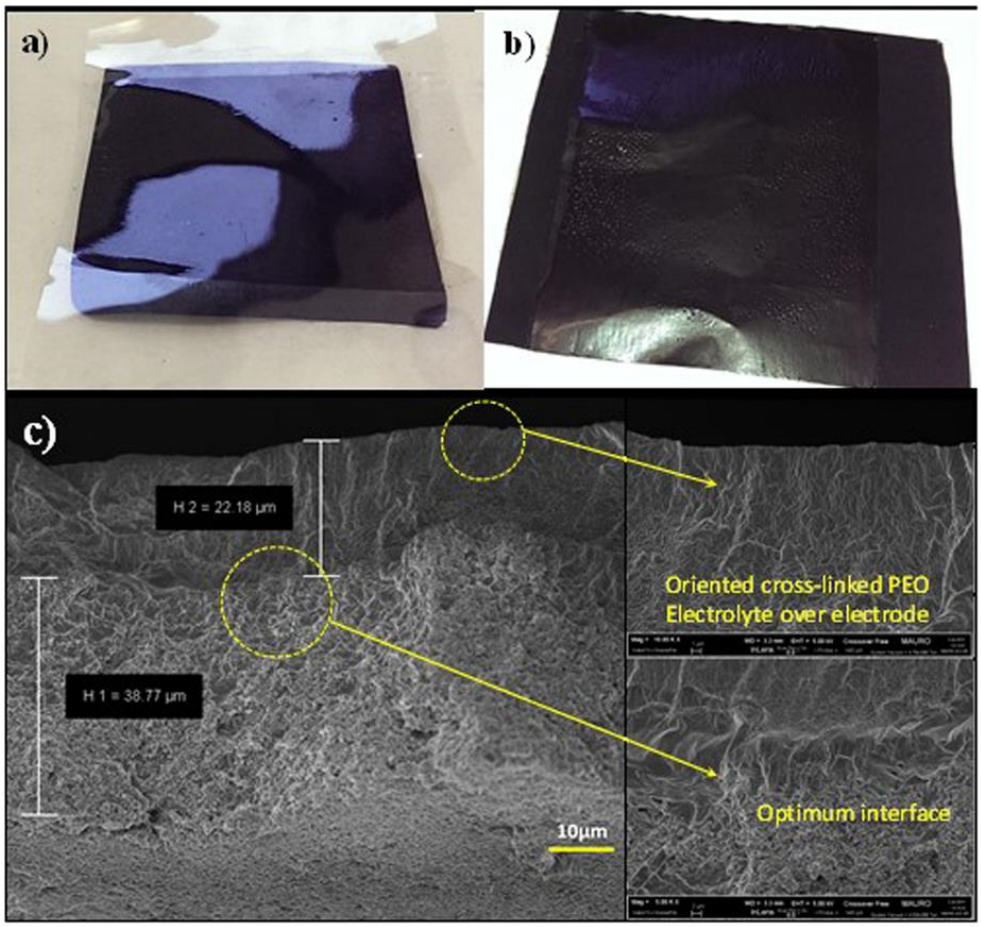


**Figure 3.13** (a) Photograph of bare $TiO_2$ based electrode and electrolyte before UV curing. (b) Freshly prepared self-supporting multiphase electrode/electrolyte composite obtained by direct hot-pressing and in situ photopolymerisation of the polymer electrolyte over the $TiO_2$-electrode film supported over copper foil. (c) Cross-sectional FESEM images showing the optimum interface achieved after UV curing.

The response of the cell at 0.1 mA $cm^{-2}$ is shown in **Figure 3.14** in terms of galvanostatic charge/discharge profiles and specific capacity vs. cycle number. The cell was prepared by just contacting a lithium metal foil at the polymer side of the electrode/electrolyte composite. The constant current charge/discharge profiles shown in plot (a) reflect the good properties of the electrolyte system, showing rather flat potential plateaus during charge and discharge cycles.

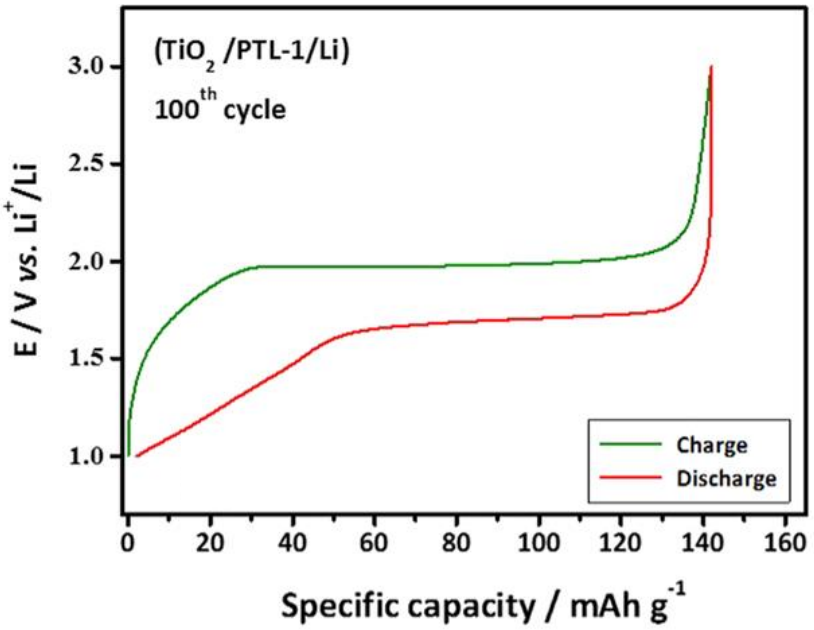


**Figure 3.14** Representative charge/discharge profiles of a cell assembled with the configuration of Li/PTL-1/$TiO_2$. The cycling test was performed at 20 °C at a current density of 0.1 mA $cm^{-2}$.

These are typical of the biphasic $Li^+$ extraction/insertion mechanism of crystalline $TiO_2$ anatase, with a steep potential increase/decay at its end. The polarization is rather limited, which accounts for an efficient redox reaction kinetics, due to the limited internal resistance at the electrode/electrolyte interface as well as the limited cell over potential contributions. In general, the material shows good cycling stability, as for the good overlapping of the charge/discharge curves, accounting for a Coulombic efficiency close to 100%, as shown in **Figure 3.15**.

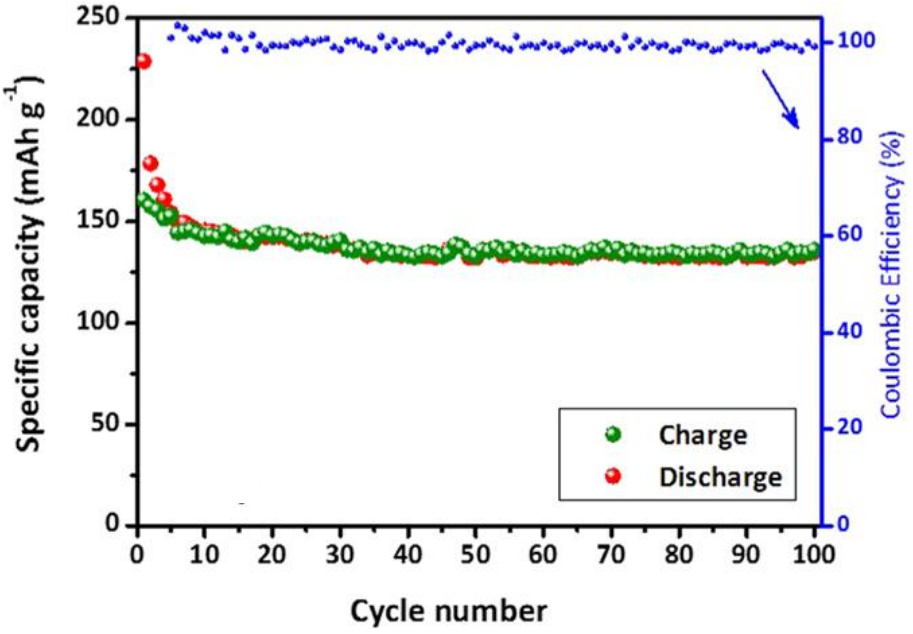


**Figure 3.15** Graph illustrating the specific capacity vs. number of cycles along with Coulombic efficiency.

The PTL-1 also demonstrated the ability to be galvanostatically cycled at 0 and 25 °C in lab-scale Li cell comprising a $LiFePO_4$-based composite cathode. Proof-of-concept charge/discharge profiles are shown in **Figure 3.16 - 17**, which clearly enlighten the possibility of designing an all-solid polymer battery system that functions at low temperature even with various electrode materials. At 0 °C, the all-solid-state cell showed an increased polarization, but still maintaining an appropriate functioning and demonstrated typical charge/discharge plateaus of $LiFePO_4$ electrode.

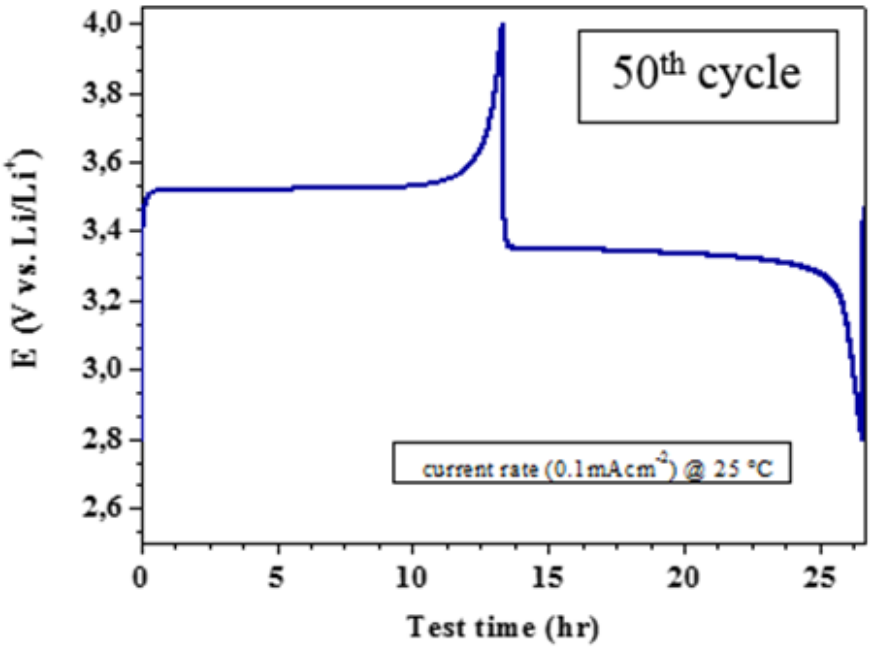


**Figure 3.16** Charge/discharge curve of a lithium test cell assembled with a configuration of Li/PTL-1/$LiFePO_4$. The test was performed at 25 °C at current densities of 0.1 mA $cm^{-2}$.

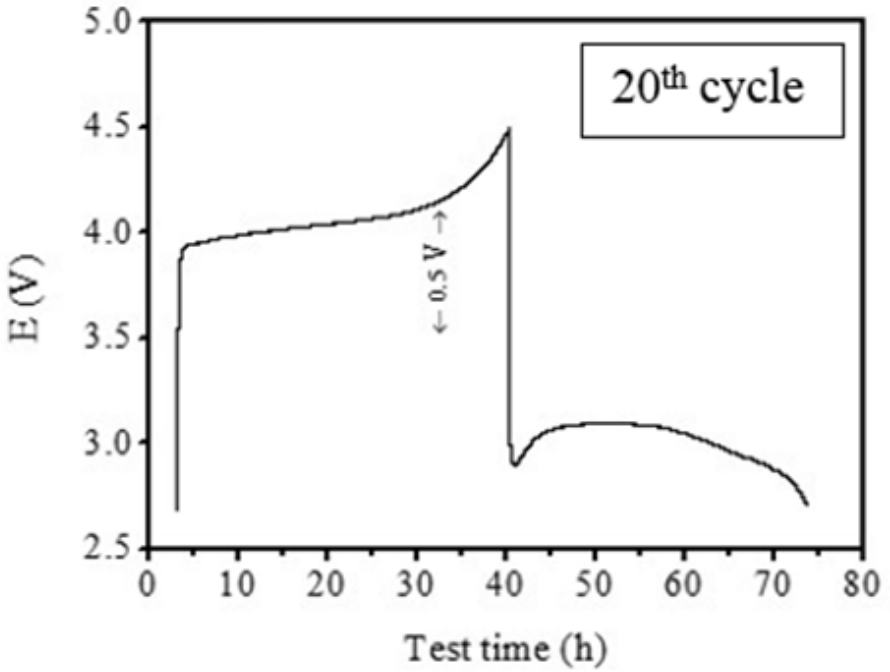


**Figure 3.17** Charge/discharge curve of a lithium test cell assembled with a configuration of Li/PTL-1/$LiFePO_4$. The test was performed at 0 °C at current densities of 0.01 mA $cm^{-2}$.

## 3.4 CONCLUSIONS

The super soft polymer electrolyte network was architectured from a thermoplastic polymer matrix of known molecular weight using the rapid and cost-effective in situ photopolymerisation technique. A multidisciplinary approach was adopted to understand the role of photopolymerisation in tailor making the integral and requisite properties of the resulting polymer electrolyte to achieve acceptable conductivity, ionic mobility and resilience

towards dendrite-induced short circuit reactions. Significantly, the feasibility of using such novel electrolyte in real cell configuration at ambient temperature with various nanostructured electrodes was established by suitably adopting in situ polymerization directly over the electrode films. The obstacles related to hazardous dendrites and reactivity towards Li-metal were nullified, leading to the assembly of superior Li-ion and Li-metal cells conceived for applications that demand high energy and/or power, including smart-grid storage and electric-/hybrid-electric vehicles.

The approach can be extended to other energy-related device applications like Na-ion batteries, dye-sensitized solar cells and supercapacitors, owing to its simple, scalable, economic and eco-friendly preparation method, and a great potential to serve as a light-designed cell component.

## REFERENCES

[1] K.M. Abraham, Z. Jiang, B. Carroll, Highly Conductive PEO-like Polymer Electrolytes, Chem. Mater. 9 (1997) 1978–1988. doi:10.1021/cm970075a.

[2] C. Zhang, D. Ainsworth, Y.G. Andreev, P.G. Bruce, Ionic Conductivity in the Solid Glyme Complexes [CH3O(CH2CH2O)nCH3]:LiAsF6 (n = 3,4), J. Am. Chem. Soc. 129 (2007) 8700–8701. doi:10.1021/ja073145f.

[3] C. Zhang, S.J. Lilley, D. Ainsworth, E. Staunton, Y.G. Andreev, A.M.Z. Slawin, et al., Structure and Conductivity of Small-Molecule Electrolytes [CH3O(CH2CH2O)nCH3]:LiAsF6 (n = 8−12), Chem. Mater. 20 (2008) 4039–4044. doi:10.1021/cm8005327.

[4] M. Barghamadi, A.S. Best, A.I. Bhatt, A.F. Hollenkamp, M. Musameh, R.J. Rees, et al., Lithium–sulfur batteries—the solution is in the electrolyte, but is the electrolyte a solution?, Energy Environ. Sci. 7 (2014) 3902–3920. doi:10.1039/C4EE02192D.

[5] M.S. Park, S.B. Ma, D.J. Lee, D. Im, S.-G. Doo, O. Yamamoto, A Highly Reversible Lithium Metal Anode, Sci. Rep. 4 (2014). doi:10.1038/srep03815.

[6] Y. Kitazawa, K. Iwata, S. Imaizumi, H. Ahn, S.Y. Kim, K. Ueno, et al., Gelation of Solvate Ionic Liquid by Self-Assembly of Block Copolymer and Characterization as Polymer Electrolyte, Macromolecules. 47 (2014) 6009–6016. doi:10.1021/ma501296m.

[7] G.T. Kim, G.B. Appetecchi, M. Carewska, M. Joost, A. Balducci, M. Winter, et al., UV cross-linked, lithium-conducting ternary polymer electrolytes containing ionic liquids, J. Power Sources. 195 (2010) 6130–6137. doi:10.1016/j.jpowsour.2009.10.079.

[8] M.W. Schulze, L.D. McIntosh, M.A. Hillmyer, T.P. Lodge, High-Modulus, High-Conductivity Nanostructured Polymer Electrolyte Membranes via Polymerization-Induced Phase Separation, Nano Lett. 14 (2014) 122–126. doi:10.1021/nl4034818.

[9] P.J. Yoo, K.Y. Suh, H. Kang, H.H. Lee, Polymer Elasticity-Driven Wrinkling and Coarsening in High Temperature Buckling of Metal-Capped Polymer Thin Films, Phys. Rev. Lett. 93 (2004) 034301. doi:10.1103/PhysRevLett.93.034301.

[10] N. Angulakhsmi, S. Thomas, J.R. Nair, R. Bongiovanni, C. Gerbaldi, A.M. Stephan, Cycling profile of innovative nanochitin-incorporated poly (ethylene oxide) based electrolytes for lithium batteries, J. Power Sources. 228 (2013) 294–299. doi:10.1016/j.jpowsour.2012.11.007.

[11] D.-J. Lee, J. Hassoun, S. Panero, Y.-K. Sun, B. Scrosati, A tetraethylene glycol dimethylether-lithium bis(oxalate)borate (TEGDME-LiBOB) electrolyte for

advanced lithium ion batteries, Electrochem. Commun. 14 (2012) 43–46. doi:10.1016/j.elecom.2011.10.027.

[12] Z. Xue, D. He, X. Xie, Poly(ethylene oxide)-based electrolytes for lithium-ion batteries, J. Mater. Chem. A. 3 (2015) 19218–19253. doi:10.1039/C5TA03471J.

[13] L.W. Hill, Calculation of crosslink density in short chain networks, Prog. Org. Coat. 31 (1997) 235–243. doi:10.1016/S0300-9440(97)00081-7.

[14] S.J. Wen, T.J. Richardson, D.I. Ghantous, K.A. Striebel, P.N. Ross, E.J. Cairns, FTIR characterization of PEO + LiN(CF3SO2)2 electrolytes, J. Electroanal. Chem. 408 (1996) 113–118. doi:10.1016/0022-0728(96)04536-6.

[15] R. Khurana, J.L. Schaefer, L.A. Archer, G.W. Coates, Suppression of Lithium Dendrite Growth Using Cross-Linked Polyethylene/Poly(ethylene oxide) Electrolytes: A New Approach for Practical Lithium-Metal Polymer Batteries, J. Am. Chem. Soc. 136 (2014) 7395–7402. doi:10.1021/ja502133j.

[16] A. Lahiri, T.J.S. Schubert, B. Iliev, F. Endres, LiTFSI in 1-butyl-1-methylpyrrolidinium bis(fluorosulfonyl)amide: a possible electrolyte for ionic liquid based lithium ion batteries, Phys. Chem. Chem. Phys. 17 (2015) 11161–11164. doi:10.1039/C5CP01337B.

[17] S.I. Smedley, Ionic Conductivity in Low-Temperature Molten Salts and Concentrated Solutions, in: Interpret. Ion. Conduct. Liq., Springer US, 1980: pp. 75–100. http://link.springer.com/chapter/10.1007/978-1-4684-3818-5_3 (accessed February 24, 2016).

[18] K.P. Barteau, M. Wolffs, N.A. Lynd, G.H. Fredrickson, E.J. Kramer, C.J. Hawker, Allyl Glycidyl Ether-Based Polymer Electrolytes for Room Temperature Lithium Batteries, Macromolecules. 46 (2013) 8988–8994. doi:10.1021/ma401267w.

[19] J. Evans, C.A. Vincent, P.G. Bruce, Electrochemical measurement of transference numbers in polymer electrolytes, Polymer. 28 (1987) 2324–2328. doi:10.1016/0032-3861(87)90394-6.

[20] N. Boaretto, A. Bittner, C. Brinkmann, B.-E. Olsowski, J. Schulz, M. Seyfried, et al., Highly Conducting 3D-Hybrid Polymer Electrolytes for Lithium Batteries Based on Siloxane Networks and Cross-Linked Organic Polar Interphases, Chem. Mater. 26 (2014) 6339–6350. doi:10.1021/cm5024647.

[21] R. Bouchet, S. Maria, R. Meziane, A. Aboulaich, L. Lienafa, J.-P. Bonnet, et al., Single-ion BAB triblock copolymers as highly efficient electrolytes for lithium-metal batteries, Nat. Mater. 12 (2013) 452–457. doi:10.1038/nmat3602.

[22] J.-N. Chazalviel, Electrochemical aspects of the generation of ramified metallic electrodeposits, Phys. Rev. A. 42 (1990) 7355–7367. doi:10.1103/PhysRevA.42.7355.

[23] K.E. Thomas, S.E. Sloop, J.B. Kerr, J. Newman, Comparison of lithium-polymer cell performance with unity and nonunity transference numbers, J. Power Sources. 89 (2000) 132–138. doi:10.1016/S0378-7753(00)00420-1.

[24] H. Wang, M. Matsui, Y. Takeda, O. Yamamoto, D. Im, D. Lee, et al., Interface Properties between Lithium Metal and a Composite Polymer Electrolyte of PEO18Li(CF3SO2)2N-Tetraethylene Glycol Dimethyl Ether, Membranes. 3 (2013) 298–310. doi:10.3390/membranes3040298.

[25] Y. Ma, M. Doyle, T.F. Fuller, M.M. Doeff, L.C.D. Jonghe, J. Newman, The Measurement of a Complete Set of Transport Properties for a Concentrated Solid Polymer Electrolyte Solution, J. Electrochem. Soc. 142 (1995) 1859–1868. doi:10.1149/1.2044206.

[26] J. Kříž, S. Abbrent, J. Dybal, D. Kurková, J. Lindgren, J. Tegenfeldt, et al., Nature and Dynamics of Lithium Ion Coordination in Oligo(ethylene glycol) Dimethacrylate-Solvent Systems: NMR, Raman, and Quantum Mechanical Study, J. Phys. Chem. A. 103 (1999) 8505–8515. doi:10.1021/jp991410g.

[27] H. Zhang, C. Liu, L. Zheng, F. Xu, W. Feng, H. Li, et al., Lithium bis(fluorosulfonyl)imide/poly(ethylene oxide) polymer electrolyte, Electrochimica Acta. 133 (2014) 529–538. doi:10.1016/j.electacta.2014.04.099.

[28] C. Laoire, S. Mukerjee, E.J. Plichta, M.A. Hendrickson, K.M. Abraham, Rechargeable Lithium/TEGDME- LiPF6 / O2 Battery, J. Electrochem. Soc. 158 (2011) A302–A308. doi:10.1149/1.3531981.

[29] E. Peled, The Electrochemical Behavior of Alkali and Alkaline Earth Metals in Nonaqueous Battery Systems—The Solid Electrolyte Interphase Model, J. Electrochem. Soc. 126 (1979) 2047–2051. doi:10.1149/1.2128859.

[30] F. Croce, R. Curini, A. Martinelli, L. Persi, F. Ronci, B. Scrosati, et al., Physical and Chemical Properties of Nanocomposite Polymer Electrolytes, J. Phys. Chem. B. 103 (1999) 10632–10638. doi:10.1021/jp992307u.

[31] G.B. Appetecchi, F. Croce, L. Persi, F. Ronci, B. Scrosati, Transport and interfacial properties of composite polymer electrolytes, Electrochimica Acta. 45 (2000) 1481–1490. doi:10.1016/S0013-4686(99)00363-1.

[32] J.L. Schaefer, D.A. Yanga, L.A. Archer, High Lithium Transference Number Electrolytes via Creation of 3-Dimensional, Charged, Nanoporous Networks from Dense Functionalized Nanoparticle Composites, Chem. Mater. 25 (2013) 834–839. doi:10.1021/cm303091j.

[33] M.C. Borghini, M. Mastragostino, A. Zanelli, Reliability of lithium batteries with crosslinked polymer electrolytes, Electrochimica Acta. 41 (1996) 2369–2373. doi:10.1016/0013-4686(96)00014-X.

[34] P. Hovington, M. Lagacé, A. Guerfi, P. Bouchard, A. Mauger, C.M. Julien, et al., New Lithium Metal Polymer Solid State Battery for an Ultrahigh Energy: Nano C-LiFePO4 versus Nano Li1.2V3O8, Nano Lett. 15 (2015) 2671–2678. doi:10.1021/acs.nanolett.5b00326.

[35] G.M. Stone, S.A. Mullin, A.A. Teran, D.T. Hallinan, A.M. Minor, A. Hexemer, et al., Resolution of the Modulus versus Adhesion Dilemma in Solid Polymer Electrolytes for Rechargeable Lithium Metal Batteries, J. Electrochem. Soc. 159 (2012) A222–A227. doi:10.1149/2.030203jes.

# CHAPTER FOUR

## *Single-ion block copoly(ionic liquid)s as electrolytes for all-solid state lithium batteries*

### 4.1. INTRODUCTION

In the previous two chapters, the incorporation of polar aprotic plasticizers was demonstrated to greatly enhance the ambient temperature ionic conductivity of PEO based polymer electrolytes, also assuring excellent chemical and thermal stability. However, despite such an increase, these polymer electrolytes struggle to meet the requirements of real devices due to limited power delivery caused by cell polarization. The main cause of cell polarization in solid polymer electrolytes (SPEs) is the formation of strong ion concentration gradients within the cell during operation [1]. For instance, lithium ions are over-concentrated at the negative electrode and depleted at the positive electrode during cell discharge, which leads to the formation of strong concentration gradients that limit the maximum current available.

Moreover, concentration gradients are suspected to favor the formation of hazardous lithium dendrites at the negative electrode. An effective way to

suppress concentration gradients is to bond anions covalently to the polymer backbone; in such a system, lithium ions are the only mobile species and, consequently, carry the bulk of the ionic current. This class of polymer electrolytes, namely single-ion conductors, was introduced in the 90's and it is attracting considerable attention nowadays. Given their single-ion nature, the lithium-ion transference number of such electrolytes noticeably approaches the unity. However, until the appearance of functional groups weakly coordinating due to highly delocalized anions, the nature of the anionic species was limited to sulfate [2,3], phosphate [4] and carboxylic [2,5,6] groups, providing poor conductivity under anhydrous conditions ($10^{-10}$ – $10^{-8}$ S cm$^{-1}$ at 25 °C).

The success in effectively improving the ionic conductivity was achieved by the development of ionic liquid like monomers (ILMs) bearing trifluoromethylsulfonylimide [7–12], tetraphenyl borate [13], tetraperfluorinated phenyl borate [14] and borabicyclo [3,3,1]nonane anionic species [15]. However, the ionic conductivity of these anionic PILs ($10^{-8}$ – $10^{-7}$ S cm$^{-1}$ at 25 °C) was still lower than the minimum targeted value of $10^{-5}$ S cm$^{-1}$ (at 25 °C) required for acceptable battery performance [16–18].

With the aim to further increase the conductivity of anionic PILs, ILMs were randomly copolymerized with various polar neutral monomers [19,20]. This led to the decrease in polyelectrolytes' $T_g$ and nearly one order of magnitude improvement in ionic conductivity, allowing the achievement of ~$10^{-6}$ S cm$^{-1}$ at 25 °C [20].

Further interest turned out to the synthesis of different anionic block copolymers [21–24], where it is possible to influence the microstructure of the resulting solid polymer electrolyte by choosing an appropriate neutral block. The most common architectures are the AB diblock and the BAB triblock copolymers, where A is the anionic block and B is the block comprising of a neutral polymer.

One of the latest examples reported by Inceoglu et al. [22] describes the anionic AB block copolymer obtained by nitroxide-mediated polymerization of lithium styrenesulfonyl(trifluoromethylsulfonyl)imide monomer onto poly(ethylene oxide). It was demonstrated that the ionic conductivity in such polymers is strongly affected by morphology. At low temperatures, an ordered lamellar phase was obtained, and the "mobile" lithium ions were trapped in the form of ionic clusters in the glassy polystyrene-rich microphase. An increase in temperature resulted in a thermodynamic transition to a disordered phase. Finally, above this transition temperature, lithium ions were released from the clusters, and the ionic conductivity increased by several orders of magnitude (from $3.0\times10^{-8}$ to $2.7\times10^{-5}$ S $cm^{-1}$ at 25 and 60 °C, respectively). Similar results on morphology-conductivity relationship for AB block copolymer were later published by Rojas et al. [24] and Elabd et al. [25,26] In 2013, Bouchet et al. [21] reported the anionic BAB triblock copolymers based on the same lithium poly(styrenesulfonyl (trifluoromethylsulfonyl)imide) as a B block and poly(ethylene oxide) as a central A block. The high ionic conductivity ($1.3\times10^{-5}$ S $cm^{-1}$ at 60 °C) of such triblock copolymer was governed by the weak interactions of the lithium ions with the delocalized anion on one hand and by their enhanced dissociation

provided by PEO part on the other one. A recent paper by Jangu et al. [23] deals with the synthesis of A−BC−A triblock copolymers featuring a microphase-separated morphology and high ion transport. The soft central "BC" block was composed of poly(4-styrenesulfonyl-(trifluoromethylsulfonyl)imide) and di(ethylene glycol)methyl ether methacrylate units, while the external A blocks were represented by polystyrene. The authors were able to achieve ionic conductivity as high as $1.3\times10^{-6}$ S $cm^{-1}$ at 25 °C. Finally, it should be mentioned that in spite of rather high gained ionic conductivity for the listed anionic PILs, only the BAB triblock copolymers were tested in real Li cell configuration demonstrating good performance at 60-80 °C [21,27].

With the aim of concurrently decreasing anionic PILs' glass transition temperature and increasing their ionic conductivity, a novel series of single-ion block copolymer electrolytes was prepared, which was based on poly(ethylene glycol) methyl ether methacrylate (PEGM) and a specifically designed ILM, namely lithium 1-[3-(methacryloyloxy)propylsulfonyl]-1-(trifluoromethylsulfonyl)imide (LiMTFSI). By controlling the macromolecular architecture of the polyelectrolytes via reversible addition−fragmentation chain transfer (RAFT) polymerization, it was possible to develop solid polymer electrolyte systems with the tailored high ionic conductivity, lithium-ion transport number close to unity and high electrochemical stability. Finally, the performance in lab-scale lithium cell prototypes is shown, which demonstrates the highly promising prospects of these materials as next-generation electrolytes for truly solid LIBs.

## 4.2. EXPERIMENTAL SECTION

### 4.2.1. MATERIALS

Poly(ethylene glycol) methyl ether methacrylate (PEGM, $M_w$ = 475 g $mol^{-1}$, Aldrich), 4-cyano-4-(phenylcarbonothioylthio)pentanoic acid (CPADB, >97%, Aldrich), thionyl chloride (>99%, Aldrich), 4-methoxyphenol (99%, Acros), trifluoromethanesulfonamide (97%, ABCR), lithium hydride (LiH, 97%, Sigma-Aldrich), tetrahydrofuran (THF, anhydrous, Acros), methanol (Acros), hexane (Acros), dicloromethane (DCM, Acros), acetonitrile (ACN, HPLC grade 99%, Acros), dimethyl formamide (DMF, Acros), carbon-coated lithium iron phosphate ($LiFePO_4$, Advanced Lithium Electrochemistry Co. Ltd.), carbon black $C_{65}$ (Timcal), carbon coated aluminum current collector (Showa Denko), lithium metal foil (Chemetall Foote Corporation) were used without further purification. 2,2'-Azobisisobutyronitrile (AIBN, initiator, 98%, Acros) was recrystallized from methanol before use. Potassium 3-(methacryloyloxy) propane-1-sulfonate (Sigma-Aldrich, 98%, Aldrich) was carefully dried under vacuum (<1 mm Hg) at 25 °C for 2 h prior to use. Carbon coated aluminum foils were provided by Lithops Srl. Spectra/Por 3 (Spectrumlabs) dialysis tubes with MWCO 3500 Dalton were used for polymer dialysis.

### 4.2.2 SYNTHESIS OF 3-(CHLOROSULFONYL)PROPYL METHACRYLATE

Potassium 3-(methacryloyloxy)propane-1-sulfonate (30.0 g, 0.122 mol) was dried under vacuum at 60 °C for three hours and, then, dispersed in 45

ml of anhydrous THF under nitrogen atmosphere. Then, 3.4 mL of DMF as catalyst were added via syringe. The reaction flask was cooled down to 0 °C and 35 ml of thionyl chloride were added dropwise. The reaction proceeded at room temperature overnight (12 h). A yellowish and viscous solution was obtained; the solution was poured into 300 mL of ice water. The lower oily layer was recovered in a decantation funnel and diluted with 110 ml of dichloromethane. The solution of 3-(chlorosulfonyl)propyl methacrylate was washed with water (6 × 40 ml) and dried over anhydrous magnesium sulfate. After filtering off $MgSO_4$, the obtained slightly yellow oil was dried under vacuum at RT overnight. Yield: 23.1 g (85%). $^1$H NMR (400 MHz, $CDCl_3$): δ = 6.05 (1H, $CH_2$=C($CH_3$)–), 5.59 (1H, $CH_2$=C($CH_3$)–), 4.29 (2H, CO-O-$CH_2$-), 3.77 (2H, -$CH_2$-$SO_2$Cl), 2.40 (2H, O-$CH_2$-$CH_2$-$CH_2$-), 1.92 (3H, $CH_2$=C($CH_3$)–), refer to **Figure 4.1**

### 4.2.3 SYNTHESIS OF TRIETHYL AMMONIUM 1-[3-(METHACRYLOYLOXY)PROPYLSULFONYL]-1-(TRIFLUOROMETHANSULFONYL)IMIDE

Trifluoromethanesulfonamide (14.6 g, 0.098 mol) was dissolved in freshly distilled triethylamine (30 ml, 0.214 mol) and cooled down to 0 °C under nitrogen atmosphere; the solution was diluted with 80 ml of anhydrous THF. A solution of 3-(chlorosulfonyl)propyl methacrylate (22.2 g, 0.098 mol) in 30 ml of anhydrous THF was added dropwise to the former mixture. The reaction proceeded at 0 °C for one hour and at RT for another hour. By means of filtration, the resulted precipitate was removed and the filtrate was

concentrated under reduced pressure at room temperature; the residual oil was dissolved in dichloromethane and washed four times with water. Anhydrous magnesium sulfate was added to remove traces of water from the solution and, consequently, removed by filtration. The solvent was removed under reduced pressure at room temperature and an orange-yellowish oil was obtained. The product was dried under vacuum at RT overnight. Yield: 33.3 g (78%). $^{1}$H NMR (400 MHz, $CDCl_3$): δ = 8.09 (1H, H–$N(C_2H_5)_3$), 6.08 (1H, $CH_2$=C($CH_3$)–), 5.56 (1H, $CH_2$=C($CH_3$)–), 4.25 (2H, CO-O-$CH_2$-), 3.25 (2H, -$CH_2$-$SO_2$-N), 3.19 (6H, H–N($CH_2CH_3$)$_3$), 2.22 (2H, O-$CH_2$-$CH_2$-$CH_2$-), 1.92 (3H, $CH_2$=C($CH_3$)–), 1.35 (9H, H–N($CH_2CH_3$)$_3$), refer to **Figure 4.2**

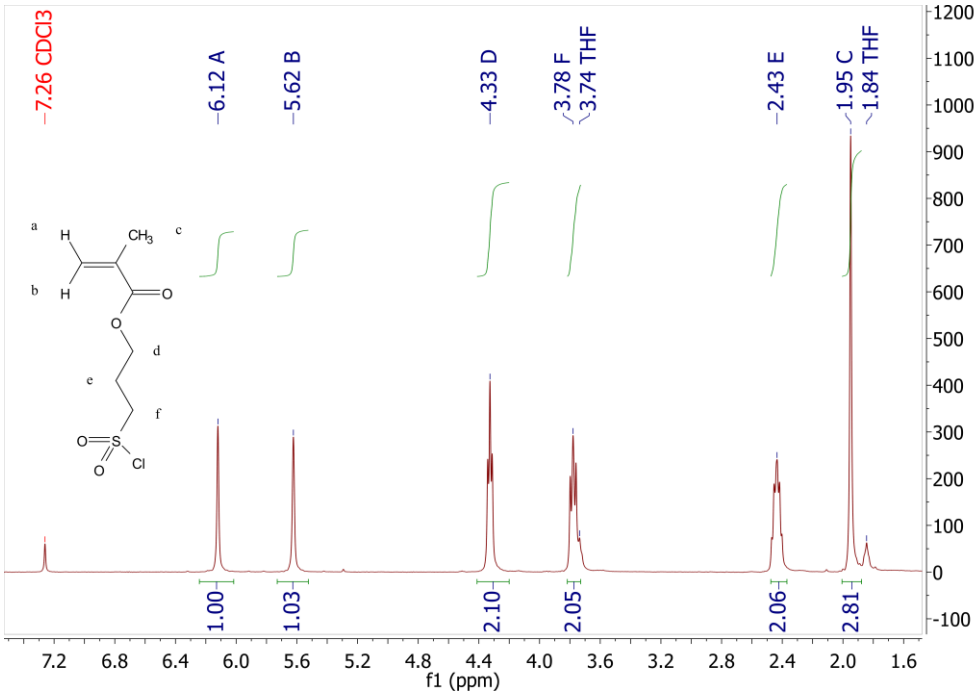


**Figura 4.1** $^{1}$H NMR of 3-(chlorosulfonyl)propyl methacrylate recorded in $CDCl_3$

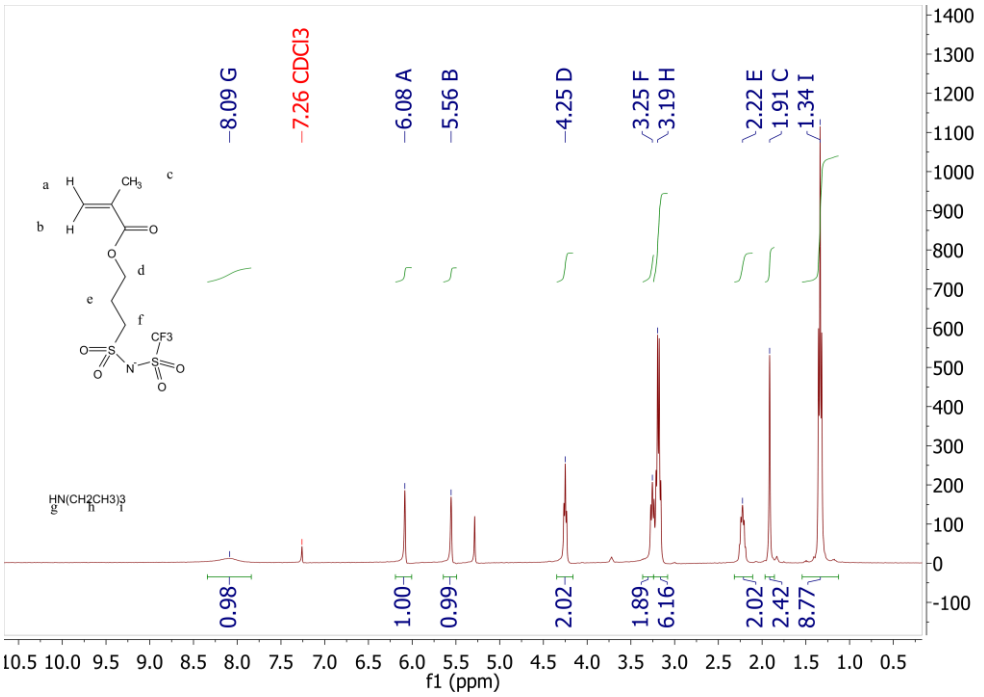


**Figura 4.2** $^{1}H$ NMR of triethyl ammonium 1-[3-(methacryloyloxy)propylsulfonyl]-1-(trifluoromethansulfonyl)imide recorded in $CDCl_3$

## 4.2.4 SYNTHESIS OF LITHIUM 1-[3-(METHACRYLOYLOXY)PROPYLSULFONYL]-1-(TRIFLUOROMETHANESULFONYL)IMIDE (LiMTFSI)

Triethyl ammonium 1-[3-(methacryloyloxy)propylsulfonyl]-1-(trifluoromethanesulfonyl)imide (30.0 g, 68.1 mmol) was dissolved in 45 mL of anhydrous THF with stirring under inert atmosphere at room temperature. Lithium hydride (1.3 g, 170.3 mmol) was added to the prepared solution in

one portion and the obtained suspension was stirred overnight at 30 °C. Then, the unreacted LiH was removed by filtration and the solution was concentrated under reduced pressure giving a yellowish viscous oil. The product was washed with hexane (3 × 40 mL), dried at 25 °C/15 mm Hg and, finally, crystallized from anhydrous DCM in the form of a white crystalline powder. The powder was collected by filtration under inert atmosphere and dried overnight at 25 $^{o}$C/1 mm Hg.

Yield: 18.8 g (80%); mp = 75.1 °C (DSC); Anal. Calcd for $C_8H_{11}F_3LiNO_6S_2\times1H_2O$ (363.3): C, 26.45%; H, 3.61%; N, 3.86; Found: C, 26.68%; H, 3.58%; N, 3.88%; $^1$H NMR (400 MHz, DMSO-$d_6$): δ = 6.04 (s, 1H, C$\underline{H}_2$=C(CH$_3$)–), 5.68 (s, H, C$\underline{H}_2$=C(CH$_3$)–), 4.17 (t, 2H, CO-O-C$\underline{H}_2$-, $J_{HH}$ = 6.5 Hz), 3.06 (m, 2H, -C$\underline{H}_2$-SO$_2$-N), 2.11 (m, 2H, O-C$\underline{H}_2$-CH$_2$-), 1.88 (s, 3H, CH2=C(CH3)–), refer to **Figure 4.3**; $^{13}$C NMR (101 MHz, DMSO-$d_6$): δ = 166.4, 135.8, 125.7, 124.9, 121.7, 118.5, 115.3, 62.7, 51.3, 23.5, 17.9; $^{19}$F NMR (376.5 MHz, DMSO-$d_6$): δ = -82.8 (s, CF$_3$); IR (ATR-mode): ν = 2981 (w, $\nu_{C-H}$), 2934 (w, $\nu_{C-H}$), 1702 (s, $\nu_{C=O}$), 1663 (w), 1637 (m, $\nu_{C=C}$), 1467 (w), 1444 (w), 1411 (w), 1322 (vs, $\nu_{asSO2}$), 1263 (s, $\nu_{asSO2}$), 1228 (w), 1182 (vs, $\nu_{CF}$), 1159 (vs, $\nu_{sSO2}$), 1127 (s), 1109 (s), 1065 (vs, $\nu_{CF}$), 1004 (m), 968 (m), 956 (m), 916 (w), 883 (w), 858 (w), 836 (w), 822 (m), 803 (m), 784 (w), 760 (w), 716 (m), 639 (s), 579 (s), 558 (m), 547 (m), 511 (s), 465 (m) cm$^{-1}$.

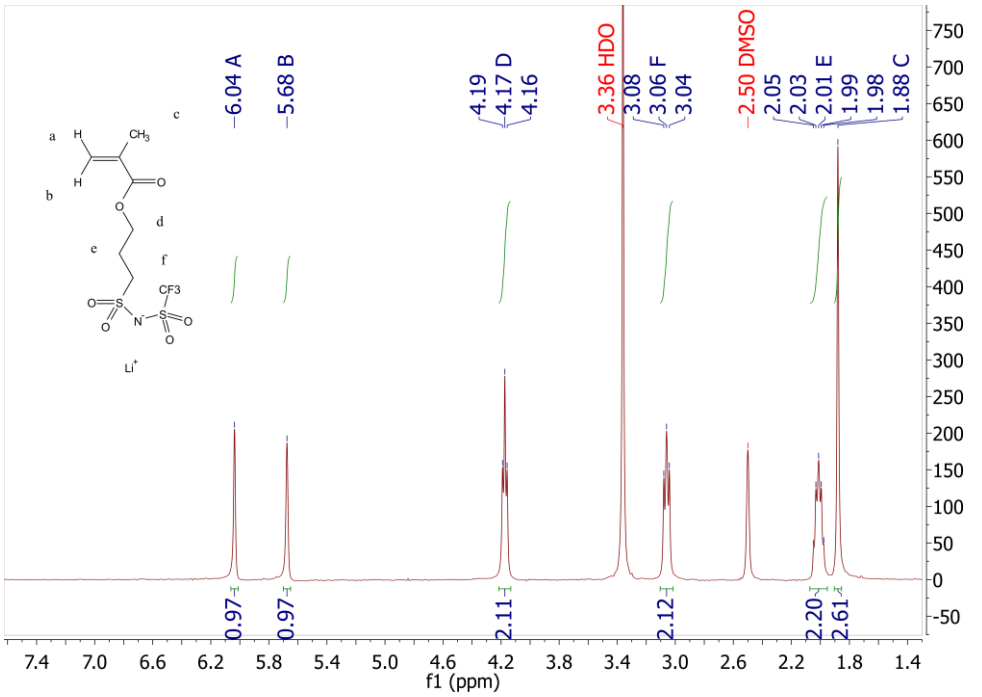


**Figura 4.3** $^{1}$H NMR of lithium 1-[3-(methacryloyloxy)propylsulfonyl]-1-(trifluoromethansulfonyl)imide recorded in DMSO-$d_6$

## 4.2.5 RAFT SYNTHESIS OF POLY(PEGM) PRECURSOR

PEGM polymer (poly(PEGM)) was prepared via RAFT polymerization and used as the starting block for copolymers' synthesis. The polymerization procedure was carried out as follows: a solution of PEGM (10.0 g, 21.1 mmol), AIBN (3.0 mg, 0.018 mmol) and CPADB (50.7 mg, 0.18 mmol) in 10.6 ml of DMF was transferred to a round-bottom Schlenk flask and degassed via three freeze-pump-thaw cycles. Then, polymerization was carried out under

inert atmosphere at 70 °C. The reaction product had a targeted molecular weight of 44 kg $mol^{-1}$ at full conversion. Aliquots were removed from the reaction flask under nitrogen atmosphere using a syringe at predetermined time intervals throughout the polymerization. $^{1}H$ NMR spectroscopy in $D_2O$ and gel permeation chromatography (GPC) in THF were used to determine the reaction kinetics and the molecular weight of the products, respectively. The desired monomer conversion of ~90% was achieved after 8 h. The resulting viscous polymer solution was diluted with milli-Q water, dialyzed against water for 3 days and freeze-dried.

### 4.2.6 RAFT SYNTHESIS OF poly(PEGM)-b-poly(LiMTFSI)

The series of four poly(PEGM)-b-poly(LiMTFSI) were prepared and coded as LiBC-1, LiBC-2, LiBC-3, and LiBC-4. The example is provided for the preparation of LiBC-4 sample: the solution of poly(PEGM) precursor (1.0 g, 44 kg $mol^{-1}$, 22.7 µmol), LiMTFSI monomer (1.0 g, 2.9 mmol) and AIBN (0.37 mg, 2.27 µmol) in 3.2 mL of anhydrous DMF was placed in a typical Schlenk tube equipped with a magnetic stir bar. The reaction mixture was subjected to three freeze−pump−thaw cycles, flashed with nitrogen and then placed into a preheated bath at 70 °C. Aliquots were removed from the reaction flask under nitrogen atmosphere using a syringe at predetermined time intervals throughout the polymerization. $^{1}H$ NMR spectroscopy in $D_2O$ and gel permeation chromatography (GPC) in 0.1 M LiCl solution in water/ACN mixture (4:1 v/v) were used to determine the reaction kinetics and the product molecular weights, respectively. The desired monomer conversion

of ~85% was achieved after 8 h. The resulting viscous polymer solution was diluted with water, dialyzed against water for 3 days and freeze-dried. Finally, the block copolymer was dried at 60 °C/1 mm Hg for 12 h. All other block copolymers (LiBC-1 - LiBC-3) were prepared similarly by changing the ratio between PEGM-based macro-RAFT initiator and lithium-ion LiMTFSI monomer. Detailed polymerization conditions are given in **Table 4.1**.

### 4.2.7 RAFT SYNTHESIS OF RANDOM poly(PEGM-r-LiMTFSI) COPOLYMER

LiMTFSI (0.60 g, 1.74 mmol), PEGM (0.60 g, 1.26 mmol), AIBN (0.23 mg, 0.0014 mmol), CPADB (3.90 mg, 0.014 mmol) and DMF (1.20 g, 1.3 mL) were gently mixed in a flask at ambient temperature. The solution was transferred into a glass ampoule where upon the same procedure was used as for RAFT polymerization of PEGM.

### 4.2.8 RAFT SYNTHESIS OF poly(LiMTFSI)

The polymerization was carried out in full accordance with the procedure described for poly(PEGM) with molecular weight of 44 kg $mol^{-1}$.

**Table 4.1 Polymerization conditions used for the synthesis of poly(PEGM)-b-poly(LiMTFSI) copolymers[a]**

| Sample | Monomer (mol × $10^{-3}$) | RAFT agent (mol × $10^{-5}$) | Initiator (mol × $10^{-5}$) | Solvent (ml) |
|---|---|---|---|---|
| poly(PEGM) | PEGM (21.3) | CPADB (18.2) | AIBN (1.83) | DMF (10.6) |
| LiBC-1 | LiMTFSI (0.61) | poly(PEGM) (2.8) | AIBN (0.19) | DMF (2.3) |
| LiBC-2 | LiMTFSI (0,69) | poly(PEGM) (2.4) | AIBN (0.24) | DMF (2.0) |
| LiBC-3 | LiMTFSI (0,98) | poly(PEGM) (2.1) | AIBN (0.21) | DMF (2.0) |
| LiBC-4 | LiMTFSI (1,74) | poly(PEGM) (1.4) | AIBN (0.27) | DMF (1.9) |

[a] Polymerization temperature: 70 °C; time: 8h.

### 4.2.9 SYNTHESIS OF RANDOM COPOLYMER VIA FREE RADICAL POLYMERIZATION

LiMTFSI (0.50 g, 1.45 mmol), PEGM (0.69 g, 1.45 mmol), DMF (3.57 g, 3.8 mL) and AIBN (0.012 g, 1.0 wt.%) were gently mixed in a flask at ambient temperature. The solution was transferred into a glass ampoule. After triple freeze-thaw-pump cycles, the ampoule was sealed under vacuum and heated to 60 °C for 6 h. The resulting transparent highly viscous polymer

solution was diluted with water, dialyzed against water for 3 days and freeze-dried. The resulting polymer was then thoroughly dried at 60 °C/1 mm Hg for 12 h. Yield: 1.20 g (60 %).

### 4.2.10 CHARACTERIZATION TECHNIQUES

The physico-chemical characterization techniques used for sample characterisation are described in the Appendix.

### 4.2.11 LI CELLS ASSEMBLY AND TESTING

A composition of 60 wt.% of carbon coated $LiFePO_4$, 30 wt.% of LiBC-1 and 10 wt.% of carbon black was used for the preparation of the positive electrodes. First, powders of active material and carbon black were gently mixed in a hand mortar and, successively, added to the 5 wt.% solution of LiBC-1 in water upon stirring. The stirring was continued at room temperature for 1 h and the suspension was finally homogenized using an ULTRA-TURRAX mixer for one hour. The obtained aqueous slurry was casted onto a carbon coated aluminum current collector using a doctor-blade with a blade height of 300 µm. Water was removed by evaporation at ambient temperature and further drying at 60 °C/1 mm Hg for 24 h. The obtained composite electrode film's thickness after drying was 50 µm. The layer of block copolymer electrolyte (LiBC-1) was applied manually directly onto the surface of the composite cathode, whereupon the assembly was again dried

at 60 °C/1 mm Hg for 2 4h and transferred inside the glove-box. Lab-scale $LiFePO_4$/LiBC-1/lithium metal battery prototypes were then assembled using ECC-Std test cells. The lithium cells were cycled at 70 °C in terms of constant current charge and discharge between 2.5 and 3.8 V vs. $Li^+/Li$ at different current regimes (C-rates).

## 4.3 RESULTS AND DISCUSSION

### 4.3.1 SYNTHESIS OF LITHIUM 1-[3-(METHACRYLOYLOXY)PROPYLSULFONYL]-1-(TRIFLUOROMETHANESULFONYL) IMIDE ANIONIC MONOMER.

The position of the cation in PIL's structure is playing a strong influence on its ionic conductivity [28]. Generally, it was demonstrated, that the cation's placement inside or near the main polymer chain leads to PILs with lower conductivity in comparison with polymer analogues having ions attached via flexible spacer. The same rule was found to be applicable for anionic PILs as well: the modification of polyanions by the introduction of a flexible spacer between the main polymer chain and the attached anion results in the increase of ions mobility [28]. This was taken into consideration for the development of the new anionic ILM with $Li^+$ cation consisting of a methacrylate reactive group, a highly delocalized and chemically bonded $TFSI^-$ anion and a flexible alkyl spacer (**Scheme 4.1**). The two initial reaction steps for the synthesis of 3-(chlorosulfonyl)propyl methacrylate and triethyl ammonium 1-[3-(methacryloyloxy)propylsulfonyl]-1-

(trifluoromethanesulfonyl) imide were performed in accordance with the method published by Shaplov et al. [11]. While for the last step, the optimal reaction conditions providing the highest yield were elaborated. It was found that this heterogeneous reaction proceeds quantitatively upon slightly heating up to 30 °C for at least 12 h. After respective crystallization, LiMTFSI could be isolated in a pure form. The structure and purity of LiMTFSI was proved by $^{1}H$, $^{13}C$ and $^{19}F$ NMR, IR spectroscopy and elemental analysis. In contrast to ILMs with heterocyclic cations, LiMTFSI represents a crystalline, hygroscopic powder at room temperature with melting point of 75 ˚C (measured by DSC).

**Scheme 4.1** Synthetic route for the preparation of LiMTFSI monomer

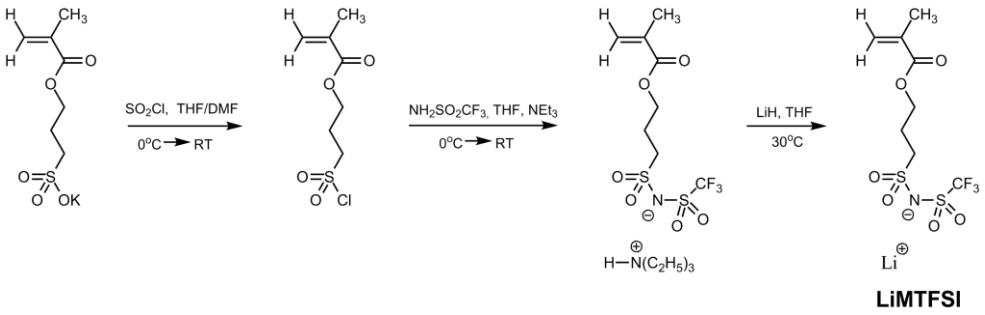


## 3.2. RAFT SYNTHESIS OF poly(PEGM)-b-poly(LiMTFSI)

First, the RAFT synthesis of poly(PEGM) precursor with 4-cyano-4-(phenylcarbonothioylthio)pentanoic acid as RAFT transfer agent was investigated. As it was previously demonstrated [29], DMF can be considered as the best organic solvent for the polymerization of ILMs in terms of

achieving high yields and high molecular weights of the resulting polyelectrolytes. Thus, DMF was selected for RAFT polymerization of PEGM and, later on, for the block extension with LiMTFSI. The block copolymers poly(PEGM)-b-poly(LiMTFSI) were synthesized by RAFT polymerization technique starting from poly(PEGM) macro-CTA precursor (**Scheme 4.2**).

**Scheme 4.2**. Synthesis of poly(PEGM)-b-poly( LiMTFSI) copolymers.

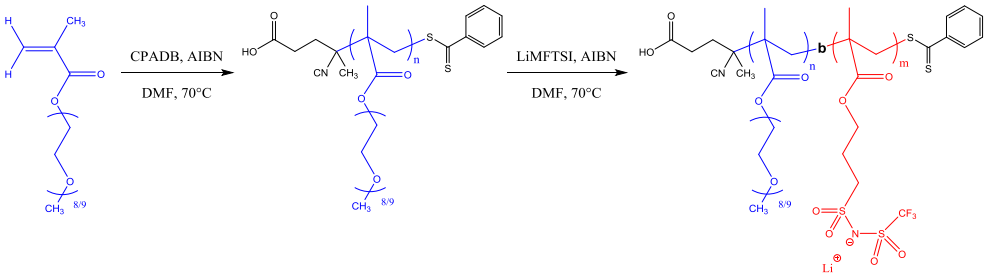


Although RAFT polymerization of PEGM was intensively studied in various solvents and with different chain transfer agents (CTAs) [30–32], it was not possible to find the information about its controlled polymerization in DMF with CPADB. Thus, initially the study of the PEGM's polymerization kinetics was carried out (**Figure 4.4**). It was revealed that quantitative conversion of the monomer (~95%) was obtained after 8 h. The experimental $M_n$ values determined by GPC in THF were close to the theoretically calculated ones, refer to **Figure 4.4 (a)**, while $M_n$ values obtained by aqueous GPC were found to be nearly two times lower than the targeted ones. This discrepancy can be explained by the strong structural difference between the linear

polystyrene and pollulan standards used for calibration and the synthesized comb-like poly(PEGM) [33].

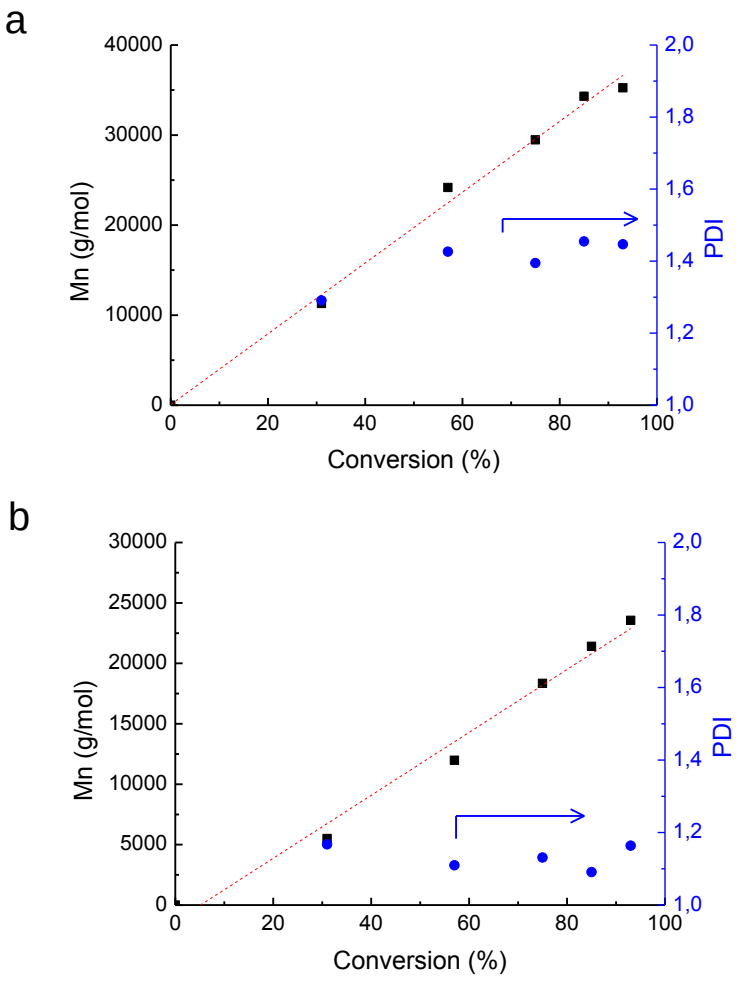


**Figure 4.4** Molar mass and PDI evolution versus conversion for RAFT polymerization of PEGM determined in THF (a) and 0.1 M LiCl solution in $H_2O$/ACN mixture (4:1 v/v) (b).

**Figure 4.5** shows the GPC traces of the poly(PEGM) samples. The shift of the GPC traces toward shorter elution time with increasing methacrylate conversion indicated the growth of the poly(PEGM) precursor. Sufficiently narrow PDIs (1.3-1.5) along with a linear increase of $M_n$ vs. conversion were observed for the poly(PEGM) samples, thus demonstrating a good control over the polymerization reaction.

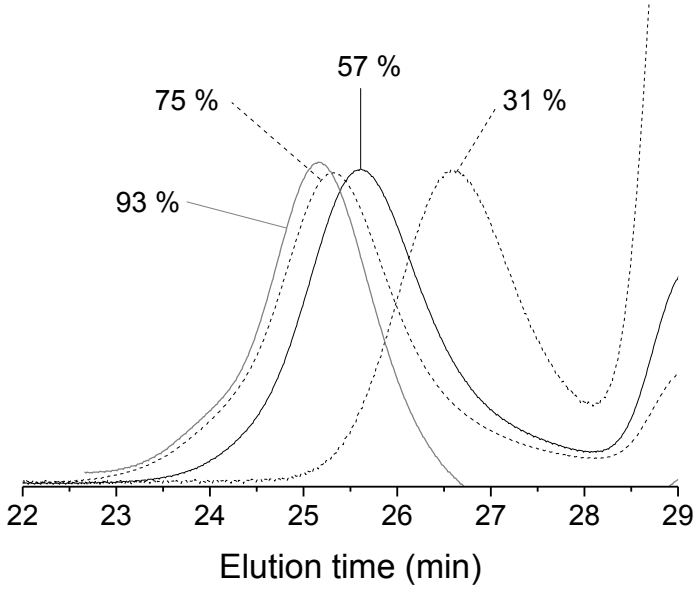


**Figure 4.5** GPC traces for the poly(PEGM) precursors in THF.

The starting poly(PEGM) macro-CTA precursor was used to synthesized block copolymers poly(PEGM)-b-poly(LiMTFSI), the chemical nature of the block copolymers was confirmed by NMR and FTIR spectroscopy, where the

repeating monomer units associated to both blocks were found in the final products. The kinetics of the reaction was found to be similar to that of poly(PEGM) (**Figure 4.6**).

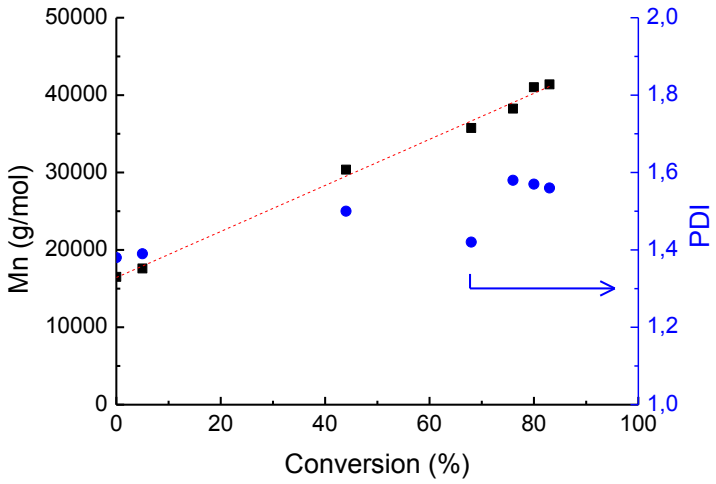


**Figure 4.6** Molar mass and PDI evolution versus conversion for RAFT extension of the poly(PEGM) block with LiMTFSI monomer.

As shown in **Figure 4.6**, the polymerization of LiMTFSI in the presence of poly(PEGM) at 70 °C reached ~85 % conversion after 8 h. The number of the average molar mass $M_n$ increases steadily with conversion, showing a linear behavior, although again the $M_n$ values of the samples were found to be lower than the theoretical ones, as shown in **Figure 4.6**. The polydispersities according to GPC were found to be satisfactory, in the range of 1.4 - 1.6. The GPC traces of the samples taken at increasing reaction times, refer to **Figure**

**4.7**, present basically unimodal peaks with decreasing elution times and reducing width proving the controlled polymerization.

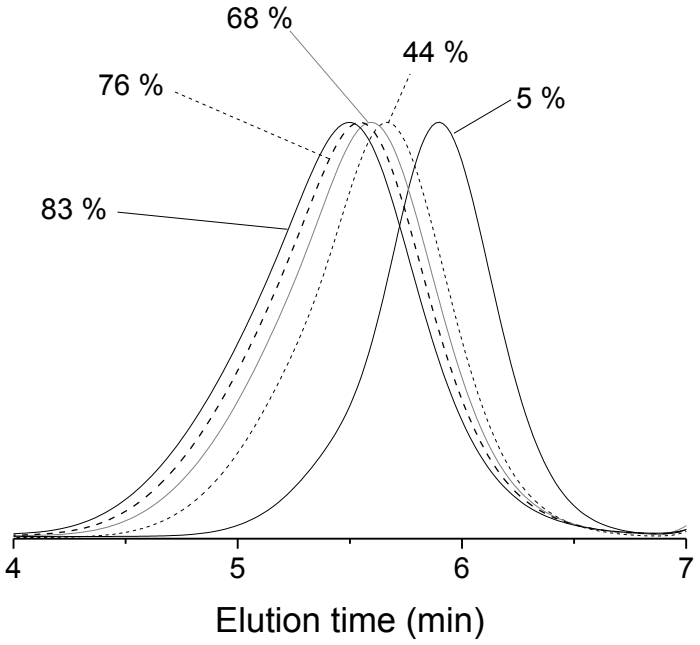


**Figure 4.7** GPC traces for RAFT extension of the poly(PEGM) block with LiMTFSI monomer.

After determination of the optimal conditions, a set of block copolymers with the fixed poly(PEGM)'s length and different size of the poly(LiMTFSI) extension were successfully prepared (**Table 4.2**, LiBC-1 – LIBC-4). The chemical structure of the synthesized block copolymers was confirmed by FTIR, $^{1}H$, and $^{13}C$ spectroscopy (**Figures 4.8 – 4.10**).

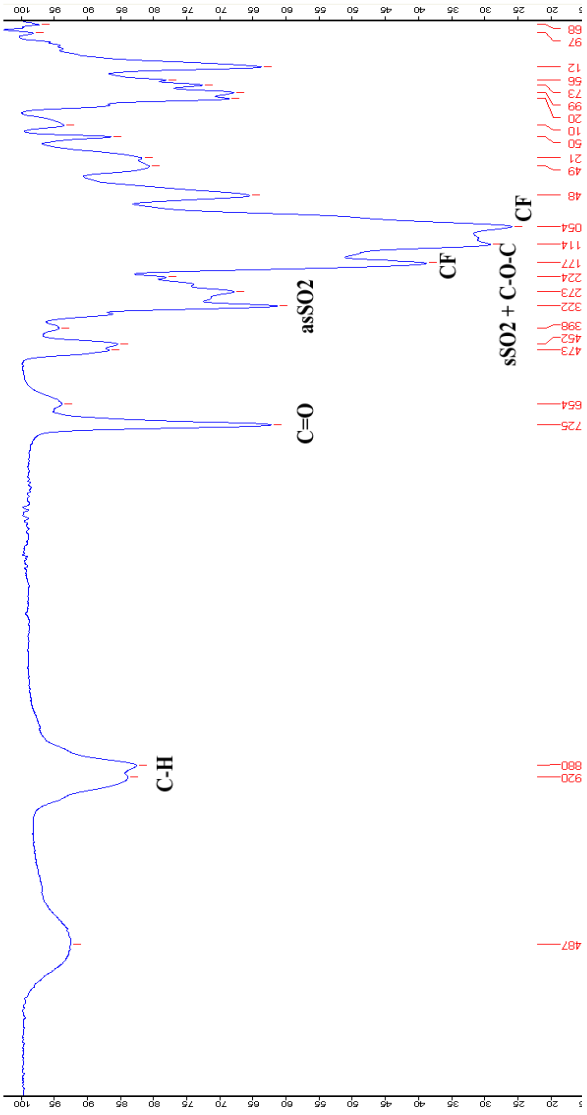


**Figure 4.10** $^{1}$H NMR spectra of poly(PEGM)-b-poly(LiMTFSI) block copolymer (LiBC-1).

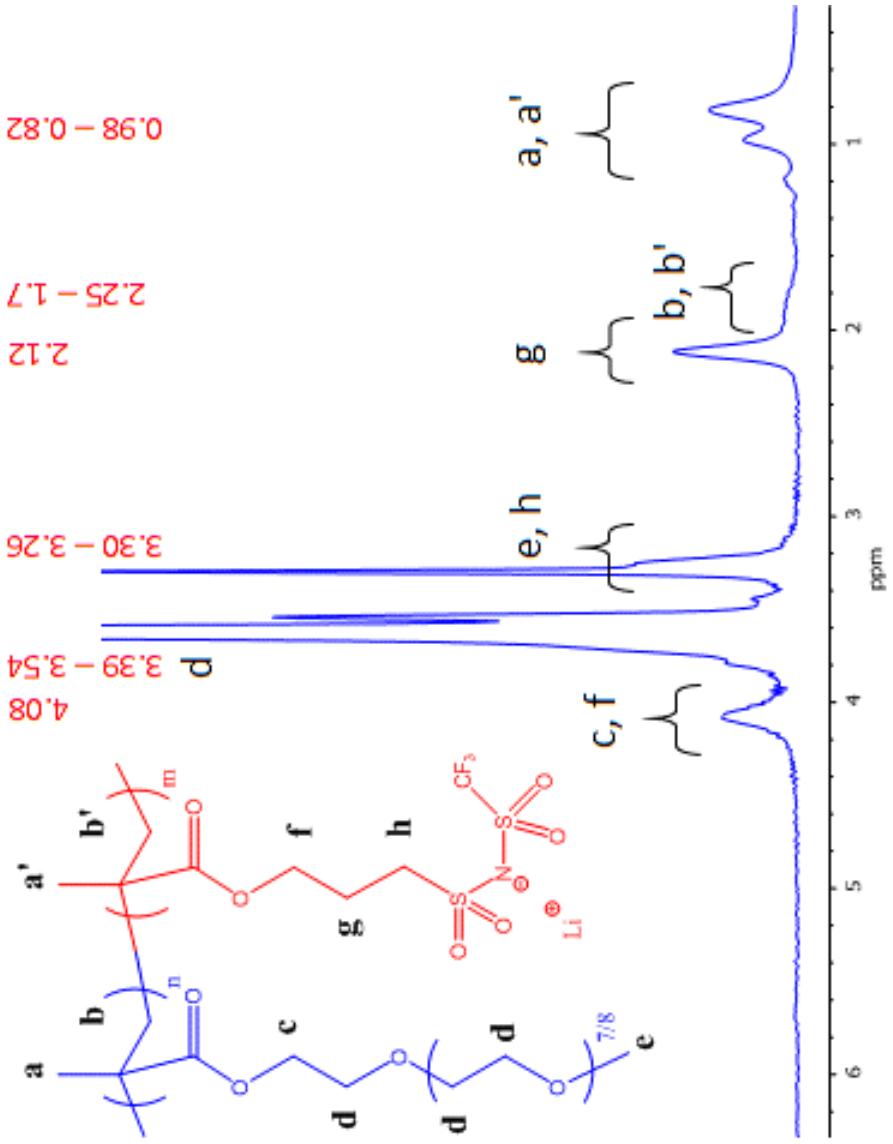


**Figure 4.10** $^{1}$H NMR spectra of poly(PEGM)-b-poly(LiMTFSI) block copolymer (LiBC-1).

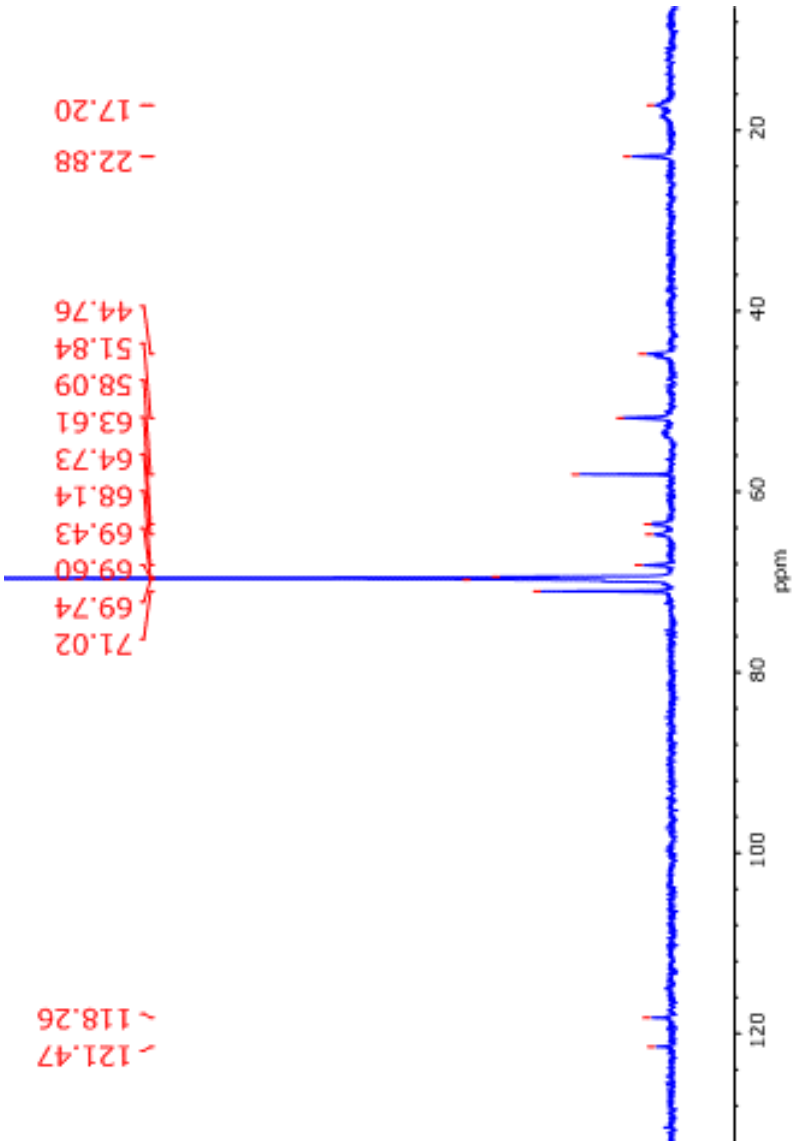


**Figure 4.10** $^{13}$C NMR spectra of poly(PEGM)-*b*-poly(LiMTFSI) block copolymer (LiBC-1).

**Table 4.2** Selected properties of the prepared polymers.

| Sample | PEGM block $M_n$ | LiMTFSI block $M_n$ | Theoretical $M_n$ | Experimental $M_n$ (PDI)[a] | $\sigma_{DC}$ at 25 °C (S/cm) | [EO]/[Li] | $T_g$ (°C) |
|---|---|---|---|---|---|---|---|
| poly(PEGM) | | - | 44000 | 23600 (1.16)[b] | - | - | -62 |
| LiBC-1 | 44000 | 7500 | 51500 | 25000 (1.46) | $2.3\times10^{-6}$ | 36 | -61 |
| LiBC-2 | | 10000 | 54000 | 31300 (1.48) | $1.5\times10^{-6}$ | 32 | -51 |
| LiBC-3 | | 16000 | 60000 | 38300 (1.53) | $1.2\times10^{-6}$ | 18 | -41 |
| LiBC-4 | | 44000 | 88000 | 68150 (1.50) | $1.6\times10^{-7}$ | 6 | 0.6 |
| poly(LiMTFSI) | - | - | 44000 | 52700 (1.20) | $1.1\times10^{-12}$ | - | 95 |
| RAFT poly(PEGM-r-LiMTFSI)[c] | - | - | 88000 | 80200 (1.34) | $1.1\times10^{-7}$ | 6 | -2 |
| free radical poly(PEGM-r-LiMTFSI)[c] | - | - | - | 375000(4.75) | $6.7\times10^{-10}$ | 6 | 10 |

[a] By GPC in 0.1 M LiCl acetonitrile/water mixture (1:4 v/v). [b] $M_n$ = 35200, PDI = 1.44 by GPC in THF. [c] For comparison: random copolymers of PEGM and LiMTFSI in 1:1 ratio, obtained by RAFT and free radical polymerization, respectively.

### 4.3.3. PHYSICO-CHEMICAL PROPERTIES OF POLYMERS

Depending on the temperature, the obtained ionic block copolymers represented rubber-like or wax like materials. Thermal properties of both poly(PEGM) and block copolymers were determined by DSC and TGA (**Figure 4.11, Figure 4.12** and **Table 4.2**).

It was found that poly(PEGM) with $M_n$ = 35.2 kg $mol^{-1}$ shows a glass-transition temperature ($T_g$) of -62 °C. The poly(LiMTFSI) demonstrates a $T_g$ of 95 °C, that is higher than a similar polymer with heterocyclic cation (viz. 14 °C [11]), but lower if compared with lithium poly(styrenesulfonyl (trifluoromethylsulfonyl)imide) (152 °C [10]). The RAFT random copolymerization of PEGM and LiMTFSI in 1:1 ratio leads to the significant decrease in $T_g$ (-2 °C) of the obtained copolymers compared to the parent poly(LiMTFSI). In its turn, the $T_g$ of the series of block copolymers LiBC-1 – LiBC-4 was found to vary in the broad range of -63 to 5 °C and moves toward lower values by decreasing the LiMTFSI content. It is worth noting that all the observed $T_g$ values for the synthetized block copolymers were much lower than that of poly(LiMTFSI) and none of the copolymers exhibited crystallinity, as the copolymerization of PEGM with LiMTFSI seems to hinder the formation of an ordered phase. The absence of two distinct $T_g$ suggests that appreciable phase separation did not occur in any of the poly(PEGM)-b-poly(LiMTFSI) copolymers. This indicates good miscibility of the parent polymers, namely poly(PEGM) and poly(LiMTFSI), most likely due to the good interactions between the ionic groups of one block and the ethylene oxide units of the other.

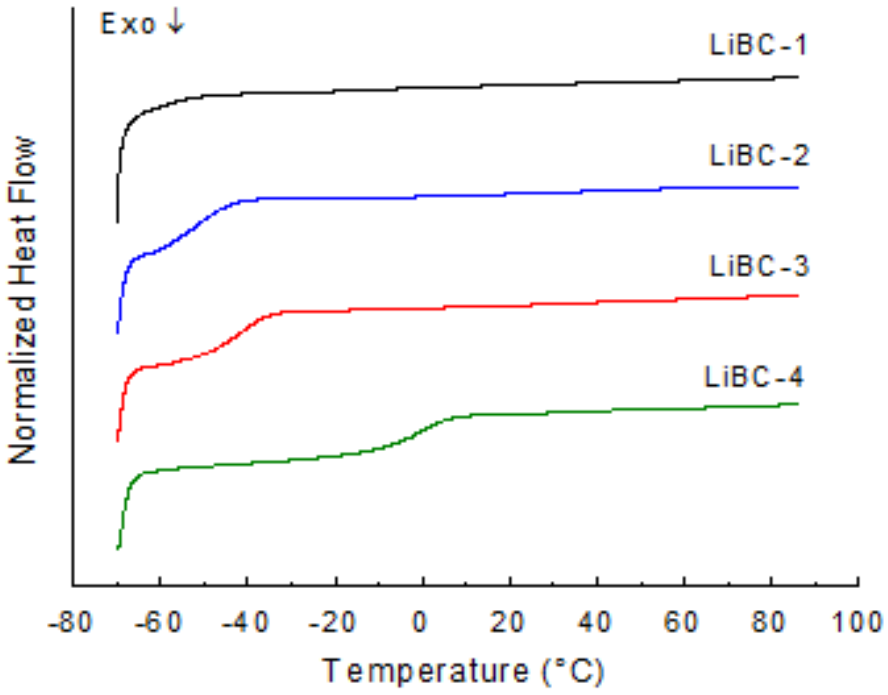


**Figure 4.11** DSC traces of poly(PEGM)-b-poly(LiMTFSI) copolymers.

According to TGA, see **Figure 4.12**, the onset mass loss temperature ($T_{onset}$) for poly(PEGM) was found to be 160 °C, while for poly(LiMTFSI) it exceeded 260 °C. TGA of the LiBC-1 copolymer shows a one-step weight-loss process starting at 170 °C. Independently on their composition, all of the other block copolymers possessed similar onset loss temperature $T_{onset}$ of ~170 °C. This result is particularly important for application in the lithium battery field, since the thermal stability of conventional liquid electrolytes is far below this value.

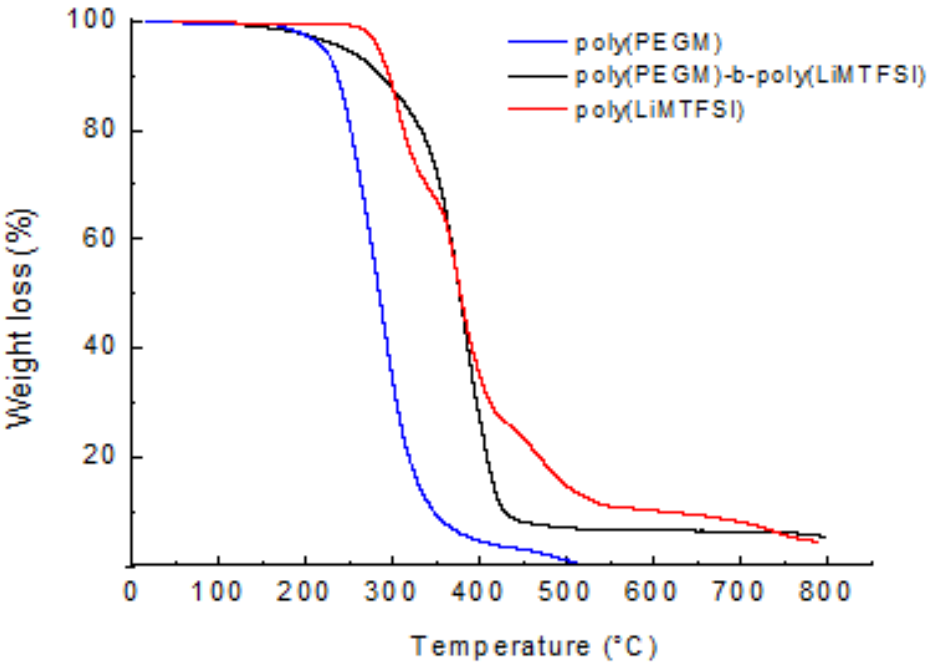


**Figure 4.12** TGA traces of LiBC-1, poly(PEGM) and poly(LiMTFSI).

The ionic conductivity of the polyelectrolytes was measured via electrochemical impedance spectroscopy and the typical Arrhenius plot is shown in **Figure 4.13**. The ionic conductivity values obtained for the block copolymers at 25 °C follow the order:

$$\sigma^{LiBC\text{-}4}\ (1.6\times10^{-7}\ S\ cm^{-1}) << \sigma^{LiBC\text{-}3} \approx \sigma^{LiBC\text{-}2} < \sigma^{LiBC\text{-}1}(2.3\times10^{-6}\ S\ cm^{-1})$$

The highest value was measured for LiBC-1 being $2.3\times10^{-6}$ S cm$^{-1}$ at 25 °C (**Table 4.2**). The observed behavior follows the general trend in relationship between the $T_g$ of the polyelectrolyte and the ionic conductivity[28]: a polymer with lower $T_g$ demonstrates the highest measured conductivity. At

higher temperatures, the curves tend to overlap, but the order described above is still generally preserved (**Figure 4.13**). It was found that the conductivity values of the block copolymers increased up to one order of magnitude and reached the targeted $10^{-5}$ S $cm^{-1}$ level at 55 °C.

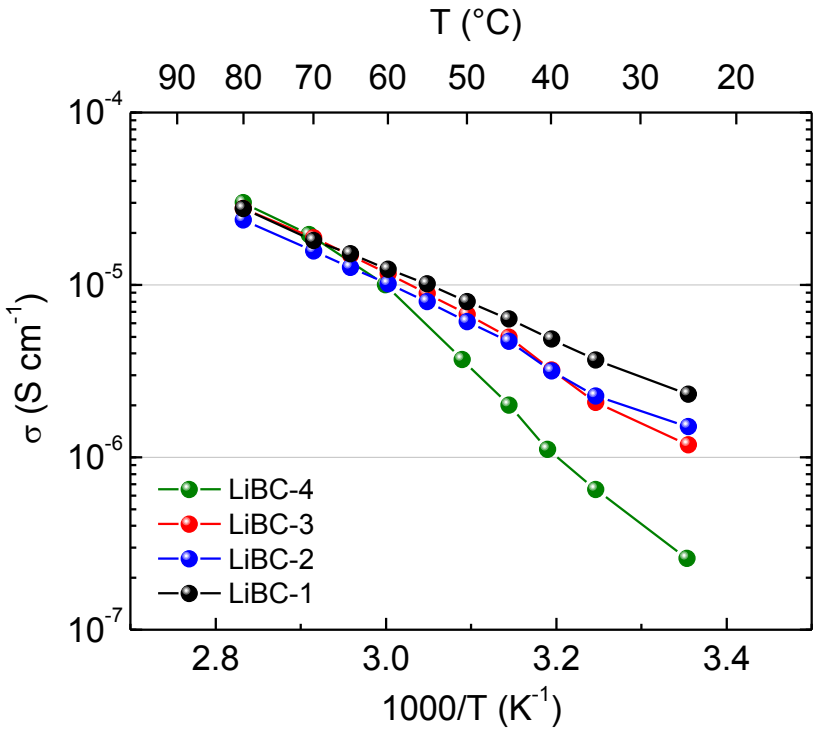


**Figure 4.13.** Arrhenius plot of ionic conductivity vs. temperature for the poly(PEGM)-b-poly(LiMTFSI) copolymers.

It was of further interest to compare the conductivity of the poly(PEGM)-b-poly(LiMTFSI) block copolymer with that of poly(LiMTFSI) and random copolymers of the same composition obtained via RAFT and free radical polymerizations (**Table 4.2**). The lowest ionic conductivity ($1.1\times10^{-12}$ S cm$^{-1}$) at 25 °C was demonstrated by poly(LiMTFSI) with a $T_g$ of 95 °C. This result can be explained by the low mobility of lithium ions in the glassy polymer phase. A two orders of magnitude higher conductivity ($6.7\times10^{-10}$ S cm$^{-1}$) was measured for the random copolymer obtained by free radical polymerization. Finally, the highest value of conductivity ($1\times10^{-7}$ S cm$^{-1}$) was observed for block and random copolymers with the same molecular weight obtained via RAFT process. Such difference in conductivity between copolymers prepared by RAFT and conventional free radical polymerization can be attributed to the distinction in their molecular weight ($M_n = 8.0\times10^4$ and $37.5\times10^4$, respectively) as it was demonstrated previously for cationic PILs [34]. However, the overlapping of the conductivity values for the block copolymer LiBC-4 and RAFT random copolymer having similar molecular mass happened more likely due the good miscibility of the parent polymers, namely poly(PEGM) and poly(LiMTFSI), and the absence of any phase separation.

The electrochemical stability window of the single-ion block copolymer LiBC-1 was studied by cyclic voltamperometry (CV) at 70 °C, this sample was selected due to its higher ionic conductivity among the prepared ones. The results are shown in **Figure 4.14**. The anodic breakdown potential of the sample was found to be 4.3 *vs*. $Li^+/Li$. Generally, the anodic stability of electrolytes is determined by the electrochemical stability of the anion, and

thus, the steep increase of current at 4.3 V is probably associated with the decomposition of the TFSI functional group of the polymer. During the second cycle of the voltammetry, the anodic limit shifts up to 4.5 *vs*. $Li^+/Li$, which can be likely explained by the growth of a passivation layer at the electrode/electrolyte interface. Regarding the cathodic scans, a highly reversible couple of peaks was observed between -0.5 and 0.48 V *vs*. $Li^+/Li$, which is evidently associated to lithium plating/stripping and confirms the efficient transfer of lithium-ions through the polymeric media.

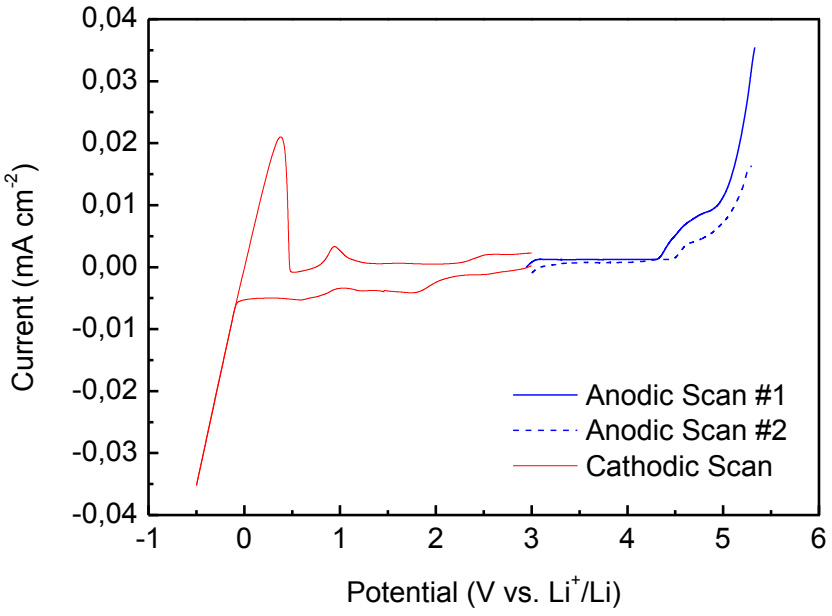


**Figure 4.14**. Electrochemical stability window obtained by CV at 1 mV $s^{-1}$ for LIBC-1 at 70 °C.

Additionally, the couple of reversible peaks at 0.7 and 1.0 V *vs*. $Li^+/Li$ may be attributed to a redox process involving species (such as oxides) at the electrode surface. The other couple of faint peaks observable in the potential range between 1.5 and 3 V is most likely associated with the multistep decomposition of some impurity traces in some of the reagents (used as received). Indeed, both peaks suddenly disappear in the subsequent voltammetric cycles, which clearly accounts for the non-reproducibility of the process and the fact that it does not influence the overall specific capacity of the system.

The lithium-ion transference number of the synthesized LiBC-1 block copolymer was determined using the method proposed by Vincent and Evans [35]. The test was performed only after the sample reached the stable interfacial resistance. Thus, major changes in resistance were not interfered in the transport properties study. The results of EIS and polarization experiments are given in **Table 4.3**.

**Table 4.3**. Lithium ion transference number measurement[a]

| | i ($\times 10^{-4}$ mA) | R (Ω) | $t_{Li^+}$ |
|---|---|---|---|
| initial | 9.62 | 2140 | 0.83 |
| steady state | 8.21 | 2182 | |

[a] potential bias applied: 10 mV

The typical Nyquist plot of a.c. impedance of a Li | LiBCE-1 | Li cell at 70 °C is shown in **Figure 4.15**. The cell impedance did not change significantly during the experiment and the initial resistance value of 2140 Ω only increased to 2182 Ω, thus proving that a stable interfacial layer was formed at the interface.

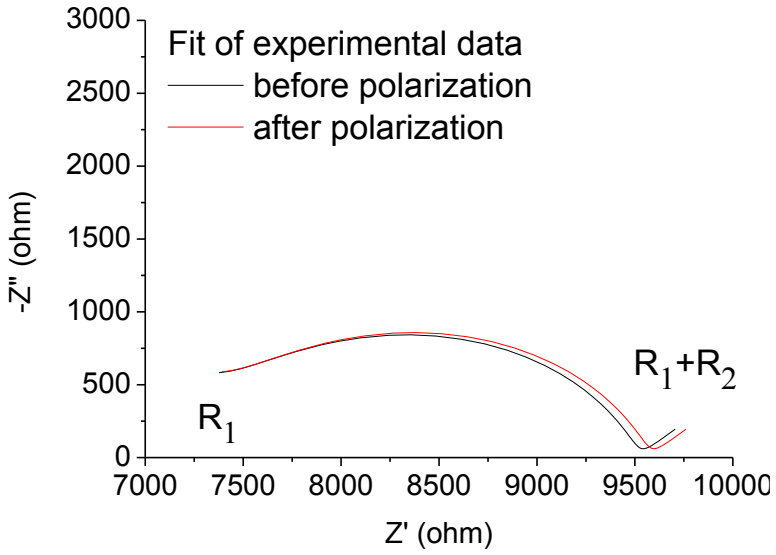


**Figure 4.15** Lithium-ion transport number analysis: (a) Typical Nyquist plot of the a.c. impedance of a Li | LiBC-1 | Li cell at 70 °C

The plot of the current response to the applied bias as a function of time is shown in **Figure 4.16**. As it can be seen, a quick drop of less than one order of magnitude (from 9.62 to 8.21 × $10^{-4}$ mA) occurs before reaching the steady

state. The obtained transport number value of 0.83 is noticeably close to the unity and, most important, is much higher than that of cationic PILs/Li salts or PEO/Li salts composite electrolytes reported previously [36]. Two main reasons can be adducted to rationalize why the transference number is not equal to unity: (1) the flexible spacer between the main polymer chain and the attached anion allows short-range motions of negative charges; (2) segmental motion of the polyanionic block may happen since the test was conducted above the glass-transition temperature of the polymer, consequently allowing additional motions of the negative charges.

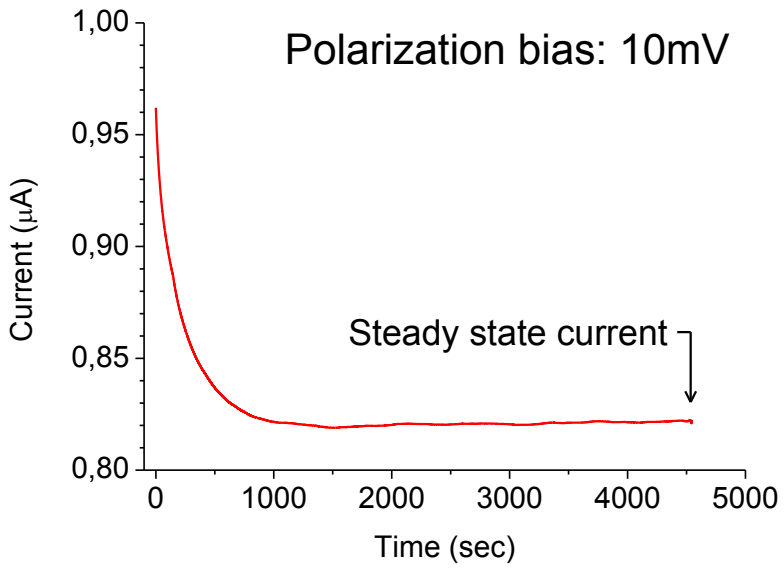


**Figure 4.16** Lithium-ion transport number analysis: (a) Typical Nyquist plot of the a.c. impedance of a Li | LiBC-1 | Li cell at 70 °C, (b) current variation with time during polarization of the symmetrical lithium cell.

### 4.3.4. ELECTROCHEMICAL BEHAVIOR IN LI CELLS

Finally, to further confirm the significance and usefulness of the newly prepared polyelectrolytes, the lab-scale lithium cell prototypes based on sample LiBC-1 were assembled using a lithium-metal negative electrode (anode) and a carbon-coated $LiFePO_4$ as a model active material for the positive electrode (cathode). The cathode for the lithium/LiBC-1/$LiFePO_4$ cells was composed of 60 wt.% of $LiFePO_4$, 30 wt.% of LiBCE-1, and 10 wt.% of carbon black. While in conventional batteries with liquid electrolyte the ion conduction inside the cathode is ensured by homogeneous wetting of the electrolyte through the porosity of the composite electrode, in solid state batteries the ionic conduction is limited to the contact area with the SPE. Therefore, a large portion of electrode's active material particles is ionically insulated when conventional neutral polymer binders are used. In the present study, to insure effective ion conduction inside the whole cathode structure, the LiBC-1 block copolymer was used as both the solid-state polyelectrolyte and the binder for the active material particles. A sketched representation of the cell assembly and the resulting morphology of the composite cathode is shown in the FESEM image of **Figure 4.17**. The particles of $LiFePO_4$ and carbon additive are uniformly coated with the block copolymer electrolyte, as it can be clearly observed in the right hand sided image. Due to the observed high contact-area between the active material and the ion conductive media an optimal ionic conduction throughout the whole thickness of the cathode is ensured.

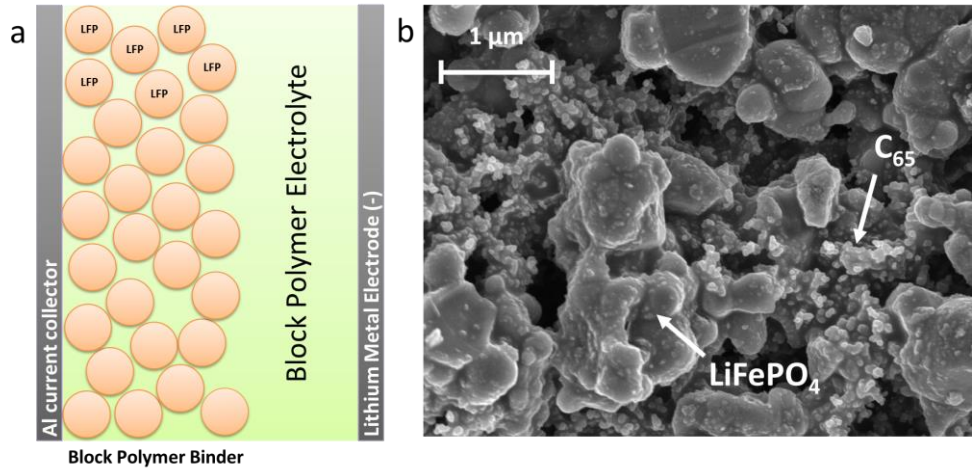


**Figure 4.17** (a) Sketched representation of the cell assembly, where the percolation of the polyelectrolyte in the whole electrode structure is clearly evidenced (b) FESEM image of the composite electrode.

The electrochemical behavior of the assembled cells was evaluated at 70 °C, and the results are shown in **Figure 4.18**. Cycling tests were conducted at different current rates, where the rate is denoted as C/n, which corresponds here to a full discharge or full charge of the theoretical cathode capacity (C, 170 mAh $g^{-1}$ for $LiFePO_4$) in n hours. The truly solid-state cells were capable of delivering large capacities up to 130 mAh $g^{-1}$ (83.3 % of the theoretical value for the $LiFePO_4$ cathode) at C/15 rate during the initial cycles. Very good rate capability for a solid polymer cell was obtained upon prolonged cycling even at higher rate (C/5). It is worth noting that despite a decrease in capacity was observed after some cycles, the cell was capable to reversibly charge and discharge at least up to 100 cycles. However, the loss of specific

capacity during cycling was observed, particularly evident during the first cycles. Such gradual decrease can be explained by the sequestration of lithium ions, possibly due to the formation of the passivation layer at the electrode/electrolyte interface.

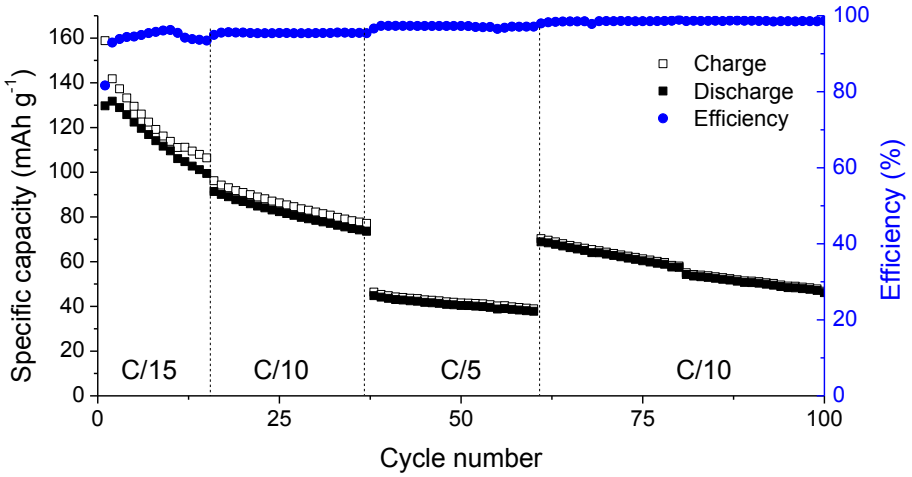


**Figure 4.18** Specific capacity vs. cycle number profile of the Li/LiBC-1/$LiFePO_4$ cell at different charge/discharge rates at 70 °C.

A constant current charge/discharge potential *vs.* specific capacity profile is shown in **Figure 4.19**. The typical potential plateau related to $Li^+$ de-insertion/insertion mechanism is clearly observed.

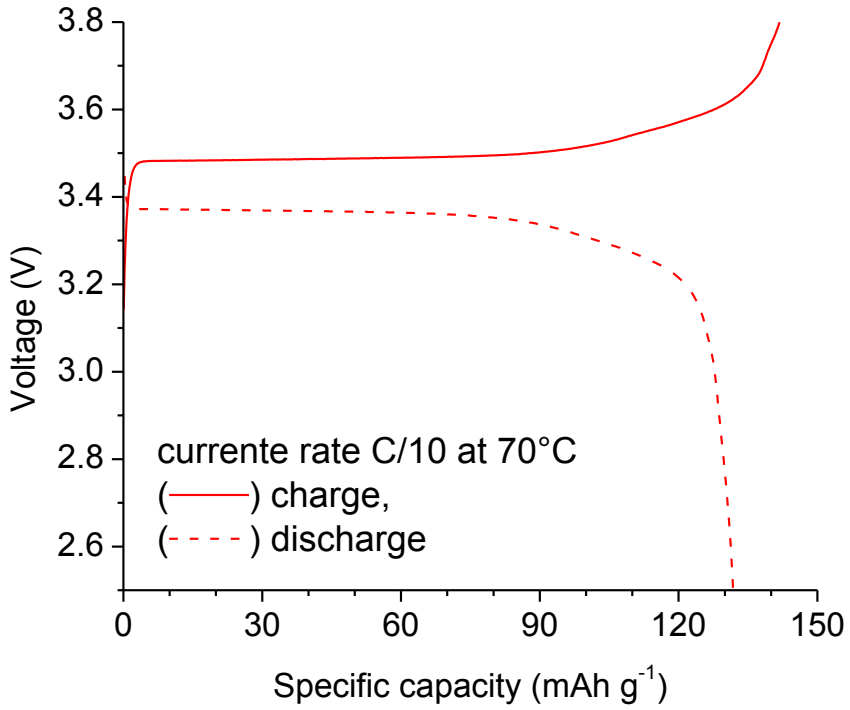


**Figure 4.19** Constant current charge/discharge potential *vs.* specific capacity profile extracted from cycle 2 at C/10 rate.

The charge/discharge efficiency was found to exceed 97 % upon initial cycling (> 99% at C/5) that confirms the reversibility of the lithium ion intercalation process as well as the electrochemical stability of the single-ion block co-polymer electrolytes developed in this study.

## 4.4 CONCLUSIONS

In this study, new family of well-defined single-ion conducting block copolymer electrolytes was synthesized via RAFT polymerization technique. Copolymers comprise a poly(PEGM) block with a fixed length and a second block based on the specifically designed ionic liquid like polymer, the length of which was varied. The detailed investigation of the physical properties of these ionic block copolymers has pinpointed the impact of polyelectrolyte's macro architecture and molecular weight on thermal and ion conducting properties. The most striking advantages of the suggested approach are summarized as follows:

1) the possibility to vary the molecular weight of polyelectrolytes and to gain the desired control over polymer's $T_g$ and ionic conductivity;
2) the preparation of solid polyelectrolytes with low $T_g$ (up to -61 °C) and comparatively high σ in a dry state (up to $2.3 \times 10^{-6}$ and $10^{-5}$ S $cm^{-1}$ at 25 and 55 °C, respectively);
3) the synthesis of polyanions with high lithium transference number (0.83) and high electrochemical stability (up to 4.5 V vs. $Li^+/Li$).

Owing to the combination of all mentioned properties, the prepared polymer materials were used as solid polyelectrolytes as well as binders in the elaboration of lithium-metal battery prototypes delivering large capacities (up to 130 mAh $g^{-1}$), with satisfying charge/discharge efficiencies and the capability to reversibly operate at medium current rates (up to C/5). Further optimization of this material must be focused in improving the performance at high rates and the stability upon prolonged cycling.

## REFERENCES


[1] D.J. Bannister, G.R. Davies, I.M. Ward, J.E. McIntyre, Ionic conductivities for poly(ethylene oxide) complexes with lithium salts of monobasic and dibasic acids and blends of poly(ethylene oxide) with lithium salts of anionic polymers, Polymer. 25 (1984) 1291–1296. doi:10.1016/0032-3861(84)90378-1.

[2] D.J. Bannister, G.R. Davies, I.M. Ward, J.E. McIntyre, Ionic conductivities for poly(ethylene oxide) complexes with lithium salts of monobasic and dibasic acids and blends of poly(ethylene oxide) with lithium salts of anionic polymers, Polymer. 25 (1984) 1291–1296. doi:10.1016/0032-3861(84)90378-1.

[3] H. Zhang, X. Zhang, E. Shiue, P.S. Fedkiw, Single-ion conductors for lithium batteries via silica surface modification, J. Power Sources. 177 (2008) 561–565. doi:10.1016/j.jpowsour.2007.11.064.

[4] L.M. Bronstein, R.L. Karlinsey, B. Stein, Z. Yi, J. Carini, J.W. Zwanziger, Solid Polymer Single-Ion Conductors: Synthesis and Properties, Chem. Mater. 18 (2006) 708–715. doi:10.1021/cm052195l.

[5] S.-W. Ryu, P.E. Trapa, S.C. Olugebefola, J.A. Gonzalez-Leon, D.R. Sadoway, A.M. Mayes, Effect of Counter Ion Placement on Conductivity in Single-Ion Conducting Block Copolymer Electrolytes, J. Electrochem. Soc. 152 (2005) A158–A163. doi:10.1149/1.1828244.

[6] J. Rolland, E. Poggi, A. Vlad, J.-F. Gohy, Single-ion diblock copolymers for solid-state polymer electrolytes, Polymer. 68 (2015) 344–352. doi:10.1016/j.polymer.2015.04.056.

[7] H.R. Allcock, D.T. Welna, A.E. Maher, Single ion conductors—polyphosphazenes with sulfonimide functional groups, Solid State Ion. 177 (2006) 741–747. doi:10.1016/j.ssi.2006.01.039.

[8] K. Matsumoto, T. Endo, Preparation and properties of ionic-liquid-containing poly(ethylene glycol)-based networked polymer films having lithium salt structures, J. Polym. Sci. Part Polym. Chem. 49 (2011) 3582–3587. doi:10.1002/pola.24795.

[9] K. Matsumoto, T. Endo, Synthesis of networked polymers by copolymerization of monoepoxy-substituted lithium sulfonylimide and diepoxy-substituted poly(ethylene glycol), and their properties, J. Polym. Sci. Part Polym. Chem. 49 (2011) 1874–1880. doi:10.1002/pola.24614.

[10] R. Meziane, J.-P. Bonnet, M. Courty, K. Djellab, M. Armand, Single-ion polymer electrolytes based on a delocalized polyanion for lithium batteries, Electrochimica Acta. 57 (2011) 14–19. doi:10.1016/j.electacta.2011.03.074.

[11] A.S. Shaplov, P.S. Vlasov, M. Armand, E.I. Lozinskaya, D.O. Ponkratov, I.A. Malyshkina, et al., Design and synthesis of new anionic "polymeric ionic liquids" with high charge delocalization, Polym Chem. 2 (2011) 2609–2618. doi:10.1039/C1PY00282A.

[12] M.M. Obadia, B.P. Mudraboyina, A. Serghei, T.N.T. Phan, D. Gigmes, E. Drockenmuller, Enhancing Properties of Anionic Poly(ionic liquid)s with 1,2,3-Triazolium Counter Cations, ACS Macro Lett. 3 (2014) 658–662. doi:10.1021/mz500310j.

[13] U.H. Choi, S. Liang, M.V. O'Reilly, K.I. Winey, J. Runt, R.H. Colby, Influence of Solvating Plasticizer on Ion Conduction of Polysiloxane Single-Ion Conductors, Macromolecules. 47 (2014) 3145–3153. doi:10.1021/ma500146v.

[14] S. Liang, U.H. Choi, W. Liu, J. Runt, R.H. Colby, Synthesis and Lithium Ion Conduction of Polysiloxane Single-Ion Conductors Containing Novel Weak-Binding Borates, Chem. Mater. 24 (2012) 2316–2323. doi:10.1021/cm3005387.

[15] A. Narita, W. Shibayama, N. Matsumi, H. Ohno, Novel ion conductive matrix via dehydrocoupling polymerization of imidazolium-type ionic liquid and

lithium 9-borabicyclo[3,3,1]nonane hydride, Polym. Bull. 57 (2006) 109–114. doi:10.1007/s00289-006-0527-1.

[16] K. Xu, Nonaqueous Liquid Electrolytes for Lithium-Based Rechargeable Batteries, Chem. Rev. 104 (2004) 4303–4418. doi:10.1021/cr030203g.

[17] P. Arora, Z. (John) Zhang, Battery Separators, Chem. Rev. 104 (2004) 4419–4462. doi:10.1021/cr020738u.

[18] M. Armand, J.-M. Tarascon, Building better batteries, Nature. 451 (2008) 652–657. doi:10.1038/451652a.

[19] S. Feng, D. Shi, F. Liu, L. Zheng, J. Nie, W. Feng, et al., Single lithium-ion conducting polymer electrolytes based on poly[(4-styrenesulfonyl)(trifluoromethanesulfonyl)imide] anions, Electrochimica Acta. 93 (2013) 254–263. doi:10.1016/j.electacta.2013.01.119.

[20] J. Li, H. Zhu, X. Wang, M. Armand, D.R. MacFarlane, M. Forsyth, Synthesis of Sodium Poly[4-styrenesulfonyl(trifluoromethylsulfonyl)imide]-co-ethylacrylate] Solid Polymer Electrolytes, Electrochimica Acta. 175 (2015) 232–239. doi:10.1016/j.electacta.2015.03.075.

[21] R. Bouchet, S. Maria, R. Meziane, A. Aboulaich, L. Lienafa, J.-P. Bonnet, et al., Single-ion BAB triblock copolymers as highly efficient electrolytes for lithium-metal batteries, Nat. Mater. 12 (2013) 452–457. doi:10.1038/nmat3602.

[22] S. Inceoglu, A.A. Rojas, D. Devaux, X.C. Chen, G.M. Stone, N.P. Balsara, Morphology–Conductivity Relationship of Single-Ion-Conducting Block Copolymer Electrolytes for Lithium Batteries, ACS Macro Lett. 3 (2014) 510–514. doi:10.1021/mz5001948.

[23] C. Jangu, A.M. Savage, Z. Zhang, A.R. Schultz, L.A. Madsen, F.L. Beyer, et al., Sulfonimide-Containing Triblock Copolymers for Improved Conductivity and Mechanical Performance, Macromolecules. 48 (2015) 4520–4528. doi:10.1021/acs.macromol.5b01009.

[24] A.A. Rojas, S. Inceoglu, N.G. Mackay, J.L. Thelen, D. Devaux, G.M. Stone, et al., Effect of Lithium-Ion Concentration on Morphology and Ion Transport in Single-Ion-Conducting Block Copolymer Electrolytes, Macromolecules. 48 (2015) 6589–6595. doi:10.1021/acs.macromol.5b01193.

[25] R.L. Weber, Y. Ye, A.L. Schmitt, S.M. Banik, Y.A. Elabd, M.K. Mahanthappa, Effect of Nanoscale Morphology on the Conductivity of Polymerized Ionic Liquid Block Copolymers, Macromolecules. 44 (2011) 5727–5735. doi:10.1021/ma201067h.

[26] Y. Ye, J.-H. Choi, K.I. Winey, Y.A. Elabd, Polymerized Ionic Liquid Block and Random Copolymers: Effect of Weak Microphase Separation on Ion Transport, Macromolecules. 45 (2012) 7027–7035. doi:10.1021/ma301036b.

[27] D. Devaux, D. Glé, T.N.T. Phan, D. Gigmes, E. Giroud, M. Deschamps, et al., Optimization of Block Copolymer Electrolytes for Lithium Metal Batteries, Chem. Mater. 27 (2015) 4682–4692. doi:10.1021/acs.chemmater.5b01273.

[28] A.S. Shaplov, R. Marcilla, D. Mecerreyes, Recent Advances in Innovative Polymer Electrolytes based on Poly(ionic liquid)s, Electrochim Acta. 175 (2015) 18–34. doi:10.1016/j.electacta.2015.03.038.

[29] A.S. Shaplov, P.S. Vlasov, E.I. Lozinskaya, D.O. Ponkratov, I.A. Malyshkina, F. Vidal, et al., Polymeric Ionic Liquids: Comparison of Polycations and Polyanions, Macromolecules. 44 (2011) 9792–9803. doi:10.1021/ma2014518.

[30] M. Mertoglu, A. Laschewsky, K. Skrabania, C. Wieland, New Water Soluble Agents for Reversible Addition−Fragmentation Chain Transfer Polymerization and Their Application in Aqueous Solutions, Macromolecules. 38 (2005) 3601–3614. doi:10.1021/ma048268o.

[31] G.N. Grover, J. Lee, N.M. Matsumoto, H.D. Maynard, Aminooxy and Pyridyl Disulfide Telechelic Poly(poly(ethylene glycol) acrylate) by RAFT

Polymerization, Macromolecules. 45 (2012) 4958–4965. doi:10.1021/ma300575e.

[32] W. Zhao, G. Gody, S. Dong, P.B. Zetterlund, S. Perrier, Optimization of the RAFT polymerization conditions for the in situ formation of nano-objects via dispersion polymerization in alcoholic medium, Polym. Chem. 5 (2014) 6990–7003. doi:10.1039/C4PY00855C.

[33] D. Rinaldi, T. Hamaide, C. Graillat, F. D'Agosto, R. Spitz, S. Georges, et al., RAFT copolymerization of methacrylic acid and poly(ethylene glycol) methyl ether methacrylate in the presence of a hydrophobic chain transfer agent in organic solution and in water, J. Polym. Sci. Part Polym. Chem. 47 (2009) 3045–3055. doi:10.1002/pola.23374.

[34] A.S. Shaplov, E.I. Lozinskaya, D.O. Ponkratov, I.A. Malyshkina, F. Vidal, P.-H. Aubert, et al., Bis(trifluoromethylsulfonyl)amide based "polymeric ionic liquids": Synthesis, purification and peculiarities of structure–properties relationships, Electrochim Acta. 57 (2011) 74–90. doi:10.1016/j.electacta.2011.06.041.

[35] J. Evans, C.A. Vincent, P.G. Bruce, Electrochemical measurement of transference numbers in polymer electrolytes, Polymer. 28 (1987) 2324–2328. doi:10.1016/0032-3861(87)90394-6.

[36] A. Manuel Stephan, K.S. Nahm, Review on composite polymer electrolytes for lithium batteries, Polymer. 47 (2006) 5952–5964. doi:10.1016/j.polymer.2006.05.069.

# CHAPTER FIVE

## *Single-ion conducting gel polymer electrolyte with wide operating temperature conditions*

### 5.1 INTRODUCTION

In the previous chapter, the control radical polymerization of a specifically designed anionic monomer was exploited to prepare a novel class of single-ion conductors. The preferential $Li^+$ transport properties were successfully demonstrated by a lithium-ion transference number approaching the unity. However, the ionic conductivity of the prepared solid polymer electrolyte (SPE) was limited to the $10^{-5}$ range. To date, the most effective approach to increase the ionic conductivity of polymeric single-ion conductors is to incorporate a liquid plasticizer into the polymer matrix, hence forming a gel polymer electrolyte (GPE). As a result, room temperature σ values in the order of $10^{-4}$ - $10^{-5}$ S $cm^{-1}$ were reported for single-ion GPEs, and the addition of plasticizer resulted in an increased number of dissociated charge carriers and faster pathways for lithium-ion diffusion in the liquid phase.

Besides good transport properties, sufficient mechanical stability is another important requirement in sight of replacement of conventional electrode separators with GPE membranes. Structural stability is usually achieved by blending with high $T_g$ materials, such as perfluorinated polymers [1–3], and chemical crosslinking [4,5]. The great potential of this novel class of electrolytes was recently demonstrated by reports on lab-scale cells operating at ambient conditions [1–3,6–9]. However, further research efforts are still required to improve the power density delivery.

In this respect, the preparation and characterization of single-ion gels is discussed here. The newly elaborated GPEs are based on a lithium anionic monomer recently developed by Shaplov et al. [10], namely lithium 1-[3-(methacryloyloxy)propylsulfonyl]-1-(trifluoromethylsulfonyl)imide (LiMTFSI), and their use as polymer electrolytes in lab-scale lithium metal cells is demonstrated. Single-ion GPEs are obtained via thermal copolymerization of LiMFTSI with mono and bifunctional poly(ethylene glycol) methyl ether methacrylate monomers (PEGM and PEGDM, respectively) in the presence of propylene carbonate (PC). The proposed "in-situ" synthesis allows to incorporate the liquid plasticizer in the gel whilst forming the covalently cross-linked network. The resulting membranes showed ionic conductivities exceeding the values usually reported for single-ion SPE, noteworthy in a wide range of temperature. They also display wide electrochemical stability window and remarkably high $t_{Li^+}$ approaching the unity. Furthermore, the self-standing nature of the polymer membranes allows their effective use as electrodes separating electrolyte. Composite electrode/electrolyte assemblies were prepared via the same simple

procedure and successfully cycled in lithium metal lab-scale prototypes in a wide temperature range even at high current rate (5C).

## 5.2. EXPERTIMENTAL

### 5.2.1. MATERIALS

Poly(ethylene glycol) methyl ether methacrylate (PEGM, $M_n$ = 500 g $mol^{-1}$, Sigma-Aldrich) and poly(ethylene glycol) dimethacrylate (PEGDM, $M_n$ = 550 g $mol^{-1}$, Sigma-Aldrich) were degassed under vacuum (<1 mm Hg). The liquid monomers were transferred inside the Ar-filled glove-box (MBraun UNILab, $O_2$ and $H_2O$ content < 0.1 ppm) and treated with molecular sieves (beads 4Å, 8-12 mesh, Sigma-Aldrich) for one week to ensure the complete removal of water prior to use. Propylene carbonate (PC, battery grade, Solvionic), *N*-methyl-2-pyrrolidone (NMP, Sigma-Aldrich), polyvinylidene fluoride (PVdF, Solvay Solef 6020), carbon-coated lithium iron phosphate ($LiFePO_4$, Advanced Lithium Electrochemistry Co. Ltd.), carbon black C65 (Timcal), lithium metal foil (Chemetall Foote Corporation) were used without further purification. 2,2'-Azobisisobutyronitrile (AIBN, Sigma-Aldrich) was recrystallized from methanol before use. Carbon coated aluminum foils were purchased from Showa Denko.

## 5.2.2. SYNTHESIS OF LITHIUM 1-[3-(METHACRYLOYLOXY) PROPYLSULFONYL]-1-(TRIFLUOROMETHANESULFONYL) IMIDE (LIMTFSI)

LiMTFSI was prepared in full accordance with the procedure reported in the previous chapter. The product was obtained in the form of a white crystalline powder. Prior to use, LiMTFSI was dried overnight under vacuum (<1 mm Hg) at 25 °C and transferred inside the Argon-filled glove-box.

## 5.2.3. PREPARATION OF SINGLE-ION GPE FILMS

The preparation of GPEs was carried inside the Ar-filled glove box to avoid moisture contamination. Calculated amounts of LiMTFSI, PEGM, PEGDM and PC were mixed in a vial and the resulting mixture was stirred until homogenization. An appropriate amount of thermal initiator (AIBN, 3 wt% with respect to monomer) was added upon stirring. The clear solution was poured into a mold made by a Teflon gasket (thickness 200 µm) clamped between two glass plates. Then, the mold was positioned inside a sealed quartz vessel and transferred outside the glovebox. Polymerization was carried out at 70 °C for 4 h in an oven. The mold was de-assembled inside the Ar-filled glove box and the obtained GPE films were used without further purification. Sample compositions and coding are given in **Table 5.1**.

**Table 5.1.** Composition (in weight %) of the prepared GPE membranes.

| Sample | LiMTFSI | PEGM | PEGDM | PC |
|---|---|---|---|---|
| GPE-1 | 6.4 | 38.6 | 5 | 50 |
| GPE-2 | 7.5 | 37.5 | 5 | 50 |
| GPE-3 | 9.0 | 36.0 | 5 | 50 |
| GPE-4 | 11.3 | 33.7 | 5 | 50 |
| GPE-5 | 15.0 | 30.0 | 5 | 50 |

### 5.2.4. CHARACTERIZATION TECHNIQUES

The physico-chemical characterization techniques used in this chapter were performed as described in the appendix.

### 5.2.5. Li BATTERIES ASSEMBLY AND TESTING

A composition of 80 wt% of carbon coated $LiFePO_4$, 10 wt% of PVdF and 10 wt% of carbon black was used for cathodes' preparation. The active material and carbon black were gently mixed in a hand mortar and added to a 5 wt% solution of PVdF in NMP. The suspension was homogenized using an ULTRA-TURRAX mixer for about half an hour. The obtained slurry was casted onto an aluminum current collector using a doctor-blade). NMP was removed from the electrodes by evaporation in an oven at 70 °C, further dried at 120 °C/1 mm Hg overnight and transferred inside the Ar-filled glove-

box. The active mass loading per unit area was found to be 3.4 mg $cm^{-2}$. The surface of the electrode was coated with a thin layer of the monomers reactive mixture in PC (thickness < 100 µm) and sealed inside the glass mold. In-situ free-radical polymerization was carried out for 4 h at 70 °C under Ar-atmosphere. Round disks of 14 mm diameter were cut out of the foil, which comprise the ready-to-use multiphase electrolyte-coated electrode foil. Lithium metal cells were then assembled in the glove-box inside ECC-Std electrochemical test cells. They were cycled at 25 and 70 °C at different current rates in terms of galvanostatic charge and discharge with an ARBIN BT2000 battery tester.

## 5.3. RESULTS AND DISCUSSIONS

### 5.3.1. PREPARATION OF SINGLE-ION CONDUCTING GPEs

The novel GPEs presented here were prepared through thermal copolymerization of a lithium anionic monomer (LiMTFSI) with poly(ethylene glycol) methyl ether methacrylate (PEGM) and a small amount of cross-linker (PEGDM) in the presence of PC as the reaction medium. As a result, a covalently bonded polymer network was formed where the PC was trapped inside, thus forming GPE membranes with single-ion conduction characteristics. **Scheme 5.1** schematically represents the one-step process to prepare single-ion GPEs. While the amounts of crosslinker and PC were kept fixed (at 5 and 50 wt. %, respectively), the ratio between LiMTFSI and PEGDM monomers was varied with the aim of tailoring the final properties

of the gels, including ionic conductivity. Despite the relevant amount of PC incorporated in the gel, the prepared films were found to be self-standing and non-tacky. Notably, polymer networks showed excellent compatibility with PC, and deswelling leakage of the liquid plasticizer was not observed even upon long storage times.

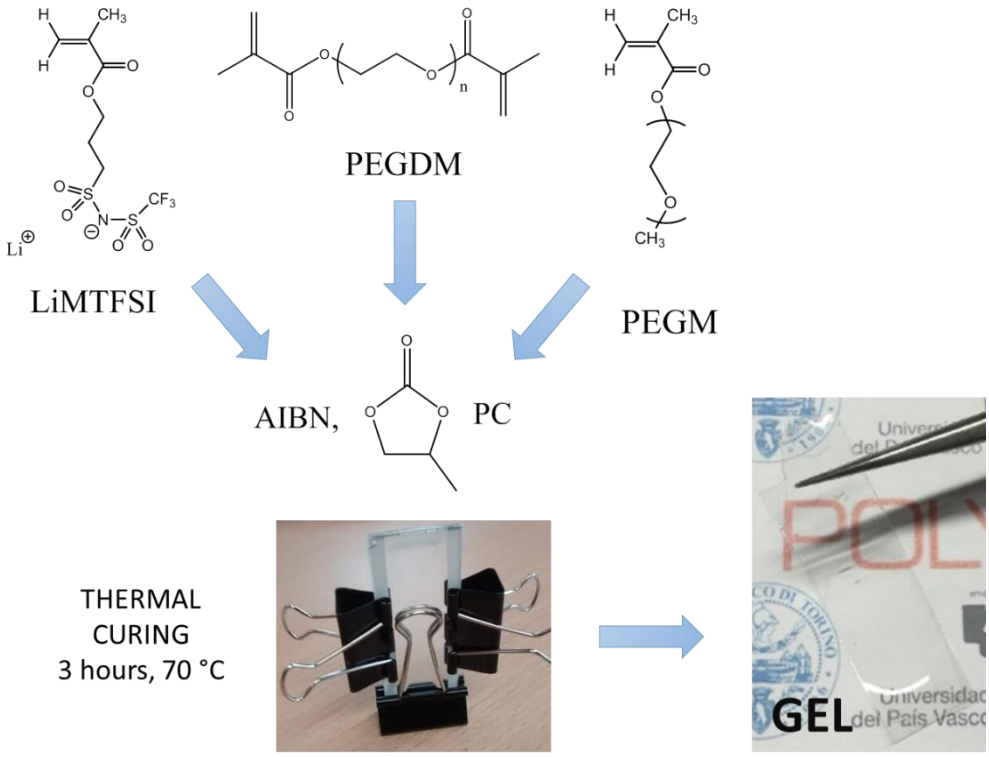


**Scheme 5.1** Sketched preparation procedure of single-ion GPEs, along with the structure of the reagents and the aspect of the final polymer electrolyte.

## 5.3.2 CHARACTERIZATION OF SINGLE ION GPEs

Viscoelastic characterization of gel-polymer electrolytes was carried out by means of DMTA analysis, by measuring the storage (*E*′) and loss (*E*″) modules and studying the variation of the damping factor *tanδ* as *E*″*/E*′ ratio. Moreover, these measurements allowed to identify the glass transition temperature ($T_g$) value as the peak of each *tanδ* curve. Given the fact that all the samples contained the same amount of plasticizer (PC) and bifunctional monomer (PEGDM), appreciable differences in $T_g$ values were not detected and all their values were found in the range of − 69±2 °C. As a representative example for all the samples prepared, the curves of *E*′ and *tanδ* as a function of the temperature for GPE-3 sample are shown in **Figure 5.1**. To highlight the role of the plasticizer within the macromolecular architecture, sample GPE-3 was prepared without introducing PC in the initial mixture, and the resulting curve is shown for comparison. The $T_g$ of this sample increased by 11 °C with respect to its PC-laden counterpart, and the plot of *E*′ (the values of which were always higher with respect to those of the PC-based sample) evidences the increased mechanical properties of the polymeric network when the plasticizer was not introduced in the initial reactive mixture. Overall, for all of the GPE samples the morphology was fully amorphous and a single $T_g$ was evidenced, which was well below room temperature, thus rendering this material suitable for actual lithium battery application.

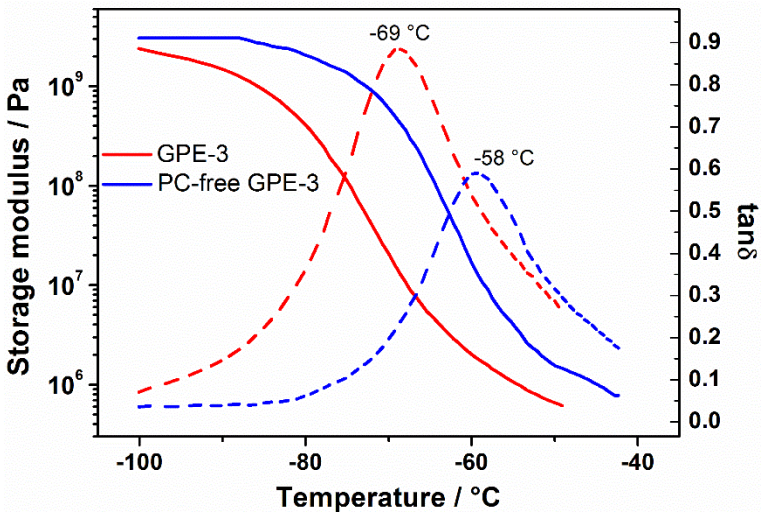


**Figure 5.1**. DMTA traces showing the variation of *E'* and *tanδ* as a function of temperature for GPE-3 sample, prepared with and without PC as a plasticizer.

Results of the thermal stability test, evaluated by thermogravimetric analysis under flowing nitrogen, are shown in **Figure 5.2**. All of the single-ion GPEs showed a two-step degradation process (see the differential curve for GPE-3 in the inset of **Figure 5.2**) corresponding to the stability of each component used for samples preparation. The first degradation step was due to the plasticizer (PC) evaporation; the onset temperature was 110 °C, whether the decomposition temperature occurred at 150 °C (50% weight loss of PC). The second step at around 400 °C was assigned to the degradation of the polymeric matrix, and was in perfect agreement with the thermal stability of methacrylic architectures. Overall, as evidenced by DMTA analysis and TGA traces, the newly proposed GPEs can be safely

implemented in lithium-based battery systems in the temperature range between –65 and 150 °C.

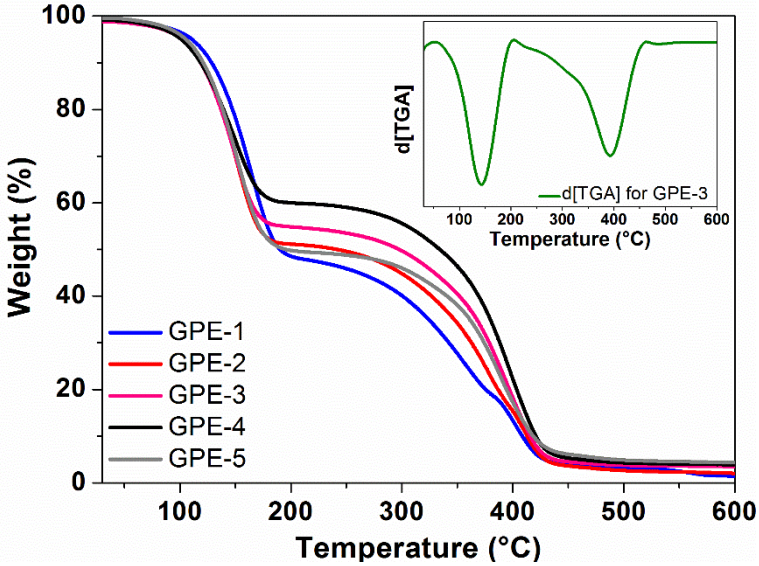


**Figure 5.2** TGA traces, measured under $N_2$ from 30 to 600 °C, of the GPE samples under study, the differential curve of sample GPE-3 is shown in the inset.

Ionic conductivity of the single-ion GPEs was measured via electrochemical impedance spectroscopy in the temperature range between 0 and 80 °C (**Figure 5.3)**. Amongst all the samples, GPE-3, corresponding to 9 wt% of LiMTFSI, showed the highest σ value both at 20 °C ($8.6 \times 10^{-5}$ S $cm^{-1}$) and 80 °C ($1.0 \times 10^{-3}$ S $cm^{-1}$). The obtained ionic conductivities approach practical values for operating a lithium-ion battery

at ambient temperature and markedly outperform the results reported for single-ion SPEs presented in the previous chapter.

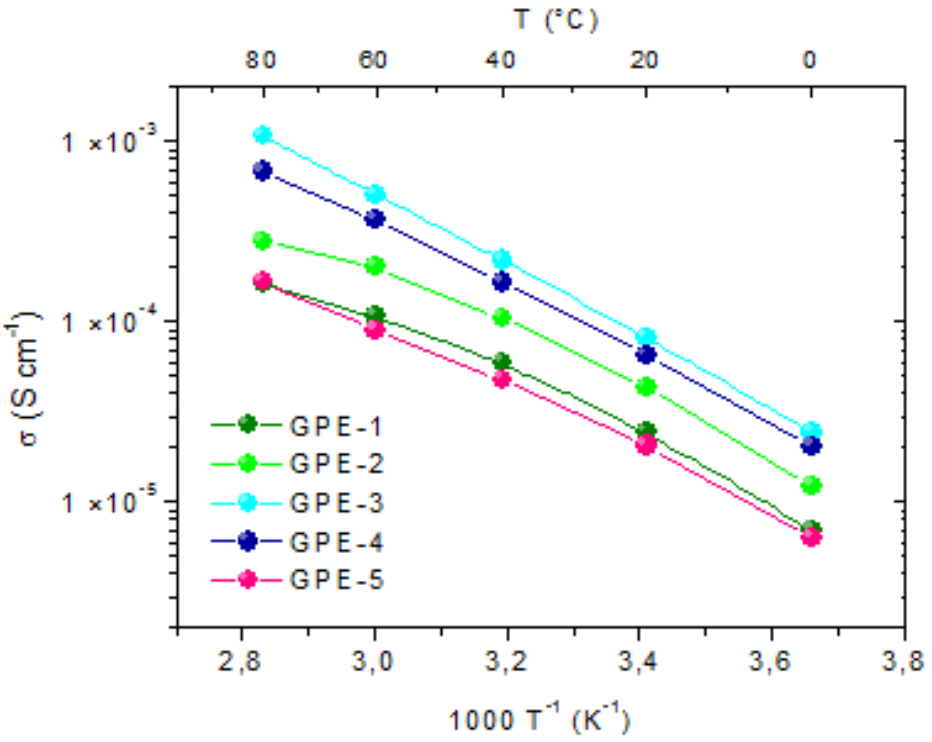


**Figure 5.3** Plot of ionic conductivity against the inverse temperature for the prepared GPEs with different amounts of lithium salt monomer.

The ionic conductivity appears to be dependent on the $Li^+$ concentration; the relationship between ionic conductivity and LiMTFSI content at 20 °C is shown in **Figure 5.4**. Under isothermal conditions, σ increased when increasing the LiMTFSI content, and such a trend was respected up to 9 wt%

content. This behavior results from the increased concentration of charge carriers in the gel. However, increasing the LiMTFSI content above the optimal value resulted in a decrease of σ. The observed trend is ascribable to the reduced lithium-ion mobility due to aggregation in ion clusters. It is worth to point out that the described trend was generally respected in the entire temperature range considered in this study (0–80 °C).

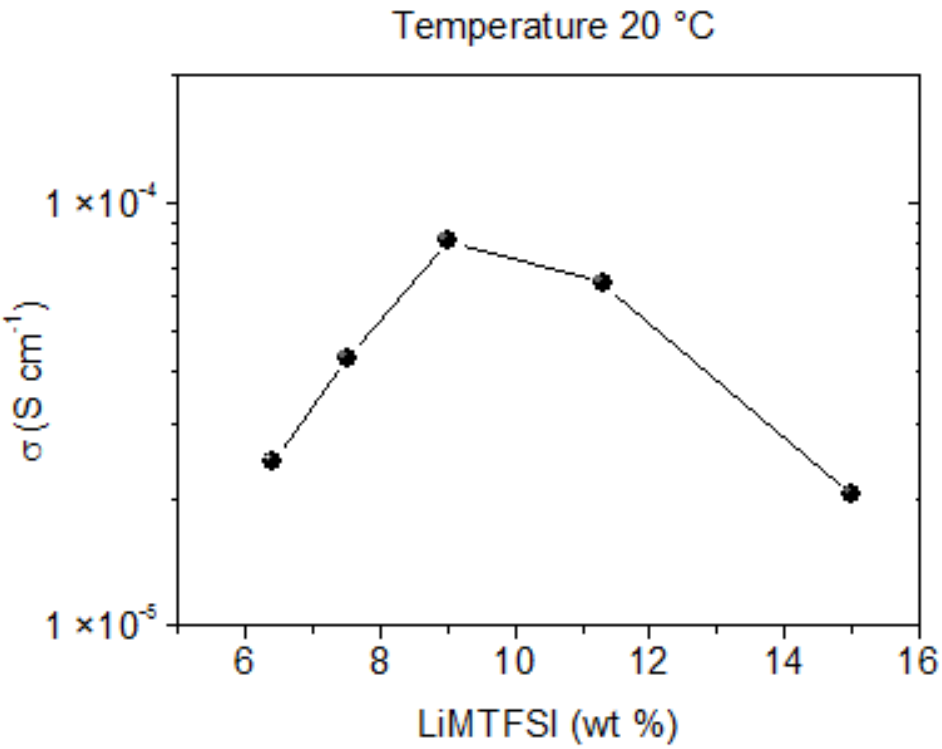


**Figure 5.4** Dependence of ionic conductivity on $Li^+$ concentration under isothermal conditions (20 °C).

It is worth to point out that the described trend was generally respected in the entire temperature range considered in this study (0–80 °C). A similar behavior was observed for solid polymer electrolytes [4,11]; interestingly, single-ion GPEs seem to follow a similar tendency. To compare directly the influence of the plasticizer on ionic conductivity, PC-free GPE-3 sample was also tested. The ionic conductivity of the dry sample was found two order of magnitude lower than that of the gel (**Figure 5.5**).

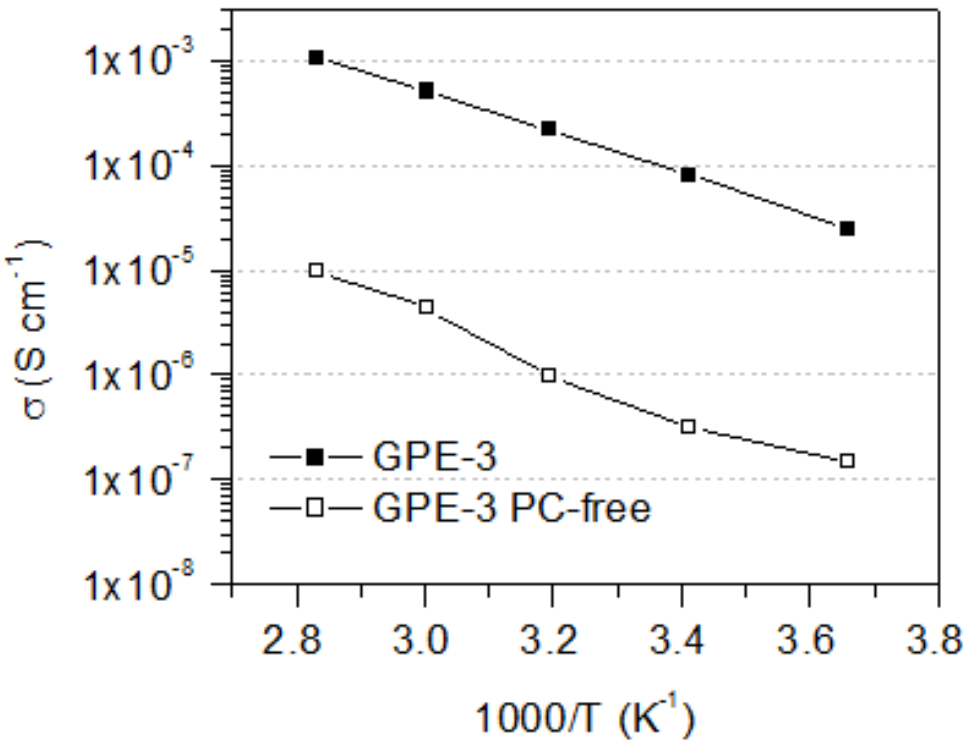


**Figure 5.5** Plot of ionic conductivity against inverse temperature for GPE membranes with and without PC as plasticizer.

Thus, the addition of PC has a twofold effect on transport properties; the most straightforward explanation is the increased mobility of lithium-ion in the plasticized medium. Furthermore, the effective concentration of mobile lithium-ion is expected to increase in virtue of the higher dielectric constant of the gel electrolyte [4,12].

Sample GPE-3, which showed the highest ionic conductivity, was selected as representative to investigate the electrochemical stability window of this new class of electrolytes. CV curves obtained at 25 and 70 °C are shown in **Figure 5.6.** At both the temperatures, cathodic scans show a couple of reversible redox peaks between -0.5 and 0.6 V vs. $Li^+/Li$; this process is associated to the reversible lithium plating and stripping onto/from the copper electrode. The current density at 70 °C appears to be roughly ten-fold greater than that at 20 °C; nevertheless, the plating-stripping process appears to be highly efficient in both cases. During anodic scans, no appreciable increase in the oxidation currents was observed up to 5.5 V vs. $Li^+/Li$. Indeed, the anions in the proposed system, responsible for electrochemical instability at high potentials [13], are covalently bonded to the polymer network and can be oxidized only at the electrode surface. Therefore, most likely accounting for the excellent electrochemical stability in the wide temperature interval between 25 – 70 °C.

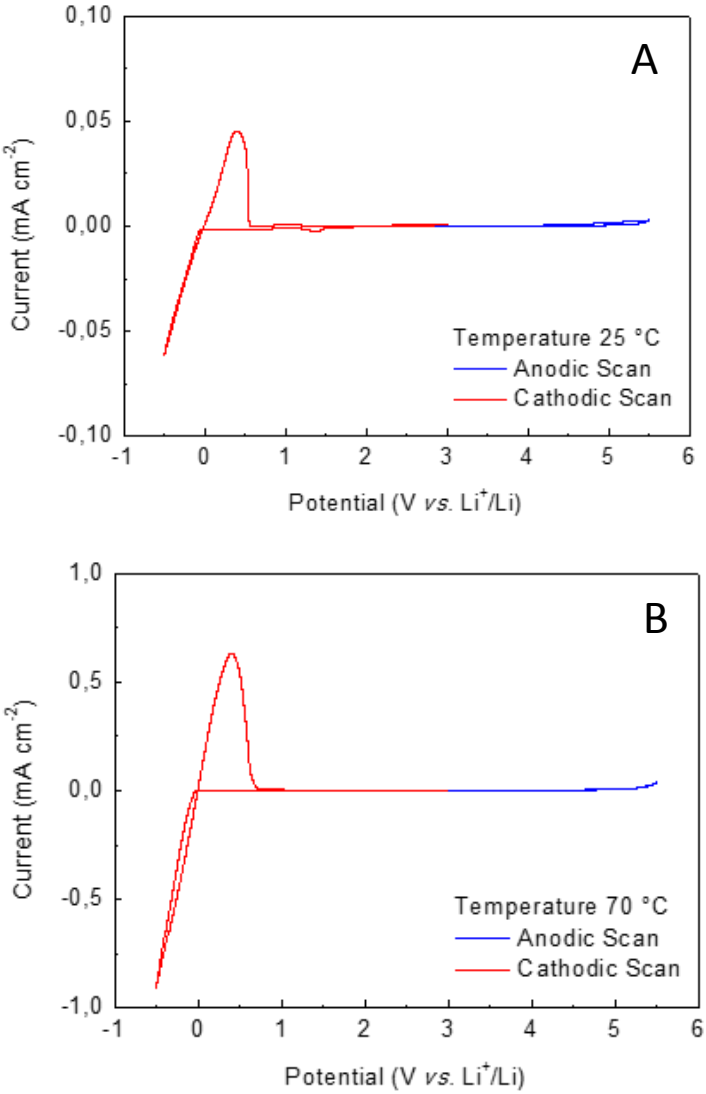


**FIGURE 5.6** Electrochemical window of GPE-3 obtained by CV in the -0.5 – 5.5 V vs. $Li^+/Li$ interval at a scan rate of 0.2 mv $s^{-1}$ and different temperatures: (a) 25 and (b) 70 °C.

The method proposed by Evans and Vincent was used to calculate the lithium-ion transference number of the prepared gel polymer electrolytes; again, data for GPE-3 are shown as representative for the series of GPEs under study. The results of EIS and polarization tests at 25 and 70 °C are given in **Table 5.2**. Tests were repeated twice on each cell to guarantee reproducibility. The value of the transference number at 25 °C was found to be 0.86 ± 0.02, while at 70 °C it slightly increased up to0.90± 0.02, thus comparable within the range of experimental error. The obtained results are in good agreement with most of the literature findings on single-ion conductors, and a transference number approaching the unity proves that - unlike a traditional binary electrolyte - the bulk of the ionic current is carried exclusively by lithium cations.

**Table 5.2.** Lithium ion transference number results for sample GPE-3[a]

| Cell | T (°C) | $R_0$ (Ω) | $R_s$ (Ω) | $I_0$ (μA) | $I_s$ (μA) | $t_{Li^+}$ |
|---|---|---|---|---|---|---|
| 1 | 25 | 760 | 780 | 4.5 | 4.1 | 0.88 |
| 1 (after 48 h recovery) | 25 | 1120 | 1123 | 4.3 | 3.9 | 0.84 |
| 2 | 70 | 24 | 25 | 38.9 | 36.0 | 0.91 |
| 2 (after 48 h recovery) | 70 | 60 | 72 | 36.5 | 32.1 | 0.89 |

[a] potential bias applied: 10 mV

In order to understand the compatibility of the single-ion conducting gel polymer electrolytes with the lithium metal electrode, two Li/GPE/Li symmetric cells were assembled, and the evolution of the interfacial resistance with time was studied at 25 and 70 °C. Measurements were carried out using electrochemical impedance spectroscopy (EIS) and resulting profiles are shown in **Figure 5.7**.

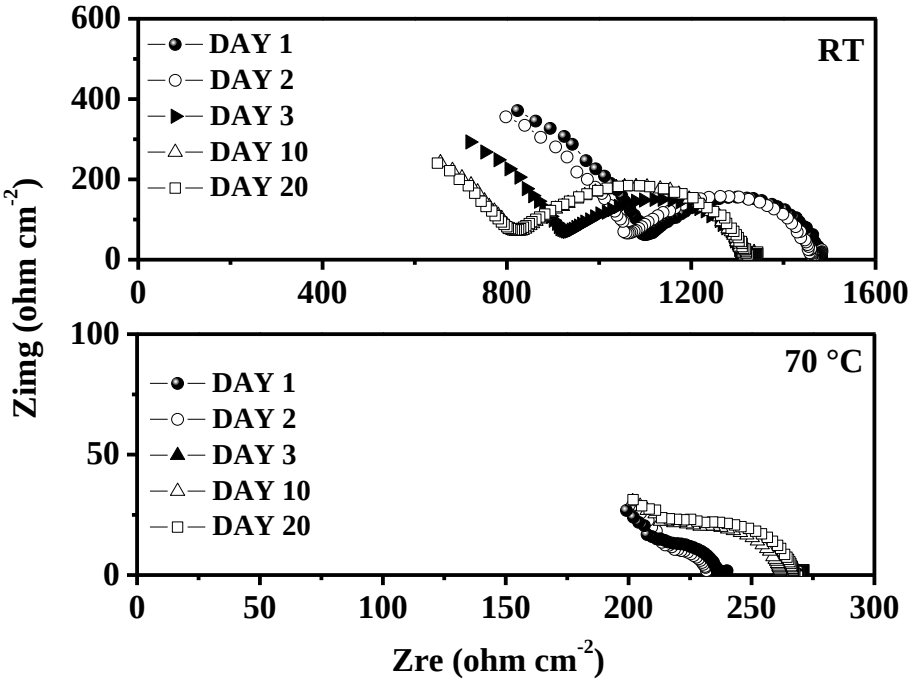


**Figure 5.7** Nyquist plots representing the time evolution of the impedance profile corresponding to the change in interfacial resistance for Li/GPE/Li symmetric cells tested at room temperature (top) and at 70 °C (bottom).

The deviation in bulk resistance ($R_b$, high frequency intercept) and interfacial resistance ($R_i$, low frequency intercept) are shown as a function of time (days). Symmetric cells tested at RT showed an increase in $R_i$ value with time, which was stabilized after some days and remained stable for long time. Indeed, $R_b$ values decreased from 1110 to 820 Ω $cm^{-2}$. It is an unusual behavior, and might be arising from the improved contact that is achieved with time between the lithium metal electrode and the polymer electrolyte. In the case of the GPE membrane tested at 70 °C, $R_b$ and $R_i$ increased with time and stabilized after few days. Then, resistance remained stable even after 20 days and this is an indication that the prepared electrolyte is pure and can form a stable interfacial layer with lithium metal, which accounts for its safe operation in lithium metal batteries.

### 5.3.3 TESTING IN LITHIUM METAL POLYMER CELLS

Constant current charge/discharge cycling in symmetric Li/GPE/Li cells was performed to determine the change in overpotential related to the lithium plating/stripping process while applying different current regimes. Measurements were performed at different current intensities starting from 3 μA $cm^{-2}$ up to 0.5 mA $cm^{-2}$ at RT; the experiment was repeated at 70 °C as well. As can be elucidated from **Figure 5.8**, the change in potential at high current density was minimal for the cell tested at 70 °C, while it was much higher when the device was tested at RT. The obtained results are also in agreement with the specific capacity values obtained when the cells were cycled at different C rates.

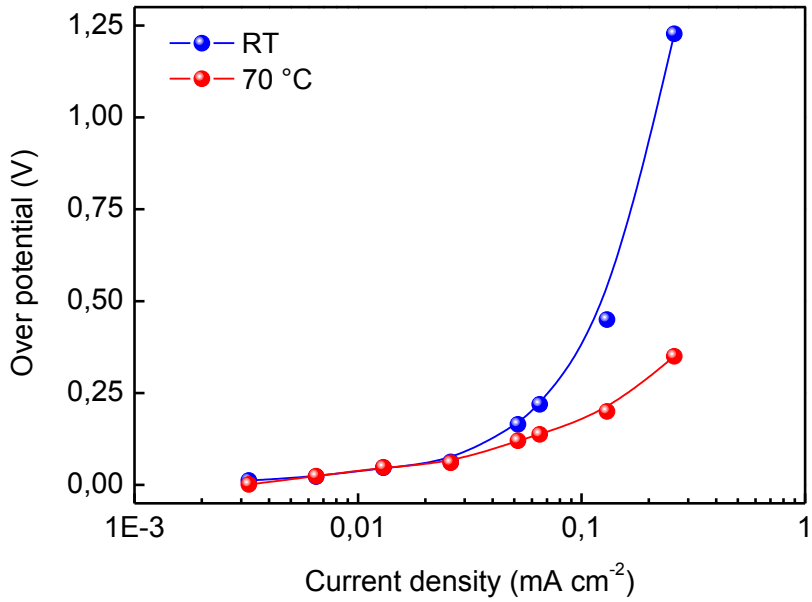


**Figure 5.8.** Plot illustrating the potential as a function of the current rate for a Li/GPE/Li symmetric cell at RT and 70 °C while performing lithium plating/stripping processes at different current densities.

GPE-3 gel polymer membrane was finally tested as electrolyte separator in a lithium metal cell having the configuration Li | GEP-3 | $LiFePO_4$. Polymerization of the monomer reactive mixture in PC was carried out directly on the electrode sheets: ready-to-use electrodes, coated with the single-ion GPE, were prepared with this simple procedure, which is detailed in the experimental section 5.2.5. This assures that no further electrode separator is needed during assembly of the lab-scale metal cells, as the GPE

films possesses sufficient mechanical stability to avoid contacts between the electrodes even upon testing at high current regimes.

Cycling tests were conducted at different temperatures (25 and 70 °C) to demonstrate the safe use of this new class of gel polymer electrolytes in a wide temperature range. The different current rates applied to fully charge/discharge the working electrode in n hours are denoted as C/n rates. **Figure 5.9** shows the plot of specific discharge capacity at different C-rates, whether the charge rate was kept fixed at C/10. The cell operating at 70 °C was able to deliver 143 mAh $g^{-1}$ at low C/10 rate, corresponding to the 84% of the theoretical capacity of $LiFePO_4$. Upon increasing the current rate, the discharge capacity decreased slightly, which is remarkable for a single-ion conducting polymer electrolyte. The cell was able to deliver up to 110 mAh $g^{-1}$ at 2C corresponding to the 65% of the theoretical capacity. The measured discharge capacity substantially decreased only at a very high rate; nevertheless, 48 mAh $g^{-1}$ were measured at 5C, which is definitely remarkable if compared to the best results reported in the literature so far [1–3,6–9]. Overall, the performance of the cell was excellent both in terms of delivered capacity at high C-rates and stable cycling at relatively high temperature. It is outstanding to pinpoint that the cell operating at 25 °C was able to deliver high specific capacity up to 126 mAh $g^{-1}$ at C/10, about 110 mAh $g^{-1}$ at C/5 and 70 mAh $g^{-1}$ at C/2. A drop in the measured discharge capacity was observed only at relatively high 1C. Overall, such a performance is definitely outstanding for a single-ion electrolyte operating at RT.

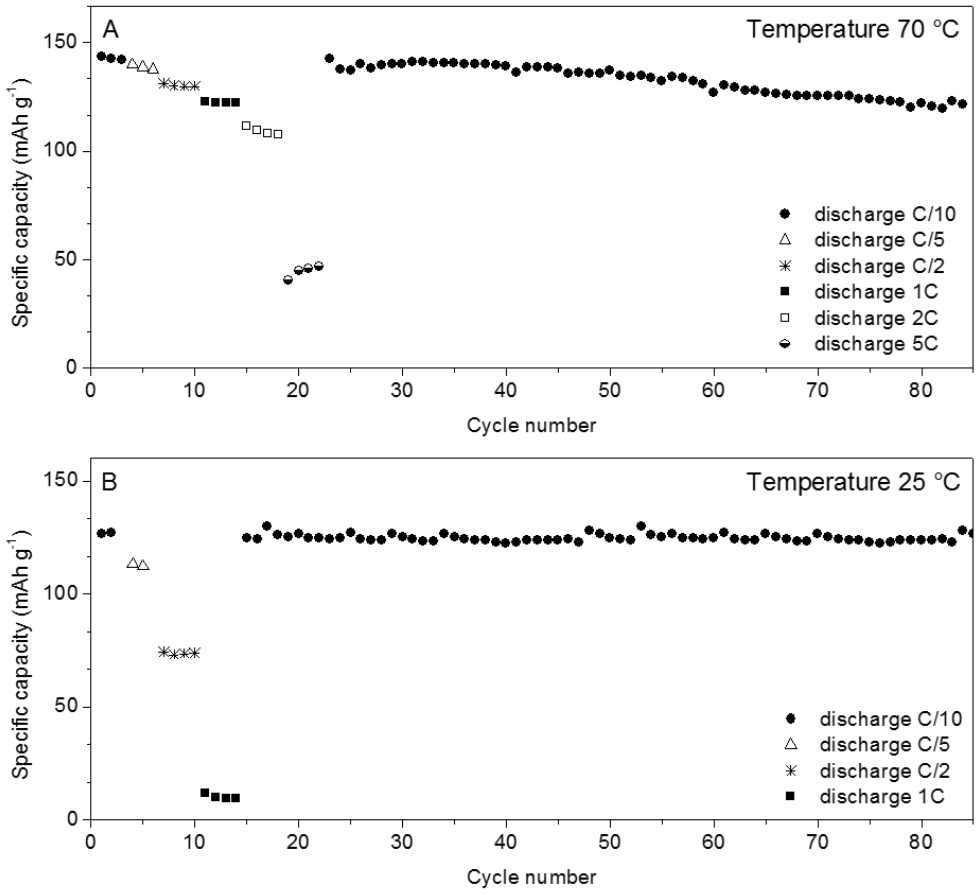


**Figure 5.9**. (a) Specific capacity vs. cycle number plots at different discharge rates and constant C/10 charge rate at 70 °C and (b) room temperature.

To investigate the cycling stability of the newly elaborated single-ion GPEs, constant current charge/discharge tests were performed at a constant C/10 discharge rate for over 80 cycles. Regardless of the operating temperature, the lithium polymer cells were able to reversibly operate

without limited capacity fading. The capacity retention at 70 °C corresponded to the 85% of the initial capacity, while at 25 °C it was equal to 98 % of the initial capacity.

Potential vs. specific discharge capacity profiles obtained at different current rates are shown in **Figure 5.10**. At both the operating temperatures, the well-known discharge curve of $LiFePO_4$ with flat plateau can be readily detected even when the current up to C/5. The typical potential plateau of $LiFePO_4$ turned into a slope when the current was further increased, along with an increased overpotential, which is more evident at lower temperature.

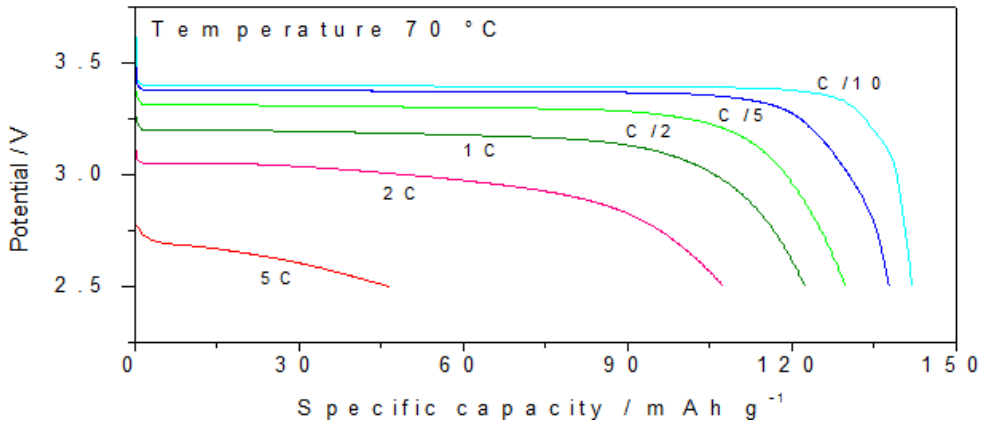


**Figure 5.10**. Potential profile vs. specific capacity plots at different discharge rates and constant C/10 charge rate at 70 °C.

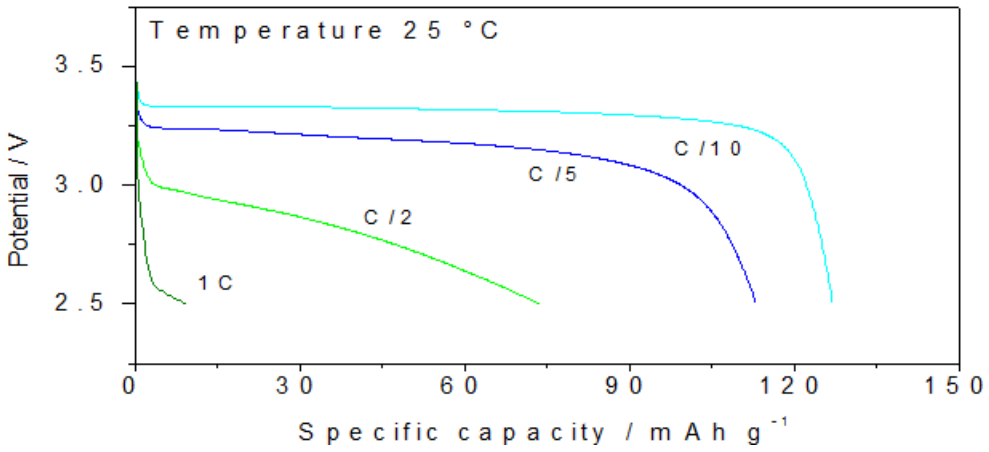


**Figure 5.11** Potential profile vs. specific capacity plots at different discharge rates and constant C/10 charge rate at room temperature.

## 5.4. CONCLUSIONS

Innovative single-ion conducting gel polymer electrolytes based on the novel LiMTFSI anionic monomer were here presented, which were prepared via a facile one-step procedure.

Gels showed sufficient mechanical properties to be self-standing and were able to retain PC inside the polymeric network upon prolonged periods of storage. Low $T_g$ values of around –70 °C were obtained due to the plasticizing effect of PC, along with thermal stability exceeding 100 °C. Ionic conductivities approaching $10^{-4}$ S $cm^{-1}$ at room temperature and wide electrochemical stability window of 5 V were measured. The single ion

conducting nature of these electrolytes was demonstrated via transference number values approaching the unity.

The sum of the positive characteristics reported above along with the remarkably stable cycling in lab-scale lithium metal cells enlighten that these gels might be an ideal candidate as electrolyte separator in the next-generation of lithium batteries safely operating in a wide temperature range.

## REFERENCES


[1] Y. Zhang, C.A. Lim, W. Cai, R. Rohan, G. Xu, Y. Sun, et al., Design and synthesis of a single ion conducting block copolymer electrolyte with multifunctionality for lithium ion batteries, RSC Adv. 4 (2014) 43857–43864. doi:10.1039/C4RA08709G.

[2] Y. Zhang, R. Rohan, Y. Sun, W. Cai, G. Xu, A. Lin, et al., A gel single ion polymer electrolyte membrane for lithium-ion batteries with wide-temperature range operability, RSC Adv. 4 (2014) 21163–21170. doi:10.1039/C4RA02729A.

[3] G. Xu, R. Rohan, J. Li, H. Cheng, A novel sp3Al-based porous single-ion polymer electrolyte for lithium ion batteries, RSC Adv. 5 (2015) 32343–32349. doi:10.1039/C5RA01126D.

[4] X.-G. Sun, C.L. Reeder, J.B. Kerr, Synthesis and Characterization of Network Type Single Ion Conductors, Macromolecules. 37 (2004) 2219–2227. doi:10.1021/ma035690g.

[5] X.-G. Sun, J.B. Kerr, Synthesis and Characterization of Network Single Ion Conductors Based on Comb-Branched Polyepoxide Ethers and Lithium

Bis(allylmalonato)borate, Macromolecules. 39 (2006) 362–372. doi:10.1021/ma0507701.

[6] X. Wang, Z. Liu, C. Zhang, Q. Kong, J. Yao, P. Han, et al., Exploring polymeric lithium tartaric acid borate for thermally resistant polymer electrolyte of lithium batteries, Electrochimica Acta. 92 (2013) 132–138. doi:10.1016/j.electacta.2013.01.026.

[7] R. Rohan, Y. Sun, W. Cai, Y. Zhang, K. Pareek, G. Xu, et al., Functionalized polystyrene based single ion conducting gel polymer electrolyte for lithium batteries, Solid State Ion. 268, Part B (2014) 294–299. doi:10.1016/j.ssi.2014.10.013.

[8] G. Xu, Y. Zhang, R. Rohan, W. Cai, H. Cheng, Synthesis, Characterization and Battery Performance of A Lithium Poly (4-vinylphenol) Phenolate Borate Composite Membrane, Electrochimica Acta. 139 (2014) 264–269. doi:10.1016/j.electacta.2014.06.173.

[9] B. Qin, Z. Liu, G. Ding, Y. Duan, C. Zhang, G. Cui, A single-ion gel polymer electrolyte system for improving cycle performance of LiMn2O4 battery at elevated temperatures, Electrochimica Acta. 141 (2014) 167–172. doi:10.1016/j.electacta.2014.07.004.

[10] A.S. Shaplov, P.S. Vlasov, M. Armand, E.I. Lozinskaya, D.O. Ponkratov, I.A. Malyshkina, et al., Design and synthesis of new anionic “polymeric ionic liquids” with high charge delocalization, Polym. Chem. 2 (2011) 2609–2618. doi:10.1039/C1PY00282A.

[11] J.F. Snyder, M.A. Ratner, D.F. Shriver, Ion Conductivity of Comb Polysiloxane Polyelectrolytes Containing Oligoether and Perfluoroether Sidechains, J. Electrochem. Soc. 150 (2003) A1090–A1094. doi:10.1149/1.1589759.

[12] S. Dou, S. Zhang, R.J. Klein, J. Runt, R.H. Colby, Synthesis and Characterization of Poly(Ethylene Glycol)-Based Single-Ion Conductors, Chem. Mater. 18 (2006) 4288–4295. doi:10.1021/cm0603699.

[13] M. Armand, Polymer solid electrolytes - an overview, Solid State Ion. 9–10, Part 2 (1983) 745–754. doi:10.1016/0167-2738(83)90083-8.

# APPENDIX

## *Description of the experimental techniques*

### A.1 GEL CONTENT: EXTRACTION OF THE SOLUBLE FRACTION

During a typical experiment, at least 0.5 grams of each sample were transferred into a Whatman glass microfibre thimble, and extracted with THF for 24 hours using a Soxhlet apparatus. After extraction, the thimble containing the insoluble fraction was thoroughly dried in an over (70 °C) to remove THF. The obtained solid was then weighted, and the gel content was calculated with the following formula:

$$gel\ content\ (\%) = \frac{wt_{final}}{wt_{initial}} \times 100$$

## A.2 FIELD EMISSION SCANNING ELECTRON MICROSCOPY (FESEM)

FESEM measurements were carried out on a ZEISS Supra 40, equipped with an energy dispersive X-ray spectrometer (EDX). Cross-sectional morphology characterizations were performed to estimate the uniformity and homogeneity across the samples thickness; test samples were cracked under cryogenic conditions after dipping in liquid nitrogen for enough time to avoid any change in the morphology. For analysis, the samples were subjected to metallization by sputtering a very thin Cr layer (~10 nm) to minimize the effect of the electron beam irradiation.

## A.3 NUCLEAR MAGNETIC RESONANCE (NMR)

$^{1}H$ and $^{13}C$-NMR spectra were obtained with a Bruker Avance II 500 MHz. Chemical shifts are reported in ppm, using the signal corresponding to the residual protons of the indicated deuterated solvent as an internal standard.

## A.4 FOURIER TRANSFORM INFRARED SPECTROSCOPY (FTIR)

A Bruker ALPHA FT-IR spectrometer was used to record FTIR spectra. The spectra were collected using 32 scans with a resolution of 2 $cm^{-1}$ in the ATR mode.

## A.5 SIZE EXCLUSION GEL PERMEATION CROMATOGRAPHY (SEC-GPC)

The molecular weights ($M_n$, $M_w$) and polydispersity index (PDI, $M_w/M_n$) of poly(PEGM) samples were determined at 35 °C on a LC-20AD gel permeation chromatograph (Shimadzu Corporation) equipped with Styragel HR columns (HR6-HR4-HR2), UV-visible detector (Waters 2487) and refractive index detector (Waters 2410). THF was used as an eluent with a flow rate of 1.0 mL $min^{-1}$. Calibration was performed with polystyrene standards (Polymer Laboratories, Varian). The molecular weights ($M_n$, $M_w$) and PDI of block copolymers were studied using on a PL-GPC 50 gel permeation chromatograph (Agilent) equipped with an integrated IR detector, a TSK-GEL® SuperAW4000 column (Tosoh) and a SuperAW-L Guard column (Tosoh). The 0.1 M LiCl and $1.5 \times 10^{-5}$ M $NaN_3$ solution in water/ACN mixture (4:1 v/v) was used as an eluent with a flow rate of 0.5 mL $min^{-1}$ at 35 °C. Calibration was performed with pullulan standards (Shodex P-82).

## A.6 DIFFERENTIAL SCANNING CALORIMETRY (DSC)

The glass transition temperature ($T_g$) and melting temperature ($T_m$) of the samples were evaluated by DSC with a METTLER DSC-30 (Greifensee, Switzerland) instrument. In a typical measurement, the samples were cooled from ambient temperature to –85 °C and then heated at 10 °C $min^{-1}$ up to 120 °C. The $T_g$ was calculated as the midpoint of the heat capacity change observed in the DSC trace during the transition from glassy to rubbery state.

## A.7 THERMO-GRAVIMETRIC ANALYSIS (TGA)

The thermal stability was tested by TGA tests using a TGA/SDTA-851 instrument from METTLER (Switzerland) over the temperature range between 25 and 600 °C under $N_2$ flux at a heating rate of 10 °C $min^{-1}$.

## A.8 DYNAMIC MECHANICAL THERMAL ANALYSIS (DMTA)

Glass transition temperature ($T_g$), storage (*E'*) and loss (*E''*) modules of the samples were measured by DMTA tests on a MK III Rheometrics Scientific Instrument at 1.0 Hz frequency on tensile configuration at a heating rate of 5 °C $min^{-1}$. The size of the specimen was about 20 mm×4 mm×0.2 mm. The storage modulus (*E*'), and the loss factor were measured from –80 up to 30 °C.

## A.9 TENSILE STRENGHT MEASUREMENT

Mechanical measurements on the samples were carried out through tensile experiments according to ASTM Standard D638, using a INSTRON 3366 dynamometer equipped electromechanical extensimeter (clip gauge) with a load cell of 500N; data were elaborated using the software provided by Instron S.r.l. A constant deformation of 10 mm $min^{-1}$ was applied on strips of 1 cm in width, which were blocked at an initial distance of 2.5 cm. At least five

specimens for each sample were tested; standard deviation in Young modulus (*E*) was 5%.

## A.10 ASSEMBLY OF TEST CELLS

All of the electrochemical techniques described below were performed using a CHI600 electrochemical analyzer/workstation (CH Instruments). Electrochemical cells model ECC-Std were used for the different tests, which were purchased from El-Cell GbmH. Cells were assembled inside the Ar-filled glove-box to avoid moisture contamination. Upon testing, the temperature was controlled using an environmental simulation chamber MK-53 (Binder); cells were allowed to reach the thermal equilibrium for at least three hour before each test.

## A.11 MEASUREMENTS OF IONIC CONDUCTIVITY ($\sigma$)

The values of $\sigma$ were determined by electrochemical impedance spectroscopy (EIS). Symmetric stainless steel/GPE/stainless steel cells were assembled. Cell complex impedance was measured by applying a 10 mV perturbation in the frequency range of 100 kHz to 1 Hz at the open circuit potential (OCV). Depending on the sample, the measurements were carried out between -20 and 90 °C with increasing 10 or 20 °C steps interval. The ohmic

resistance ($R_\Omega$) of the samples, obtained from the Nyquist plot at the low frequency end of the semicircle, was used to calculate the ionic conductivity using the following equation ($l$ is the distance between the electrodes and $A$ is their area):

$$\sigma = \frac{l}{A}\frac{1}{R_\Omega}$$

The activation energy was calculated from conductivity values obtained at various temperature and the resulting values are fitted with Vogel–Tamman–Fulcher (VTF) equation, which is typically used to describe the relation between viscosity and temperature near the $T_g$ of the polymer matrix. The equation used is given below:

$$\ln \sigma = \ln \sigma_0 - \frac{E_a^{VFT}}{R} \cdot \frac{1}{T - T_0}$$

where $\sigma$ is the ionic conductivity, $E_a^{VFT}$ is equivalent to the activation energy, $R$ is the gas constant, $T$ is the experimental temperature and $T_0$ is a fitting parameter, usually corresponding to a temperature which is 50 °C below the $T_g$.

## A.12 MEASUREMENTS OF LITHIUM IONS DIFFUSION COEFFICIENTS

The $Li^+$ diffusion coefficients were estimated using the method proposed by Ma *et al.* [1] as a function of salt concentration. Symmetrical cells were assembled sandwiching the sample in between lithium foils. A constant current was applied to the cell for a sufficient amount of time to set up a salt concentration gradient. Then, the current was interrupted, and the potential of the cell monitored as the concentration profiles relaxed. The curve of the natural log of potential (V) versus time (t) was plotted. The $D_{Li+}$ values were calculated from the slope of the linear curves using the following equation:

$$Slope = -\frac{\pi^2 \cdot D_{Li+}}{L^2}$$

where *L* is the thickness of the sample under study. Tests were performed at least trice to confirm the obtained results.

## A.13 ELECTROCHEMICAL STABILITY WINDOW (ESW)

Cyclic voltammetry (CV) was used to determine the ESW of the gel polymer electrolytes. Electrochemical test cells were assembled by sandwiching sample film between the working electrode and a lithium disk as counter electrode; lithium also served as reference electrode. Stainless steel and copper disks were used as working electrode during anodic and cathodic stability measurements,

respectively. Potential scans were carried out between OCV and 5.5 V vs. $Li^+/Li$ at a constant rate of 0.1-2 mV $s^{-1}$ to determine the anodic limit. To determine the cathodic limit, potential was scanned between OCV and -0.5 V vs. $Li^+/Li$ at the same constant rate.

## A.14 MEASUREMENTS OF INTERFACIAL STABILITY TOWARDS LITHIUM

Polymer electrolyte samples were characterized in terms of their stability towards Li-metal surface (interfacial stability) by monitoring the evolution of the complex impedance response with time of a symmetric Li/GPE/Li cell under OCV conditions. The test was carried out applying a 10 mV perturbation in the frequency range between 100 kHz and 0.01 Hz.

## A.15 ELECTROCHEMICAL STABILITY WINDOW (ESW)

The lithium-ion transference number ($t_{Li^+}$) was determined using the method described by Evans and Vincent [2]. Symmetrical cells were assembled sandwiching the sample in between lithium foils. Cells were subjected to a 10 mV polarization bias ($\Delta V$) to determine the initial ($I_i$) and steady state ($I_S$) currents. EIS was performed by applying a 10 mV perturbation between 100 kHz and 1 Hz at the open circuit potential (OCV) to obtain the resistance of the

passivation layer before ($R_i$) and after ($R_S$) polarization. $t_{Li^+}$ was calculated using the following equation:

$$t_{\mathrm{Li}^+} = \frac{I_\mathrm{s}(\Delta V - I_i R_\mathrm{i})}{I_\mathrm{i}(\Delta V - I_\mathrm{s} R_\mathrm{s})}$$

## REFERENCES

[1] Y. Ma, M. Doyle, T.F. Fuller, M.M. Doeff, L.C.D. Jonghe, J. Newman, The Measurement of a Complete Set of Transport Properties for a Concentrated Solid Polymer Electrolyte Solution, J. Electrochem. Soc. 142 (1995) 1859–1868. doi:10.1149/1.2044206.

[2] J. Evans, C.A. Vincent, P.G. Bruce, Electrochemical measurement of transference numbers in polymer electrolytes, Polymer. 28 (1987) 2324–2328. doi:10.1016/0032-3861(87)90394-6.

# *CONCLUDING REMARKS*

A major challenge in the development of next-gen lithium ion batteries is represented by the design of new electrolyte materials. In the last decades, polymer electrolytes have been extensively studied due to their enhanced safety features with respect to conventional non-aqueous liquid electrolytes. Among different systems, polyethylene oxide (PEO) based ones have attracted considerable attention due to its unique lithium-ion transport mechanism. However, practical application of such materials is still precluded due to their insufficient ionic conductivity at ambient temperature. Nevertheless, PEO remains one of the most promising candidate to accomplish the goal.

Considering the challenges and expectation for this key component, this Ph.D. work was focused on the development of novel strategies to improve the two main properties that control the transport of lithium ions in polymer electrolytes, namely ionic conductivity and lithium transference number.

In the first part of the experimental work, UV-induced cross-linking has demonstrated to be a versatile tool to prepare two different families of truly quasi-solid polymer electrolytes. A room temperature ionic liquid, namely 1-ethyl-3-methylimidazolium bis(trifluoromethylsulfonyl)imide was used as liquid plasticizer in the former case, whereas tetraethylene glycol dimethyl ether was

employed in the latter. In both systems, the presence of a high boiling point liquid plasticizer was essential to increase substantially the ionic conductivity at ambient temperature (up to $10^{-4}$ at 25 °C). Noteworthy, the obtained crosslinking assured the mechanical properties to be well retained despite the relatively high plasticizer contents. The materials showed outstanding characteristics in terms of thermal stability (> 170 °C) and electrochemical window ( > 4.5 in both cases). Additionally, the feasibility of using such material in LIBs at different temperatures was established, also thanks to a suitable in situ polymerization procedure directly onto the surface of the electrode films, fundamental to obtain an intimate interfacial adhesion. Lab-scale lithium cell showed stable charge/discharge characteristics without any capacity fading even at 0.2C current regime over prolonged cycling. The simplicity of the proposed process, along with the wide availability of the materials used, make these systems very promising and ready to be industrially scaled-up following the main principles of green chemistry. Indeed, it is worth to be noted that the newly developed preparation method has led to an international patent recently published.

In the second part of the Ph.D, work, the attention was focused on single-ion conducting polymer electrolytes. These systems have been recently proposed as alternatives to conventional complexes of lithium salts and polymers. An anionic monomer having a $Li^+$ as counter ion, namely lithium 1-[3-(methacryloxy) propylsulfonyl]-1-(trifluoromethanesulfonyl) imide, was synthetized and used to prepare the single-ion conducting polyelectrolytes.

Different macromolecular architectures were prepared: random or block copolymers with poly(ethylene glycol) methyl ether methacrylate and crosslinked networks with poly(ethylene glycol)dimethacrylate. All the described systems showed lithium transference number approaching the unity, which is a fundamental requirement to reduce cell polarization at high current rates. By changing the polyelectrolyte microstructure, it was also possible to tailor the ionic conductivity of both systems. In particular, solid-state single-ion conducting electrolytes exhibited ionic conductivity values ($10^{-5}$ S $cm^{-1}$ at 55 °C) lower than homologous dual ion electrolytes; prolonged cycling in lithium cells was nonetheless demonstrated at 70 °C. The ionic conductivity of the networked single ion conducting polymers was then substantially enhanced (up to $8.6 \times 10^{-5}$ S $cm^{-1}$ at 20 °C) by the incorporation of propylene carbonate as liquid plasticizer. The obtained gel electrolytes were tested in lab-scale lithium cells, which showed outstanding performance in terms of rate capability (up to 5C and 1C current rates respectively at 70 °C and ambient temperature) and cycling stability upon prolonged cycling (more than 3 months of un-interrupted testing), outperforming the current reports on single-ion conducting gelled systems.

In conclusion, the strategies presented in this PhD work in terms of performance optimization of different polymer electrolytes, as well as the engineering and synthetic procedures here suggested will optimistically represent reliable solutions for the scientific community for the development of

the next-generation of safe, cost-effective and environmentally friendly lithium-ion as well as lithium metal batteries.

# *ACKNOWLEDGMENTS*

First of all I would like to thank my advisor, Prof. Claudio Gerbaldi, for his mentorship, support and research freedom. Their guidance, constructive comments and suggestions have provided a good basis that made me able to organize responsibly the scientific research work. Thanks are also due to Prof. David Mecerreyes for giving me the opportunity to join his group at POLYMAT, Centre for Polymeric Materials (University of the Basque Country) where I have worked in well-equipped laboratories and I was given the opportunity to learn much about polymer chemistry. I would like to thank Prof. Alexander S. Shaplov for his availability at all times, his priceless professional and personal suggestions, and for making me understand the importance of collaboration in science.

My deep gratitude goes to the actual and former members of GAME Group@PoliTO: Dr. Jijeesh Ravi Nair, Dr. Federico Bella, Dr. Giuseppina Meligrana and Francesca Colò. Also, I would like to thank all the group members of POLYMAT, during the months I have spent in Donostia I have meet brilliant scientist and colleagues that have taught me a lot about science but more importantly, I have met true friends there. Lastly, and most importantly, I want to express my gratitude to my family, who supported me during these long three years.